BIOREACTORS, AIR-LIFT REACTORS

J.C. MERCHUK
M. GLUZ
Ben-Gurion University of the Negev
Beer-Sheva, Israel

KEY WORDS

Bubble column
Fluid dynamics
Gas hold-up
Heat transfer
Liquid flow
Mass transfer
Scale-up
Three-phase airlift reactors

OUTLINE

INTRODUCTION

General

The term *airlift reactor* (ALR) covers a wide range of gas–liquid or gas–liquid–solid pneumatic contacting devices that are characterized by fluid circulation in a defined cyclic pattern through channels built specifically for this purpose. In ALRs, the content is pneumatically agitated by a stream of air or sometimes by other gases. In those cases, the name *gas lift reactors* has been used. In addition to agitation, the gas stream has the important function of facilitating exchange of material between the gas phase and the medium; oxygen is usually transferred to the liquid, and in some cases reaction products are removed through exchange with the gas phase.

The main difference between ALRs and bubble columns (which are also pneumatically agitated) lies in the type of fluid flow, which depends on the geometry of the system. The bubble column is a simple vessel into which gas is injected, usually at the bottom, and random mixing is produced by the ascending bubbles. In the ALR, the major patterns of fluid circulation are determined by the design of the reactor, which has a channel for gas–liquid upflow—the riser—and a separate channel for the downflow (Fig. 1). The two channels are linked at the bottom and at the top to form a closed loop. The gas is usually injected near the bottom of the riser. The extent to which the gas disengages at the top, in the section termed the *gas separator*, is determined by the design of this section and the operating conditions. The fraction of the gas that does not disengage, but is entrapped by the descending liquid and taken into the downcomer, has a significant influence on the fluid dynamics in the reactor and hence on the overall reactor performance.

Airlift Reactor Morphology

Airlift reactors can be divided into two main types of reactors on the basis of their structure (Fig. 1): (1) external-loop vessels, in which circulation takes place through separate and distinct conduits; and (2) baffled (or internal-loop) vessels, in which baffles placed strategically in a single vessel create the channels required for the circulation. The designs of both types can be modified further, leading to variations in the fluid dynamics, in the extent of bubble disengagement from the fluid, and in the flow rates of the various phases.

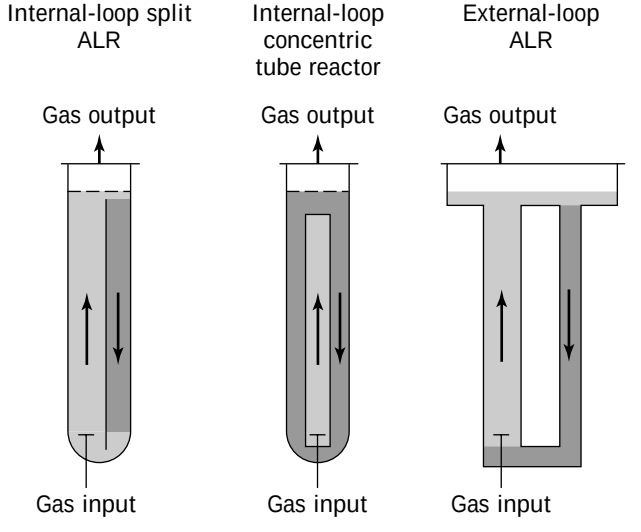

Figure 1. Different types of ALRs.

All ALRs, regardless of the basic configuration (external loop or baffled vessel), comprise four distinct sections with different flow characteristics:

- *Riser*. The gas is injected at the bottom of this section, and the flow of gas and liquid is predominantly upward.
- *Downcomer*. This section, which is parallel to the riser, is connected to the riser at the bottom and at the top. The flow of gas and liquid is predominantly downward. The driving force for recirculation is the difference in mean density between the downcomer and the riser; this difference generates the pressure gradient necessary for liquid recirculation.
- *Base*. In the vast majority of airlift designs, the bottom connection zone between the riser and downcomer is very simple. It is usually believed that the base does not significantly affect the overall behavior of the reactor, but the design of this section can influence gas holdup, liquid velocity, and solid phase flow (1,2).
- *Gas separator*. This section at the top of the reactor connects the riser to the downcomer, facilitating liquid recirculation and gas disengagement. Designs that allow for a gas residence time in the separator that is substantially longer than the time required for the bubbles to disengage will minimize the fraction of gas recirculating through the downcomer (Fig. 2).

Momentum, mass transfer, and heat transfer will be different in each section, but the design of each section may influence the performance and characteristics of each of the other sections, since the four regions are interconnected.

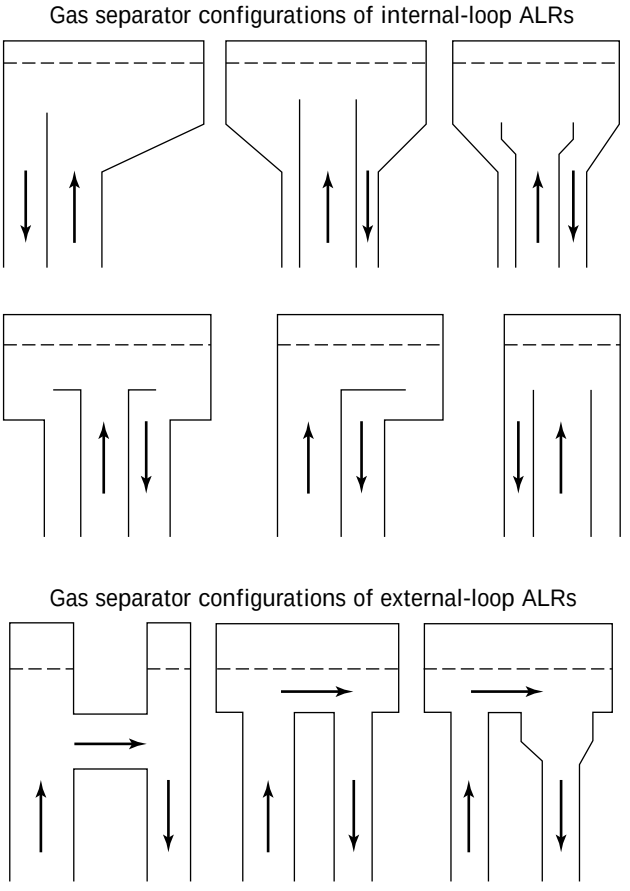

Figure 2. Different types of gas separators.

Advantages of Airlift Bioreactors

For the growth of microorganisms, ALRs are considered to be superior to traditional stirred-tank fermenters despite the fact that the conventional fermenters provide the major requirements for culturing microorganisms: gas–medium interface for the supply of oxygen and the removal of waste gases; means of agitation to ensure proper nutrient distribution and to minimize damage resulting from addition of concentrated acid or base (for pH control); means of heat transfer (for temperature control); and a contamination-free environment. Therefore, the reason for the more successful growth reported in ALRs (3,4) appears to lie in the difference in the fluid dynamics between ALRs and the more conventional fermenters. In conventional stirred tanks or bubble columns, the energy required for the movement of the fluids is introduced focally, at a single point in the reactor, via a stirrer or a sparger, respectively. Consequently, energy dissipation is very high in the immediate surroundings of the stirrer and decreases away from it toward the walls. Similarly, shear will be greatest near the stirrer (5), since the momentum is transferred directly to the fluid in that region (6), which, in turn, transfers this energy to the slower-moving, more distant elements of the fluid. This results in a wide variation of shear forces; for example, the maximum shear gradient in a stirred tank with a flat-blade turbine has been reported to be approximately 14 times the mean shear gradient (7).

Cells in culture may thus be exposed to contrasting environments in a mechanically stirred vessel, either to minimal shear forces that may generate potentially undesirable gradients in temperature and in substrate, metabolite, and electrolyte concentrations or, alternatively, to highly turbulent zones, with no problems of heat or mass transfer, but with very high shear gradients that may endanger cell integrity or exert some influence on cell morphology and metabolism (6). Changes in the morphology of microorganisms associated with high shear forces in the medium have frequently been observed (8–10). The nature of the relationship between such morphological changes and the rates of growth and metabolite production is still not properly understood, although it may be of great importance in the design and scale-up of bioreactors.

In ALRs, as in bubble columns, the gas is injected at a single point, but in ALRs the direct contribution of gas injection to the dynamics of the system is small; circulation of liquid and gas is facilitated by the difference in gas holdup between the riser and the downcomer, which creates a pressure difference at the bottom of the equipment:

$$\Delta P_b = \rho_L g(\varphi_r - \varphi_d) \quad (1)$$

where ΔP_b is the pressure difference, ρ_L is the density of

the liquid (the density of the gas is considered to be negligible), g is the gravitational constant, and φ_r and φ_d are the fractional gas holdup of the riser and downcomer, respectively. The pressure difference forces the fluid from the bottom of the downcomer toward the riser, generating fluid circulation in the ALR. Since φ_r and φ_d are both average values integrated along the height of the reactor, it follows that there are no focal points of energy dissipation and that shear distribution is homogeneous throughout the ALR. There is thus a relatively constant environment, with minimization of sharp changes in the mechanical forces acting on suspended particles. Because good mixing is required, shear forces cannot be avoided completely. One of the most critical points is the bottom, where there is a sharp 180° turn.

Shear-sensitive mammalian and plant cells in culture should benefit from such an environment. Currently, the research and development of new bioreactors for mammalian cells is indeed focusing on the issue of shear-related damage to suspended cells (8,11–24).

Mammalian and plant cells in culture are more susceptible than microorganisms to the reactor conditions. Mammalian cells, which lack the rigid cell wall of microorganisms, have a larger size (one order of magnitude) than microorganisms and are very sensitive to mechanical stress. Plant cells have a rigid cellulose wall, but they are also much larger than microorganisms (usually by about an order of magnitude) and are therefore also sensitive to reactor conditions. Kolmogoroff's model of isotropic turbulence (25) indicates that serious damage may occur at relatively large values of the length scale. The last length is a parameter of the model and indicates the size of the eddy where energy starts to be dissipated by viscous resistance. Indeed, it has been observed that plant cells, in spite of their rigid wall, are shear-sensitive, and difficulties have been found in stirred-tank cultures. This is especially true when large-scale systems are considered. Although high agitation rates may be detrimental to cell growth, low agitation rates lead to an increase in the number and size of cell aggregates—also an undesirable phenomenon. The aggregates are formed as a result of daughter cells failing to separate after division and as a consequence of the stickiness of the polysaccharides excreted by the cells, especially at the end of the growth phase. An optimal shear rate between these two extremes must be found for each culture.

It has recently been shown experimentally that velocity fluctuations related to turbulent shear are relatively homogeneously distributed in an ALR (26,27). The measurements of fluctuating velocity made by Tan et al. (26) show that the liquid turbulence in ALRs is homogeneously distributed in both the riser and the downcomer. It thus seems reasonable to assume that the homogeneity of the stress forces is the main advantage offered by ALRs and that this homogeneity is responsible for the success of shear-sensitive cultures in the ALR type of fermenter (3,28–31).

Another advantage of the ALR is the mechanical simplicity of the device. The absence of a shaft and of the associated sealing, which is always a weak element from the point of view of sterility, confers on the ALR an obvious advantage over agitated tanks. This consideration is especially important in processes involving slow-growing cultures, such as animal and plant cells, for which the risk of contamination is large.

All the points mentioned above are particularly relevant for sophisticated processes in which the product is usually of high value. But ALRs may be used also for processes involving low-value products, in which case efficiency of energy use may well become the key point for design, as in the use of ALRs for wastewater treatment (32). The superiority of ALRs over mechanically agitated contactors in terms of mass transfer rates for a given energy input has been demonstrated by Legrys (33). Comparison of the efficiency of oxygen transfer, that is, the mass of oxygen absorbed per unit energy invested and unit time, showed that the efficiency of the ALR is among the highest in agitated systems (32). The ALRs are particularly suited to processes with changing oxygen requirements because aeration efficiency and performance are relatively insensitive to changes in operating conditions. Performance decreases markedly in mechanically stirred systems as the energy input (or oxygen transfer rate) increases, but it is quite constant in ALRs (34) (Fig. 3).

The efficiency of ALRs decreases relatively slowly as the energy input per unit volume of reactor is increased, as is shown in Figure 4 (32). In contrast, in the operation of stirred tanks, the mass transfer rate can be easily increased by increasing the power input, but this improvement is achieved at the cost of a considerable decrease in the efficiency of oxygen transfer. This decrease may constitute a crucial disadvantage in a process like wastewater treatment, where the energy input is an important element in the cost of the final product and flexibility of operating conditions is required because of the constant change of feed composition and flow rate.

Energy economy in the ALR may be improved by placing a second sparger in the upper part of the downcomer (32,35,36). If the liquid velocity is greater than the free rising velocity of the bubbles generated, the gas is carried down, resulting in a longer contact time between the bubble and the liquid. This diminishes the energy requirements, since part of the gas is injected against a lower hydrostatic pressure.

The advantages described above counterbalance the obvious disadvantage of ALRs, which is the requirement for a minimum liquid volume for proper operation. Indeed, the changes in liquid volume in these reactors are limited to the region of the gas separator, since the liquid height must always be sufficient to allow liquid recirculation in the reactor and must therefore be above the separation between the riser and the downcomer.

FLUID DYNAMICS

The interconnections between the design variables, the operating variables, and the observable hydrodynamic variables in an ALR are presented diagramatically in Figure 5 (37). The design variables are the reactor height, the riser-to-downcomer area ratio, the geometrical design of the gas separator, and the bottom clearance (C_b, the distance between the bottom of the reactor and the lower end of the draft tube, which is proportional to the free area for

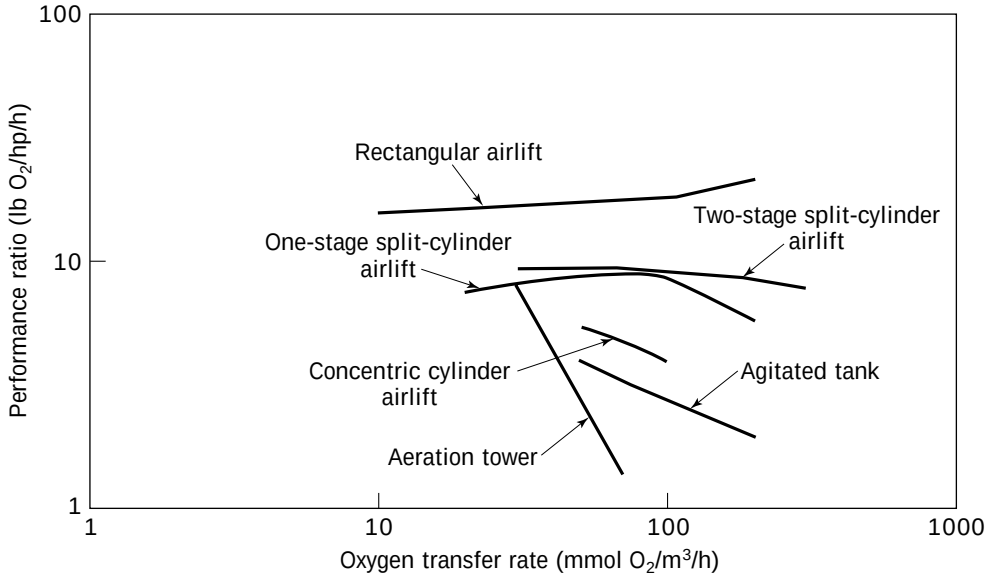

Figure 3. Performance ratio as a function of oxygen-transfer rate, showing that aeration efficiency and performance are relatively insensitive to changes in operating conditions in different types of ALRs (1–5) versus an agitation tank (6) and an aeration tower (7). Adapted from Orazem and Erickson (34).

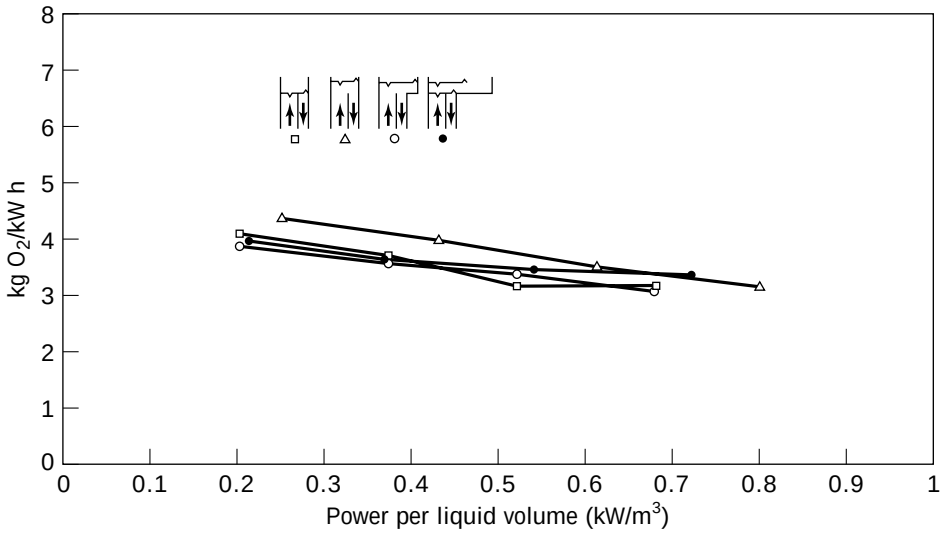

Figure 4. Aeration efficiency as a function of pneumatic power of gas input per unit volume in a straight-baffle ALR. The level indicated corresponds to no-aeration conditions. Adapted from Siegel et al. (32).

flow in the bottom and represents the resistance to flow in this part of the reactor). The main operating variables are primarily the gas input rate and, to a lesser extent, the top clearance (C_t, the distance between the upper part of the draft tube and the surface of the nonaerated liquid). These two independent variables set the conditions that determine the liquid velocity in the ALR via the mutual influences of pressure drops and holdups, as shown in Figure 5 (37). Viscosity is not shown in Figure 5 as an independent variable because in the case of gas–liquid mixtures, it is a function of the gas holdup (and of liquid velocity in the case of non-Newtonian liquids), and because in a real process, it will change with time due the changes in the composition of the liquid.

Flow Configuration

Riser. In the riser, the gas and liquid flow upward, and the gas velocity is usually larger than that of the liquid. The only exception is homogeneous flow, in which case both phases flow at the same velocity. This can happen only with very small bubbles, in which case the free-rising velocity of the bubbles is negligible with respect to the liquid velocity. Although about a dozen different gas–liquid flow configurations have been developed (38), only two of them are of interest in ALRs (39,40):

1. Homogeneous bubbly flow regime, in which the bubbles are relatively small and uniform in diameter and turbulence is low

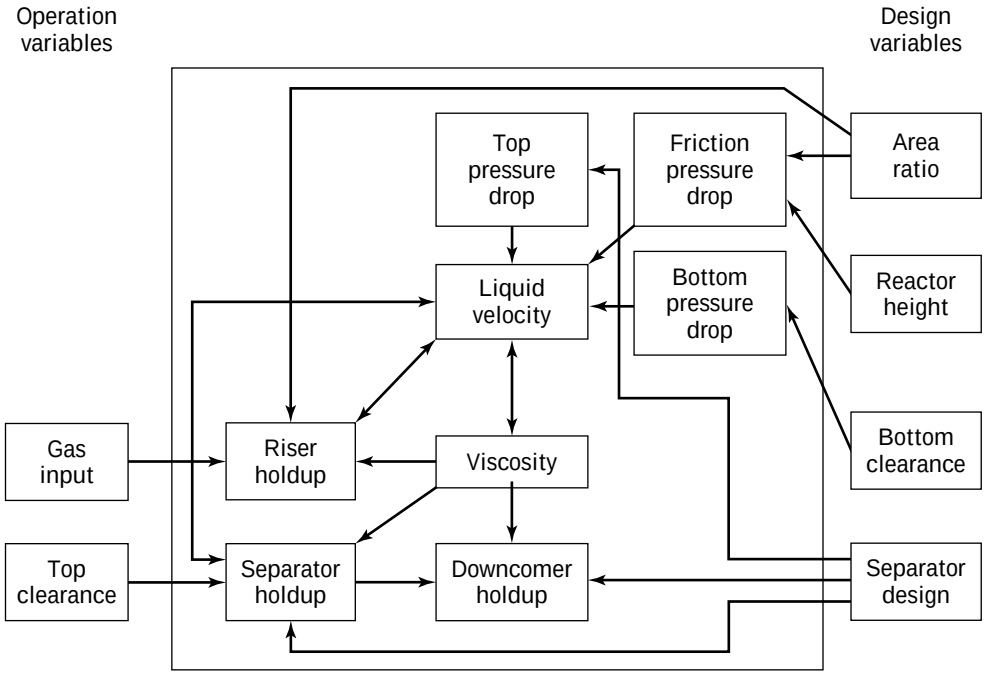

Figure 5. Interaction between geometric and fluid dynamic variables in an ALR. Adapted from Merchuk et al. (37).

2. Churn-turbulent regime, in which a wide range of bubble sizes coexist within a very turbulent liquid

The churn-turbulent regime can be produced from homogeneous bubbly flow by increasing the gas flow rate. Another way of obtaining a churn-turbulent flow zone is by starting from slug flow and increasing the liquid turbulence, by increasing either the flow rate or the diameter of the reactor, as can be seen in Figure 6 (41). The slug-flow configuration is important only as a situation to be avoided at all costs, because large bubbles bridging the entire tower cross-section offer very poor capacity for mass transfer.

Downcomer. In the downcomer, the liquid flows downward and may carry bubbles down with it. For bubbles to be entrapped and flow downward, the liquid velocity must be greater than the free-rise velocity of the bubbles. At very low gas flow input, the liquid superficial velocity is low, practically all the bubbles disengage, and clear liquid circulates in the downcomer. As the gas input is increased, the liquid velocity becomes sufficiently high to entrap the smallest bubbles. Upon a further increase in liquid velocity larger bubbles are also entrapped. Under these conditions the presence of bubbles reduces the cross-section available for liquid flow, and the liquid velocity increases in this section. Bubbles are thus entrapped and carried downward, until the number of bubbles in the cross-section decreases, the liquid velocity diminishes, and the drag forces are not sufficient to overcome the buoyancy. This feedback loop in the downcomer causes stratification of the bubbles, which is evident as a front of static bubbles, from which smaller bubbles occasionally escape downward and larger bubbles, produced by coalescence, escape upward. The bubble front descends, as the gas input to the system is increased, until the bubbles eventually reach the bottom and recirculate to the riser. When this point is reached, the bubble distribution in the downcomer becomes much more uniform. This is the most desirable flow configuration in the downcomer, unless a single pass of gas is required. The correct choice of cross-sectional area ratio of the riser to the downcomer will determine the type of flow.

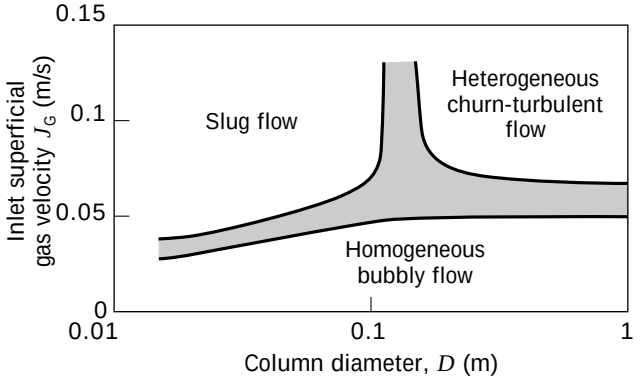

Figure 6. Map of flow configurations for gas–liquid concurrent flow in a vertical tube. Adapted with permission from Wiswanathan (40).

Gas Separator. The gas separator is often overlooked in descriptions of experimental ALR devices, although it has considerable influence on the fluid dynamics of the reactors. The geometric design of the gas separator will determine the extent of disengagement of the bubbles entering from the riser. In the case of complete disengagement, clear liquid will be the only phase entering the downcomer.

In the general case, a certain fraction of the gas will be entrapped and recirculated. Fresh gas may also be entrapped from the headspace if the fluid is very turbulent near the interface. The extent of this entrapment influences strongly gas holdup and liquid velocity in the whole reactor.

It is quite common to enlarge the separator section to reduce the liquid velocity and to facilitate better disengagement of spent bubbles. Experiments have been reported in which the liquid level in the gas separator was high enough to be represented as two mixed vessels in series (42,43). This point will be analyzed further in the section devoted to mixing.

Gas Holdup

Gas holdup is the volumetric fraction of the gas in the total volume of a gas–liquid–solid dispersion:

$$\varphi_i = \frac{V_G}{V_L + V_G + V_S} \tag{2}$$

where the subindexes L, G, and S indicate liquid, gas, and solid, and *i* indicates the region in which the holdup is considered, that is, gas separator (s) the riser (r), the downcomer (d), or the total reactor (T).

The importance of the holdup is twofold: (1) the value of the holdup gives an indication of the potential for mass transfer, since for a given system a larger gas holdup indicates a larger gas–liquid interfacial area; and (2) the difference in holdup between the riser and the downcomer generates the driving force for liquid circulation. It should be stressed, however, that when referring to gas holdup as the driving force for liquid circulation, only the total volume of the gas is relevant. This is not the case for mass-transfer phenomena, in this case, the interfacial area is of paramount importance, and therefore some information on bubble size distribution is required for a complete understanding of the process.

Because gas holdup values vary within a reactor, average values, referring to the whole volume of the reactor, are usually reported. Values referring to a particular section, such as the riser or the downcomer, are much more valuable, since they provide a basis for determining liquid velocity and mixing. However, such values are less frequently reported.

The geometric design of the ALR has a significant influence on the gas holdup. Changes in the ratio A_d/A_r, the cross-sectional areas of the downcomer and the riser, respectively, will change the liquid and gas residence time in each part of the reactor and hence their contributions to the overall holdup. Gas holdup increases with decreasing A_d/A_r (44–47).

Gas Holdup in Internal Airlift Reactors. Correlations presented for internal-loop ALRs are shown in Table 1. These take into account liquid properties and geometric differences within a particular design. Most of the correlations take the form:

$$\varphi_r = a(J_G)^{\alpha}\left(\frac{A_d}{A_r}\right)^{\beta}(\mu_{ap})^{\gamma} \tag{3}$$

where φ_r is the gas holdup in the riser, J_G is the superficial gas velocity (gas volumetric flow rate per unit of cross-sectional area), μ_{ap} is the effective viscosity of the liquid, and α, β, γ, and a are constants that depend on the geometry of the reactor and the properties of the liquid. The correlation can be used to predict the holdup in a system that is being designed or simulated as a function of the operating variables, the geometry of the system, or the liquid properties. Such correlations are effective for fitting data for the same type of reactor (e.g., a split-vessel reactor) with different area ratios or even different liquid viscosities, but they are mostly reactor-type specific.

The cyclic flow in the ALR complicates the analysis of the system. The riser gas holdup depends strongly on the geometric configuration of the gas–liquid separator and the water level in the gas separator. This has been shown experimentally in a split-vessel rectangular ALR (60), but the premise can essentially be extended to any internal-loop ALR. Analysis of the system revealed that these factors influence the gas disengagement and hence the gas recirculation in the downcomer. When this influence is taken into account and the holdup is plotted against the true gas superficial velocity, $J_{G,true}$, which is defined as the sum of the gas superficial velocity due to the freshly injected gas, Q_{in}, and to the recirculated gas, Q_d, that is,

$$J_{G,true} = \left(\frac{Q_{in} + Q_d}{A_r}\right) \tag{4}$$

then all the data for the different gas separators may be represented by a single relationship, such as equation 3. In other words, if the actual gas flow is known, the influence of gas recirculation (which depends on A_d/A_r and the design of the gas separator) has been already taken into account and does not need to be considered again. Nevertheless, this simple approach has a drawback in that the true gas superficial velocity is difficult to measure because the gas recirculation rate is usually not known. A method for evaluation of the extent of the maximum gas recirculation has recently been developed and will be discussed later in this article.

Thus, correlations that take into account all the variables, which may be easily measured, remain the option of choice. Table 1 shows most of the correlations of this type that have been proposed for the riser holdup in internal-loop ALRs. Comparison of a number of these correlations shows that there is reasonable agreement between the predictions of the different sources (Fig. 7).

Figure 7 can be used as an example of the actual state-of-the-art in ALR design. A number of correlations have been proposed, and three variables (A_d/A_r, μ_{ap}, and J_G) have been tested by most researchers. The ranges in which these variables were studied varies from source to source. In addition, some other variables (such as bottom clearance, top clearance or gas separator design, and surface tension) have been used by some authors but ignored by others. One example is the disengagement ratio defined by Siegel and Merchuk (64), which represents the mean horizontal path of a recirculating bubble relative to the external diameter and is equivalent to the parameter obtained by dimensional analysis (1) as:

$$M = \frac{D_S}{4D}$$

where D is the diameter of column and D_s the diameter of

Table 1. Gas Hold-Up in Internal-Loop ALR

No.	Formula	Ref.
1	$\varphi_r = 0.441 J_{Gr}^{0.841} \mu_{ap}^{-0.135}$ $\varphi_d = 0.297 J_{Gr}^{0.935} \mu_{ap}^{-0.107}$	48
2	$\varphi_r = 2.47 J_{Gr}^{0.97}$	49
3	$\varphi_r = 0.465 J^{0.65}\left(1 + \frac{A_d}{A_r}\right)^{-1.06} \mu_{ap}^{-0.103}$	50
4	$\varphi_r = 0.65 J_{Gr}^{(0.603 + 0.078 C_0)}\left(1 + \frac{A_d}{A_r}\right)^{-0.258}$ $\varphi_d = 0.46\varphi_r - 0.0244$	51
5	$\varphi_r = (0.491 - 0.498) J_{Gr}^{0.706}\left(\frac{A_d}{A_r}\right)^{-0.254} D_u \mu_{ap}^{-0.0684}$	52
6	$\varphi_r = 0.16\left(\frac{J_{Gr}}{J_{1r}}\right)^{0.57}\left(1 + \frac{A_d}{A_r}\right)$ $\varphi_d = 0.79\varphi_r - 0.057$	45
7	$\varphi_r = 0.364 J_{Gr}$	53
8	$\frac{\varphi_r}{1 - \varphi_r} = \frac{J_{Gr}^{n+2/2(n+1)}}{2^{3n+1/n+1} n^{n+2/2(n+1)}\left(\frac{K}{\rho_1}\right)^{1/2(n+1)} g^{n/2(n+1)}\left(1 + \frac{A_d}{A_r}\right)^{3(n+2)/4(n+1)}}$	54
9	$\frac{\varphi}{(1 - \varphi)^4} = \frac{0.124\left(\frac{J_G \mu_1}{\sigma_1}\right)^{0.996}\left(\frac{\rho_1 \sigma_1^3}{g\mu_1^4}\right)^{0.294}\left(\frac{D_r}{D}\right)^{0.114}}{1 - 0.276(1 - e^{-0.0368 Ma})}$	55
10	$\varphi_r = \frac{Fr}{0.415 + 4.27\left(\frac{J_{Gr} + J_{1r}}{\sqrt{gD_r}}\right)\left(\frac{g\rho_1 D^2}{\sigma_1}\right)^{-0.188} + 1.13 Fr^{1.22} Mo^{0.0386}\left(\frac{\Delta\rho}{\rho_1}\right)^{0.0386}}$	56
11	$\frac{\varphi}{(1 - \varphi)^4} = 0.16\left(\frac{J_G \mu_1}{\sigma_1}\right) Mo^{-0.283}\left(\frac{D_r}{D}\right)^{-0.222}\left(\frac{\rho_1}{\Delta\rho}\right)^{0.283} * (1 - 1.61(1 - e^{-0.00565 Ma}))^{-1}$	2
12	$\varphi_d = 4.51 \cdot 10^6 Mo^{0.115}\left(\frac{A_r}{A_d}\right)^{4.2} \varphi_r$ when $\varphi_r < 0.0133\left(\frac{A_d}{A_r}\right)^{-1.32}$ and $\varphi_d = 0.05 Mo^{-0.22}\left[\left(\frac{A_r}{A_d}\right)^{0.6} \varphi_r\right]^{0.31 Mo^{-0.0273}}$ when $\varphi_r > 0.0133\left(\frac{A_d}{A_r}\right)^{-1.32}$	57
13	$\varphi_r = 0.0057\left[(\mu_1 - \mu_w)^{2.75} - 161\frac{73.3 - \sigma}{79.3 - \sigma}\right] \cdot J_{Gr}^{0.88}$	58
14	$\varphi_r = \frac{0.4Fr}{1 + 0.4Fr\left(1 + \frac{J_1}{J_{Gr}}\right)}$	57
15	$\varphi = 0.24 n^{-0.6} Fr^{0.84 - 0.14n} Ga$	59

gas separator. If this parameter is not taken into account, then studies of the influence of the top clearance (42,65) are incomplete and difficult to extrapolate to other designs. The same can be said about the filling factor (66) given by the ratio of the gas separator volume to the total volume.

The foregoing discussion thus explains why all the correlations coincide for some ranges of these secondary variables while in other ranges they may diverge. In addition, in some cases the number of experiments may not have been sufficient to provide correlations or they may have been ill-balanced from the statistical point of view. The obvious solution to this problem lies in the collection of a large and detailed bank of reliable data that will constitute the basis for correlations with greater accuracy and validity.

The safest procedure for the prediction of the gas holdup in an ALR under design is to take data provided by researchers who have made the measurements in that par-

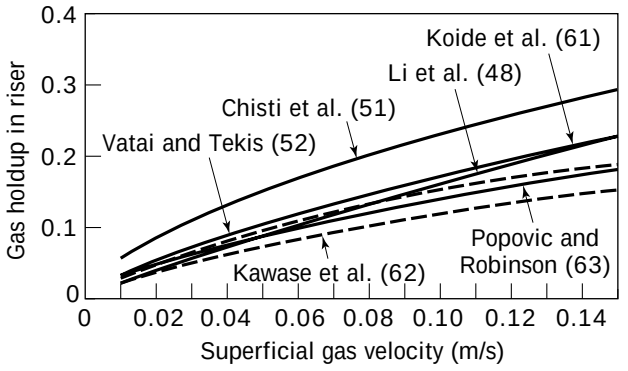

Figure 7. Some correlations proposed for prediction of gas holdup in the riser of internal-loop ALRs (Table 1). Gas holdup (φ_r) is presented as a function of superficial gas velocity (J_G). Other parameters related to geometry and physicochemical properties that were used in the calculations are shown on the figure.

ticular type of reactor with the same physicochemical properties of the system. If this option is not available, then correlation 9 in Table 1 (55) is recommended for prediction of the gas holdup in the riser.

Gas holdup in the downcomer is lower than that in the riser. The extent of this difference depends mainly on the design of the gas separator (67). The downcomer gas holdup is linearly dependent on the riser holdup, as a consequence of the continuity of liquid flow in the reactor. Many expressions of this type have been published (68). At low gas flow rates, φ_d is usually negligible, since most of the bubbles have enough time to disengage from the liquid in the gas separator. This usually happens at the low gas flow rates frequently used for animal cell cultures.

The gas holdup in the separator is very close to the mean gas holdup in the whole reactor (1) as long as the top clearance C_t is relatively small (one or two diameters). For larger top clearances, the behavior of the gas separator begins to resemble that of a bubble column, and the overall performance of the reactor is influenced by this change.

External-Loop Airlift Reactors. From the point of view of fluid dynamics, neither the external configuration (shape and architecture) nor the fact that both riser and downcomer are easily accessible is the most important difference between external- and internal-loop reactors. The most important point is that the gas separator of the external-loop ALR is built in such way that gas disengagement is usually much more effective in this type of reactor. This can be easily seen in Figure 2. In concentric tubes or split vessels, the shortest path that a bubble has to cover from the riser to the downcomer is a straight line across the baffle that separates the two sections. In the case of external-loop ALRs, there is usually a minimum horizontal distance to be covered, which increases the chances of disengagement of the bubbles. In this case, it is worth pointing out that if gas does appear in the downcomer, then most of it will be fresh air entrained in the reactor because of interfacial turbulence or vortices that appear in the gas separator above the entrance to the downcomer. In many of the studies reported in the literature on holdup in external-loop ALRs, total disengagement is attained. No such data are available for the concentric tubes of split-vessel ALRs, since total disengagement is possible only at very low gas flow rates.

Several authors (37,69–73) have presented their results of gas holdup as the gas velocity versus the superficial mixture velocity, based on the drift flux model of Zuber and Findlay (74). These authors derived general expressions for prediction of the gas holdup and for interpretation of experimental data applicable to nonuniform radial distributions of liquid velocity and gas fraction. The drift velocity is defined as the difference between the velocity of the particular phase (U) and the volumetric flux density of the mixture (J) where:

$$J = J_G + J_L \tag{5}$$

The drift velocities of the gas and liquid phases may thus be expressed as:

$$J_G = U_G - J \tag{6}$$

$$J_L = U_L - J \tag{7}$$

Zuber and Findlay (74) derived the relationship [8], which has been shown to be more than adequate to provide a correlation of gas holdup measurements in tower reactors with high liquid velocities, such as ALRs (71):

$$U_G = \frac{J_G}{\varphi} = C_0 J + \frac{\frac{1}{A}\int \varphi(U_G - J)dA}{\frac{1}{A}\int \varphi \cdot dA} \tag{8}$$

where A is cross-sectional area, C_0 is distribution parameter, J is superficial velocity, J_G is superficial gas velocity, U_G linear gas velocity, and φ is gas holdup.

Equation 7 describes the relationship between the gas velocity in a two-phase flow and the volumetric flow density of the mixture, J.

As stressed by Zuber and Findlay (74), J has the advantage of being independent on space coordinates for both one-dimensional flow and multidimensional irrotational flows. The distribution parameter C_0 is given by (75):

$$C_0 = \frac{\frac{1}{A}\int_A \varphi J \cdot dA}{\left[\frac{1}{A}\int_A J \cdot dA\right]\left[\frac{1}{A}\int_A \varphi \cdot dA\right]} \tag{9}$$

The value of C_0 depends mainly on the radial profile of the gas holdup. Zuber and Findlay (74) calculated $C_0 = 1$ for a flat profile and $C_0 = 1.5$ for a parabolic profile. Experimental values have been reported in the range of 1.03–1.2 for upflow (69–73,76) and 1.0–1.16 for downflow (70,73).

Equation 9 shows that this parameter is a function of the profiles of velocities and holdup. The last term of the right-hand side of equation 8 is the weighted mean value of the drift velocity:

$$U_{GI} = U_G - J \tag{10}$$

The drift velocity of a swarm of bubbles can be evaluated by using the expression given by Zuber and Findlay (74).

$$U_{2J} = 1.53 \cdot \left[\frac{\sigma g \Delta\rho}{\rho_L^2}\right]^{0.25} (1 - \varphi)^{1.5} \tag{11}$$

where U_{2J} is the velocity of the swarm of bubbles, g is gravitational acceleration, ρ_L is the density of liquid, $\Delta\rho$ is the density difference, σ is the surface tension, and φ is the gas holdup. This equation is valid for bubble diameters of the order of 0.1 to 2 cm, which covers the population usually observed in ALRs.

It has, however, been shown (71) that a plot of U_G versus J gives a straight line, suggesting that a constant value of the drift velocity satisfactorily represents the two-phase flow in the riser of an external-loop ALR. In this plot, the distribution parameter was $C_0 = 1.03$, and U_{GS}, the value of the slip velocity of a bubble, was taken as the mean drift velocity. Siegel et al. (35) applied the same model for the study of gas recirculation in a split-vessel ALR and obtained the values of $C_0 = 1.11$. The slip velocity that they obtained fitting their data to equation 8 was 0.238 m/s. It has been suggested (71) that this simplification holds as long as coalescence is not a predominant factor in the process.

It is very important to stress the difference between holdup, φ, and the flowing volumetric concentration (β), which is defined as:

$$\beta = \frac{Q_G}{Q_G + Q_L} = \frac{J_G}{J} \tag{12}$$

Zuber–Findlay's drift flux model allows us to derive the following equation, which establishes a connection between the gas holdup and β.

$$\frac{\beta}{\varphi} = C_0 + \frac{U_{b\infty}}{J} \tag{13}$$

where C_0 is the distribution parameter, J is the superficial velocity, $U_{b\infty}$ is the terminal gas velocity, β is the flowing volumetric concentration, and φ is the gas holdup.

Figure 8 gives a representation of the $\varphi - \beta$ plane. The 45° line indicates that $\varphi = \beta$, an equality that is true only for nonslip flow, where the velocity of the gas is equal to the velocity of the liquid. Such a situation can be visualized for the case of very small bubbles in a relatively fast liquid. In this case, there is no influence of one phase on the motion of the other. As indicated in Figure 8, all the points below the 45° line indicate operation situations in which the liquid is driven by the gas:

$$U_G > U_L;\ \varphi < \beta \tag{14}$$

This happens in the riser of ALRs. For all points above the line the opposite is true:

$$U_G < U_L;\ \varphi > \beta \tag{15}$$

This latter condition reflects the operation of the downcomer.

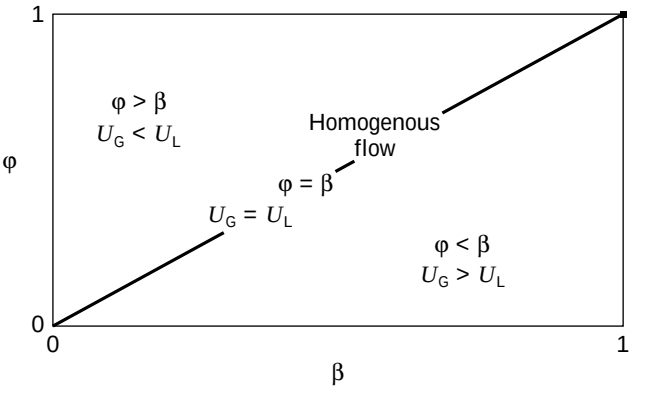

Figure 8. Gas flow holdup (φ) vs. flowing volumetric concentration (β). The different zones in the plane φ–β identify the two-phase flow. Adapted from Merchuk and Berzin (77).

A number of authors (71,76,78,79) have measured the local holdup profile along the riser of an external-loop ALR. In general, it was found that the holdup increases with height. This finding concurs with the expected expansion of gas bubbles as regions of lower pressure are reached. Common sense indicates that this situation must be limited to a certain range; an increase in bubble size will enhance turbulence and result in an increase in bubble encounters, leading eventually to bubble coalescence. The larger bubbles will rise much faster, resulting in a decrease in holdup. Such a scenario was indeed observed by Merchuk and Stein (71), as is illustrated in Figure 9. Merchuk and Stein (71) reported a maximum in the holdup profile for the case of a single-orifice gas distributor. For a multiple-orifice sparger, producing a more homogeneous bubble size distribution, a maximum was not observed within the studied length of the riser, which was 4 m.

Literature data from different sources for gas holdup in the riser under conditions of little or no carryover of gas from the separator into the downcomer for different A_d/A_r and top clearance C_t may be represented by the simple exponential:

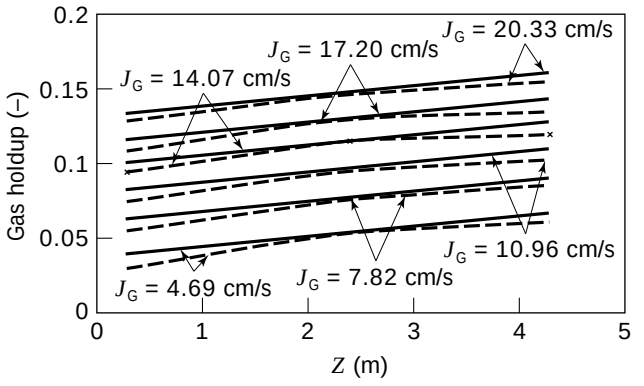

Figure 9. Dependence of the riser gas holdup in a 4-m high external-loop ALR with a multiple-orifice sparger (*solid lines*) and a single-orifice sparger (*broken lines*). Adapted from Merchuk and Stein (71).

$$\varphi_r = \alpha J_G^{\beta} \tag{16}$$

where the constant α depends on the friction losses in the loop, and β is usually a value between 0.6 and 0.7, as is illustrated in Figure 10 (65). The fact that neither the area ratio nor the top clearance affects the gas holdup demonstrates the role of the gas–liquid separator in determining the performance of the reactor in general. In the absence of gas recirculation, there is no effect on these variables. Moreover, this means that under conditions of no gas entrainment from the separator to the downcomer, it is possible to predict the riser gas holdup as a function of the riser superficial gas velocity alone, which is of great importance for design purposes.

It is accepted that liquid velocity has a mild negative effect on gas holdup in the riser. This effect is usually studied by reducing the liquid flow; this is achieved by adding resistance to the liquid loop by means of a valve or other controlled obstruction (71,78,82) under conditions of low or nil gas recirculation. Such experiments, which are relatively simple in external-loop ALRs, indicate that the holdup decreases as the liquid velocity is increased from zero (bubble column) to 0.3 m/s (which is close to the bubble free-rise velocity). For higher velocities, the effect of U_L is small. These findings add to our understanding of the fluid dynamics in the column. At liquid velocities that are smaller than the bubble free-rising velocity, the liquid transported in the wake of the bubbles, which must return downward to balance the mass flux, is the cause of the meandering and loops that typically appear in bubble column operation (83). As the overall liquid flux increases, the patterns straighten out, the bubbles begin to ascend in a straight pattern, and the holdup goes down. When the liquid velocity is higher than the free-rise velocity of the bubbles, piston flow of bubbles ensues in the tube, and the decrease in holdup for further increases in liquid velocity is due solely to the change in the ratio of gas–liquid volumetric flow rates.

When there is gas recirculation, the area ratio A_d/A_r becomes an important variable affecting gas holdup. The effect of A_d/A_r starts in the region in which gas entrainment from the separator to the downcomer occurs. If it is assumed that the riser cross-sectional area A_r remains unchanged and the downcomer cross-sectional area A_d is increased, then it can be expected that the liquid velocity in the riser will increase as a result of the smaller resistance to flow in the loop, which in turn leads to a decrease in the riser gas holdup. An increase in A_d/A_r will result in a decrease in the liquid velocity in the downcomer, which leads to a decrease in the gas recirculation, since fewer bubbles are entrapped in the downcomer. The final outcome of increasing A_d/A_r is thus a decrease is the riser gas holdup. A similar argument can be applied in the discussion of the effect of reactor height on the riser gas holdup, that is, an increase in the height of the downcomer will result in a higher liquid velocity, which will in turn lead to a decrease, as in the former case, in the holdup in the riser. In contrast, an increase in A_d/A_r will lead to an increase in the extent of bubble entrapment in the downcomer, which will serve to inject some additional gas into the riser. On the other hand, an increase of gas holdup in the downcomer diminishes the driving force for recirculation, as shown in equation 1, and this will moderate the increase of liquid velocity generated by the larger height. This feedback control of the liquid velocity is one of the characteristics particular to ALRs.

Table 2 shows most of the expressions published for the correlation of experimental data obtained in external-loop ALRs. Some of these expressions are presented in Figure 11. The differences between the predictions obtained with the different correlations are probably due to the design of the gas separator. The equation given by Popovic and Robinson (63) seems to give an average of the proposed correlations.

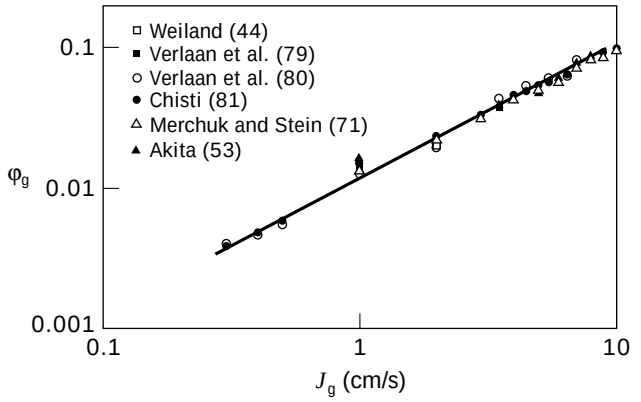

Figure 10. Gas holdup reported by various sources for the riser of airlift reactors under conditions of little or no gas recirculation. The data correspond to different A_d/A_r ratios.

Table 2. Gas Hold-up in External-Loop ALR

No.	Formula	Ref
1	$\varphi_r = \dfrac{0.6\rho_G^{0.062}\rho_l^{0.069}\mu_G^{0.107}}{\mu_l^{0.053}s_l^{0.185}} \cdot \dfrac{J_{Gr}^{0.936}}{(J_{Gr} + J_{lr})^{0.474}}$	84
2	$\varphi_r = 0.16\left(\dfrac{J_G^2}{J_{lr}}\right)^{0.56}\left(1 + \dfrac{A_d}{A_r}\right)$	85
	$\varphi_d = 0.89\varphi r$	
	$\varphi_r = 1.07Fr^{0.333}$	
3	$Fr = \dfrac{J_G^2}{gD_r}$	62
4	$\varphi = 0.55J_{Gr}^{0.78}F^{0.2}D_r^{0.42}$	66
	$F = \dfrac{V_{ls}}{V_l}$	
5	$\varphi_r = 0.203\dfrac{Fr_*^{0.31}}{Mo^{0.012}}\left(\dfrac{J_{Gr}}{J_{lr}} \cdot \dfrac{A_r}{A_d}\right)^{0.74}$	86
	$Mo = \dfrac{g(\rho_l - \rho_G)}{\sigma_l\rho_l^2} \cdot K^4\left(\dfrac{8J_{lr}}{D_r}\right)^{4(n-1)}\left(\dfrac{3n+1}{4n}\right)^{4n}$	
	$Fr_* = \dfrac{(J_{lr} + J_{Gr})^2}{gD_r}$	
6	$\varphi_d = 0.997\varphi_r$	81
7	$\varphi_r = 0.16\left(\dfrac{J_{Gr}}{J_l}\right)^{0.56}\left(1 + \dfrac{A_d}{A_r}\right)$	45

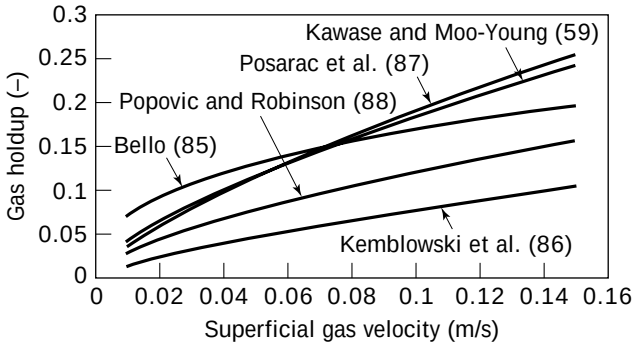

Figure 11. Some correlations proposed for prediction of gas holdup in the riser of external ALRs (Table 2). The gas holdup is presented as a function of the superficial gas velocity.

Effects of Liquid Rheology. The effect of rheology on the reactor behavior and performance is of great interest because in most biotechnological processes an increase in biomass provokes changes in the rheology of the fluid, especially in the case of mycelial growth. This effect is enhanced when in addition to the biomass growth, a product of the process is released into the medium in appreciable amounts. A good example of this scenario is the biosynthesis of polysaccharides, which cause an increase in the liquid viscosity.

The effect of viscosity on gas holdup in bubble columns has been studied by a number of authors. The main problem to be overcome is that of non-Newtonian flow. If the viscosity is not constant, but changes with changes in the shear rate, then the evaluation of shear rates becomes particularly relevant for the identification of the system. Several authors have confronted this issue. Nishikawa et al. (89,90) analyzed the problem of heat transfer in a bubble column with non-Newtonian liquids. They found a direct proportionality between the superficial gas velocity and the global shear rate:

$$\gamma = 5000 \cdot J_G \quad (J_G > 0.04\text{m/s}) \tag{17}$$

This global shear rate was then used to calculate a global viscosity. In shear-sensitive cultures, the definition of a global shear rate in itself is of great importance.

A number of researchers, Henzler (91), Kawase and Moo-Young (59), Schumpe and Deckwer (92,93) have followed the approach of Nishikawa et al. (89) but have suggested different proportionality constants relating the global shear rate to the superficial gas velocity. This approach is questionable from the rheological point of view because it will predict the same shear rate for a certain superficial gas velocity, no matter which liquid is used. El-Tamtamy et al. (94) introduced an improvement by calculating the shear rate from the bubble velocity divided by the bubble diameter. However, accurate evaluation of the latter two parameters is difficult. Henzler and Kauling (95) suggested relating the shear rate to power input based on dimensional analysis by expressing the shear rate as a function of the power input per unit volume, $(P/[V\rho\nu])^{1/2}$. Their analysis gives different shear rates for liquids that are rheologically different.

The above-described relationships predict different shear rates that vary in up to three orders of magnitude. It is thus generally agreed that the correct solution is still to be found. Recently, a more general approach, known as a global approach, has been proposed by Merchuk and Ben-Zvi (Yona) (96). The shear stress in a bubble column was defined as being equal to the acting force, which can be calculated from the power input divided by the sum of the areas of all the bubbles:

$$\tau = \frac{P}{L_R} S_{ab} \tag{18}$$

where L_R is an effective length that represents the mean circulation path of a bubble in the system considered, P is the power input, S_{ab} is the total surface of all of bubbles, and τ is the shear stress.

Assuming ideal gas isothermal expansion, the power input P can be calculated. The interfacial area can be evaluated from correlations or can be obtained by direct measurement if available. A correlation taking into account other variables, like sparger configuration, surface tension, etc., will broaden the range of applications of this approach.

If a constitutive equation describing the rheology of the system is available (such as the power law, which has been reported to correspond to many biological systems), equation 17 facilitates the calculation of a global shear force acting on the liquid. The shear rate can be in this case expressed as:

$$\gamma = \left[\frac{\tau}{k}\right]^{1/n}$$

where γ is shear rate and κ is behavior coefficient, and equation 17 can be now used to express γ as:

$$\gamma = \left[\frac{p_1 J_G \ln\left(\frac{p_1}{p_2}\right)}{aL_R^2\kappa}\right]^{1/n} \tag{19}$$

where the subindexes 1 and 2 represent the two extremes of the section considered.

Equation 19 thus gives a global shear rate that is a function of both fluid dynamics and rheology. This approach has been found to be useful for the presentation of results on mass transfer rates in bubble columns (96).

In contrast to the marked influence of rheology on gas holdup in bubble columns, the data available for ALRs show clearly that the effect of liquid viscosity is less dramatic, but not simpler. Figure 12 (65) illustrates the effect of the addition of glycerol to water in an internal-loop ALR. At low concentrations of glycerol, a moderate increase of the gas holdup is evident, particularly in the downcomer but also in the riser. These increases are caused by the lower free rise velocity of the bubbles, which increase the gas retention due to the longer residence time. In addition, the entrapment of the bubbles is increased, and this is reflected mainly in φ_d. When the concentration of glycerol becomes too high, a strong decrease of the gas holdup is

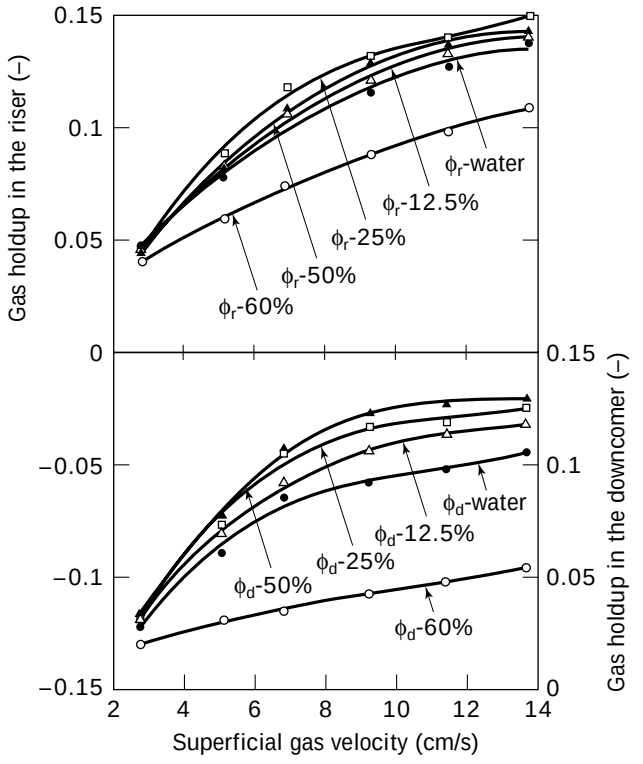

Figure 12. Effect of liquid viscosity on the gas holdup in the riser and in the downcomer of an internal-loop ALR. The viscosity corresponding to the solutions used was 4–14 mPa s. Percentages refer to percent glycerol in water (65).

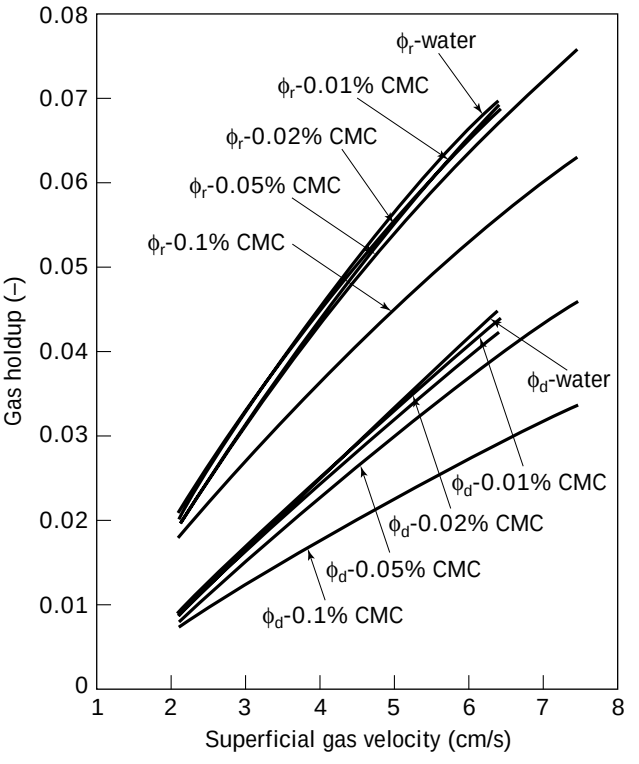

Figure 13. Effect of liquid rheology on the gas holdup in the riser and in the downcomer of an internal-loop ALR with a non-Newtonian liquid. The apparent viscosity corresponding to the solutions used, calculated for $\gamma = 50\ s^{-1}$, was 5–56 mPa s (65).

seen. This decrease is probably due to the onset of coalescence, which produces larger bubbles that ascend faster in the liquid and easily disengage in the gas separator. The viscosities corresponding to these solutions ranged from 4 mPa s to 14 mPa s. In Figure 13, the addition of carboxymethyl cellulose (CMC) to water is shown (65). The change in CMC concentration had only a slight effect on the gas holdup for additions in the range 0.01 to 0.05% CMC. Only for solutions with concentrations higher than 0.5% CMC was an appreciable decrease in holdup seen.

Effect of Liquid Level. The influence of the liquid level C_t on the gas holdup is exerted as a consequence of changes in the extent of disengagement of the bubbles in the gas separator. This influence is therefore dependent on the geometric design of this section. Whether a bubble will disengage or will be entrapped into the downcomer depends on the interrelationship of several parameters—the free rising velocity of the bubble $U_{b\infty}$ (a function of size and viscosity), the liquid velocity in the downcomer U_{Ld} (a function of the difference in gas holdup between the riser and the downcomer and frictional losses), and the residence time of the bubble in the gas separator (a function of geometric design and liquid height). For a given bubble size, if U_{Ld} is smaller than the $U_{b\infty}$ corresponding to the smallest bubble, then there is no carryover. For smaller bubbles, the balance between the time required to cover the path from the end of the riser to the zone near the entrance of the downcomer and the time needed for disengagement will give the fraction of bubbles recirculated. It should nevertheless be kept in mind that this is a feedback process. A higher bubble disengagement rate leads to a lower gas holdup in the downcomer, which in turn increases the liquid velocity, enabling larger bubbles to be trapped, until the system eventually reaches a steady state.

Due to the above-explained influence of the geometric design, the influence of the liquid height is completely different in internal- and external-loop ALRs. In internal-loop reactors, an increase in C_t increases the zone of the separator in which the gas holdup is higher, and as a result, the gas holdup increases. The extent of this increase depends, as said earlier, on the free-rise velocity of the bubbles. Figure 14 (1) shows the gas holdup in the riser and downcomer of a 30-liter ALR for two values of the top clearance, $C_t = 0.178$ m and $C_t = 0.308$ m, for two different liquids, water and a 0.5% CMC solution. It can be seen that although for water C_t has a small effect, this is not so for the more viscous solution. In the latter, the lower rising velocity of the bubbles causes a greater number of bubbles to be entrained and carried down by the liquid. Thus, the residence time in the disengagement section becomes very important in determining the fraction of bubbles that recirculate. A lower C_t will give a shorter residence time in the separator, a larger bubble recirculation, and, hence, a larger gas holdup.

In external-loop ALRs, the opposite effect is obtained, as may be seen in Figure 15 (65). The data in Figure 15,

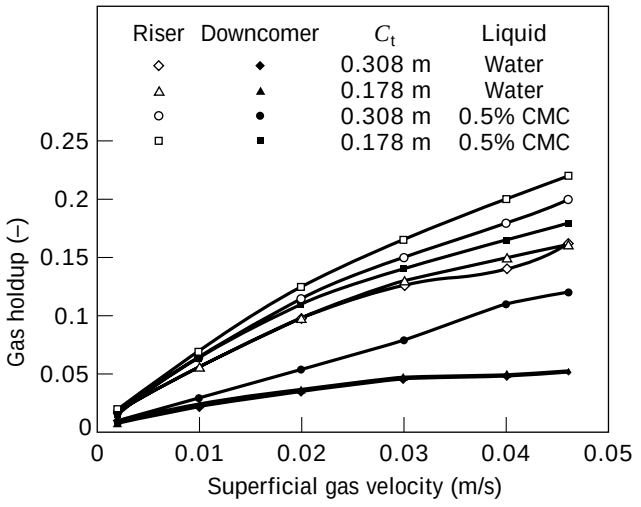

Figure 14. Riser and downcomer gas holdup in an internal-loop ALR for two different top clearances and two liquids. Adapted from Merchuk et al. (1).

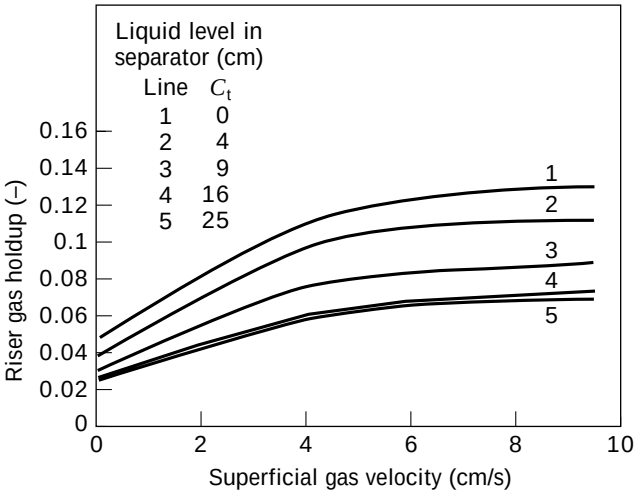

Figure 15. Gas holdup in the riser of an external-loop ALR for several top clearances. Adapted from Hallaile (65).

obtained for a 4-m high external-loop ALR, show that the holdup in the riser decreases as C_t increases. This is due to the construction of these reactors, in which much of the gas that enters into the downcomer is trapped from the headspace due to the turbulence in this zone. An increase in the liquid height serves to reduce the amount of gas trapped, so that less gas circulates in the downcomer and the liquid velocity increases. The final result is a reduction in the gas holdup, both in the riser and the downcomer (65).

Gas Recirculation

The degree to which gas flowing in the riser is entrapped and recirculated through the downcomer is an important variable, since it influences not only the flow configuration in the downcomer, but also the overall performance of the ALR. The liquid velocity depends mainly on the difference in holdup between the riser and the downcomer, and it in turn influences the gas holdup in the riser. Despite the importance of recirculation, very little quantitative data are available on this phenomenon. Siegel et al. (35) evaluated the gas recirculation in a split-vessel ALR by an indirect method based on holdup measurements. From their results, shown in Figure 16, it may be seen that the recirculation rate remains fairly constant for changing gas flow rates in the riser for high values of the last variable. Thus, the recirculation rate is determined largely by the geometric configuration of the gas–liquid separator and the liquid level in the separator.

Three zones are evident in Figure 16; they represent operating conditions giving oscillating, borderline, and straight bubble flow in the downcomer. Oscillating flow patterns produce much larger fractions of gas retained in the downcomer, but they are much more sensitive to J_G. At low superficial gas velocity, the recirculation increases very sharply with J_G. The bubbles exhibit an oscillating swirling flow pattern, with some larger bubbles escaping toward the top. The borderline condition is defined as oscillatory bubble flow at a low gas flow rate that shifts to straight bubble flow with increasing input gas flow rate. The straight flow operation zone is distinguished by bubble flow in a straight, well-defined flow pattern for all the input gas flow rates studied. If a straight bubble flow pattern is desired, the reactor should be operated at high riser gas flow rates, at which the reactor will shift toward stable operation.

Lubbert et al. (97) attempted to evaluate the recirculation of gas during the cultivation of yeast (*Saccharomyces cerevisiae*) on waste from a starch factory in a 4-m^3 pilot plant. They used microprocessor-aided pseudostochastic tracer input and cross-correlation techniques, which facilitated very reduced tracer feeds due to a high signal-to-noise ratio. The response to a pulse of helium was measured directly at the surface of the liquid in the separator by a quadruple mass spectrometer. The peak obtained showed pronounced shoulders (Fig. 17) which could be interpreted as superimposition of a second peak that represents the helium tracer one loop after. The fitting of such

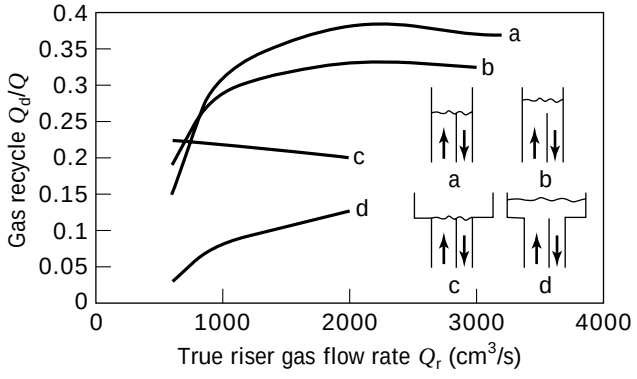

Figure 16. Gas recirculation in a split-cylinder ALR. The level indicated corresponds to no-aeration conditions. Adapted from Siegel et al. (35).

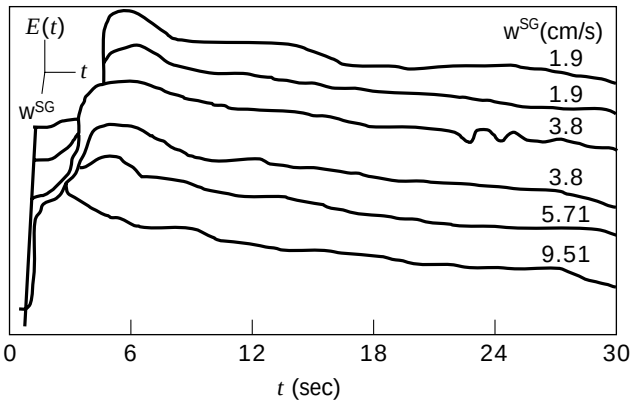

Figure 17. Response to a pulse of helium in an airlift reactor. The pronounced shoulders could be interpreted as the result of superimposing a second peak, which represents the He tracer one loop after. Reprinted with permission from Lubbert et al. (98).

a model to the experimental data suggested recirculation of 25% of the gas. This figure is in the range of the recirculation rates presented by Siegel et al. (35), considering the differences in the coalescing properties of the liquids used in these two works and the corresponding differences in the downcomer holdup.

Recently, Merchuk and Berzin (77) developed a mathematical model based on the application of the first law of the thermodynamics to each of the regions of an ALR. This model facilitates the evaluation of the maximum liquid recirculation possible in the system. The calculation is based on the premise that the gas recirculated must be compressed from the pressure at the top of the downcomer to the pressure at its bottom. The mathematical expression that gives this maximal gas recirculation is:

$$Q_d = \frac{Q_L(P_2 - P_3) + Q_L\rho_L gh - \frac{1}{2}\rho_L C_d A_d(1 - \varphi_d)U_L^3}{P_4 \ln\left(\frac{P_3}{P_2}\right)} \quad (20)$$

where Q_d is the gas flow rate in the downcomer, Q_L is the liquid circulation flow rate, P_i is pressure at point i of the reactor (1 is top of the riser, 2 is top of the downcomer, 3 is bottom of the downcomer, 4 is bottom of the riser), C_d is the hydraulic resistance coefficient, A_d is the downcomer cross-sectional area, U_L is the linear liquid velocity, g is the gravitational acceleration, ρ_L is the liquid density, and φ_d is the downcomer gas holdup.

The calculation of Q_d thus requires knowledge of the liquid flow rate, the pressures, and the geometry of the reactor. This equation represents the maximum recycling of gas in the downcomer, which will take place only if all the energy dissipated in the downcomer is invested in gas compression.

Liquid Velocity

The liquid velocity is one of the most important parameters in the design of ALRs. It affects the gas holdup in the riser and downcomer, the mixing time, the mean residence time of the gas phase, the interfacial area, and the mass and heat transfer coefficients.

Circulation in ALRs is induced by the difference in hydrostatic pressure between the riser and the downcomer as a consequence of a difference in gas holdup. Liquid velocity—like gas holdup—is not an independent variable, because (see Fig. 5) the gas flow rate is the only variable that can be manipulated. As shown in Figure 5, the geometric design of the reactor will also influence the liquid velocity, but this remains constant during operation. Experiments have been carried out in devices specially designed to artificially change the resistance to flow, with the aim of studying the effect of the velocity at a fixed rate of aeration (71,79). The information emerging from these experiments indicates that an increase in the liquid velocity leads to a decrease in the mean residence time of bubbles in the riser and hence of the gas holdup in the riser. In practice, when the gas flow rate is increased, the higher liquid velocity increases the carryover of bubbles from the gas separator into the downcomer; the carryover dampens the liquid flow by reducing the hydrostatic driving force. As a result, the overall change in liquid velocity is tempered.

Liquid Velocity Measurement. Several different methods can be used for measuring the liquid velocity. The most reliable ones are based on the use of tracers in the liquid. If a tracer is injected and two probes are installed in a section of the tube, the velocity of the liquid traveling the distance between probes can be taken directly from the recorded peaks, as the quotient of the distance between the two electrodes and the time required by the tracer to travel from the one to the other. The latter is obtained as the difference of between the first moments of the two peaks. A second method is to calculate the liquid velocity (U_L) from the circulation time (t_c) and holdup (φ) as:

$$U_L = \frac{\text{liquid volume}}{t_c \times A \times (1 - \varphi)} \quad (21)$$

where A is cross-sectional area.

In this case, only one electrode is necessary, φ is the holdup at the point at which the electrode is installed, and the circulation time is obtained from two successive peaks recorded by the electrode.

Modeling of Liquid Flow. A number of expressions are available for the estimation of the liquid velocity. Two main methods have been used for the modeling of two-phase flow in ALRs—energy balances and momentum balances. Chakravarty et al. (58) used the energy balance approach to obtain a relationship between superficial gas velocity, holdup, and liquid velocity. Lee et al. (99) calculated U_L by a similar type of model for a series of published data for concentric and external-loop ALRs and from their own results for split vessels. In both the above-mentioned models, constants accounting for friction losses were obtained by adjusting the models to the experimental data. Jones (100), on the other hand, managed to express the results of his energy balance (based on previous work of Niklin

[101] and Freedman and Davidson [73]) in a relationship free of empirical constants. His results, however, fit the experimental data only qualitatively, and the fit is satisfactory only for very small diameters. An improvement of this method was suggested by Clark and Jones (102), who took into account the radial distribution of the gas holdup through the drift flux model. However, the values of the distribution coefficient C_0 needed for satisfactory fitting of the experimental data for lager diameters is far from the range usual in this type of flow.

Chisti and Moo-Young (103) extended a model originally proposed by Bello (85), based on an energy balance over the airlift loop. Their expression for the average superficial liquid velocity is:

$$U_{Lr} = \left(\frac{2gH_d(\varphi_r - \varphi_d)}{\frac{K_t}{(1-\varphi_r)^2} + K_B\left(\frac{A_r^2}{A_d}\right)\frac{1}{(1-\varphi_d)^2}} \right)^{0.5} \qquad (22)$$

where U_L is the superficial liquid velocity, A_r is the riser cross-sectional area, A_d is the downcomer cross-sectional area, H_d is the downcomer height, K_b and K_t are the hydraulic pressure loss coefficients, φ_r is the riser gas holdup, and φ_d is the downcomer gas holdup.

By choosing suitable values for the friction coefficients in each case, the authors showed that much of the published data on liquid velocity for the different types of ALRs could be satisfactorily correlated by equation 22. Only one coefficient has to be adjusted, since the authors assume that K_t, the friction coefficient at the top of the loop, is negligible in concentric-tube type reactors and that in external-loop reactors K_t can be taken as equal to K_b, the friction coefficient for the bottom of the loop. Equation 22 has thus been adopted by many scientists. Wachi et al. (104) claimed that their derivation of the same equation gives a clearer physical meaning to the adjustable parameters. Equation 22 can also be also derived from a simple momentum balance (77).

Chisti et al. (51) presented an empirical correlation for K_b obtained by comparison of results obtained from several sources:

$$K_b = 11.402 \cdot \left(\frac{A_d}{A_b}\right)^{0.789} \qquad (23)$$

where A_b is the minimal cross section at the bottom of the airlift reactor and A_d is the downcomer cross-sectional area.

Equation 22 has the particularly that the gas flow rate, which is the main, and often the only, manipulable variable in the operation, is not present directly, but exerts its influence through the gas holdup. Therefore, either experimental data or a valid mathematical expression for the gas holdup in both the riser and the downcomer are required.

Chisti and Moo-Young (103) extended this model further in order to facilitate the prediction of liquid circulation in ALRs operating with pseudoplastic fluids, such as mold suspensions. This improvement is very important, since many commercial fermentation processes involve such non-Newtonian liquids. Kemblowski et al. (86) presented a method for the prediction of gas holdup and liquid circulation in external-loop ALRs. In their experiments there was almost no gas recirculation, because of the large size of the gas separators used.

Garcia Calvo (105) presented an ingenious model based on energy balances and on an idea originally proposed by Richardson and Higson (106), and Garcia Calvo and Leton (107) extended the model to bubble columns. The model is based on the assumption that the superficial gas velocity (J_G) in any region can be considered to be the sum of two streams (J' and J'') as follows. The J' stream has a velocity equal to that of the liquid and can therefore be treated by the laws of homogeneous two-phase flow (no slip between the bubbles and the liquid). The second stream (J'') is considered to be responsible for all the energy loses at the gas–liquid interface. The concept in itself is simple and elegant, and it is possible to envisage its application even to the flow in the downcomer, where $U_G < U_L$. In such a case, we would divide the gas flow rate into two parts as follows: One part would be larger than the actual flow rate, i.e., it would have the same velocity as the liquid. In order to arrive at the actual gas flow rate, the second flow rate must have the reverse direction. This type of gas flow can actually be seen under certain conditions, such as when there is coalescence of bubbles and larger bubbles ascend along the walls of the downcomer.

Another technique used by several researchers to predict liquid velocity is the momentum balance of the ALR. This method has been used by Blenke (108) in jet-loop reactors and by Hsu and Dudukovic (109), Kubota et al. (36), Bello (85), Koide et al. (47), and Merchuk and Stein (71). The latter authors presented a simple model for the prediction of the liquid velocity as a function of the gas input in an ALR. They assumed that the pressure drop between the bottom and the top of their external-loop reactor could be expressed as a continuation of the downcomer, using an equivalent length L_E. This length was set as an adjustable parameter describing the pressure loss in the loop. Kubota et al. (36) used a similar approach for the analysis of Imperial Chemical Industries' deep-shaft reactor. They were able to simulate the operation of the reactor and to predict the minimum air supply required to prevent flow reversal.

Verlaan et al. (76) used a similar model, in combination with the expression of Zuber and Findlay (74), to calculate the friction coefficients from experimental data reported by several authors for a wide range of reactor volumes. Koide et al. (47) presented an analysis of the liquid flow in a concentric-tube ARL that was also based on a momentum balance. The main difference between this model and that used by Merchuk and Stein (71) was that Koide et al. used a convergence–divergence flow model for the bottom and the top of the loop. At the bottom, the effect of flow reversal on the pressure drop was included in the effective width of the gas-liquid flow path under the lower end of the draft tube h_l, which was smaller than the actual gap. Miyahara et al. (57), who studied both the bubble size distribution in an internal-loop ALR and the pressure drop at the top and the bottom of the draft tube, also presented a model facilitating the prediction of the liquid velocity.

Other models use the drift-flux model (59) presented in equations 5–7, as:

$$U_{Lr} = \frac{J_{Gr}\left(\frac{1}{\varphi_r} - C_0\right) - U_{GJ}}{C_0(1 - \varphi_r)} \quad (24)$$

U_{GJ} can be taken from equation 10. The range of variation of C_0 is rather narrow, as shown in the previous section, and therefore it is not difficult to make a judicious guess as to the value of C_0 in an unknown system. The drift flux model has also been used together with energy balances (110) or with the momentum balance (111). Some studies on liquid measurement present the results in the form of empirical correlations (42,52,112). The usefulness of these correlations depends on the amount of data and the number of parameters taken into account.

Most of those correlations are shown on Table 3, and some of them are presented in Figure 18. In general, the superficial liquid velocity increases with an increase in the superficial gas velocity, but its rate of increase is much lower at high superficial gas velocities. From Table 3, it can be seen that the riser-to-downcomer cross-sectional area ratio and the reactor height are the main parameters that affect the superficial liquid velocity at constant superficial gas velocity. The superficial liquid velocity increases with an increase in A_d/A_r.

The effect of the properties of the liquid, such as viscosity, surface tension, and ionic strength, on the superficial liquid velocity are much milder in ALR than in bubble columns (113). It is expected that increasing the liquid viscosity will decrease the liquid velocity because of frictional losses, but this, in turn, will increase the gas holdup in the riser and consequently increase the driving force for liquid recirculation. Hence, it seems that these two effects balance each other partially and result in a milder effect on the superficial liquid velocity. The effects of the surface tension and the ionic strength are also exerted via their influence on the gas holdup, as analyzed above.

As a rule, it can be recommended that the Zuber-Findlay expression (equation 20) be used when the holdup is known and the liquid circulation velocity is high. For low liquid velocity, a correlation obtained in a piece of equipment as similar as possible to the one under design should be used.

Table 3. Liquid Circulation Velocity in ALRs

No.		Formula	Ref.
1	ELR	$J_{Lr} = 1.55 J_{Gr}^{0.33}\left(\frac{A_d}{A_r}\right)^{0.74}$	45
	ILR	$J_{Lr} = 0.66 J_{Gr}^{0.33}\left(\frac{A_d}{A_r}\right)^{0.78}$	
2	Bubbly	$J_{Lr} = 0.024 J_{Gr}^{0.322}\left(\frac{A_d}{A_r}\right)^{0.794} \mu_{ap}^{-0.395}$	50
	Slug flow	$J_{Lr} = 0.052 J_{Gr}^{0.322}\left(\frac{A_d}{A_r}\right)^{0.794} \mu_{ap}^{-0.395}$	
3	Slug flow	$J_{Lr} = 0.23 J_{Gr}^{0.322}\left(\frac{A_d}{A_r}\right)^{0.97} \mu_{ap}^{-0.39}$	63
4		$J_{Lr} = 2.858 J_{Gr}^{0.482}\left(\frac{A_d}{A_r}\right)^{0.97} 416\mu_{ap}^{-0.0105}$	52
5		$J_{Lr} = \left[\frac{2gH_d(\varphi_r - \varphi_d)}{K_b\left(\frac{1}{(1-\varphi_r)^2} + \left(\frac{A_d}{A_r}\right)^2 \frac{1}{(1-\varphi_d)^2}\right)}\right]^{0.5}$	103
		$K_b = 11.4\left(\frac{A_d}{A_r}\right)^{0.79}$	

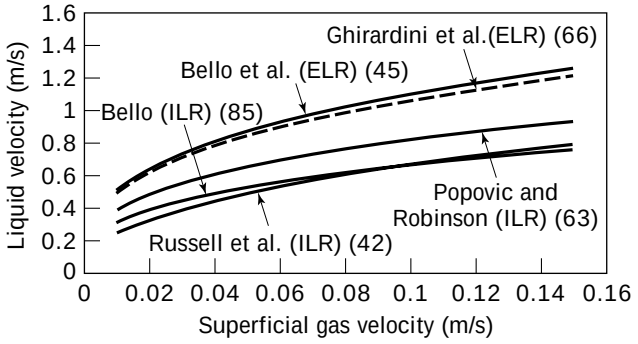

Figure 18. Liquid velocity predicted by some of the proposed correlations from Table 3. ILR, internal-loop ALR; ELR, external-loop ALR.

Liquid Mixing

For the design, modeling, and operation of ALRs, a thorough knowledge of mixing behavior is necessary. This is of particular importance during the process of scale-up from laboratory-scale to industrial-scale reactors. The optimum growth rate of a microorganism or the optimum production rate of a specific secondary metabolite usually relates to well-defined environmental conditions, such as pH range, temperature, substrate level, limiting factors, dissolved oxygen, and inhibitor concentration in a specific well-mixed laboratory-scale vessel. Because of the compromises made during scale-up, it is difficult to keep, at different scales of operation, the same hydrodynamic conditions established in the laboratory; mixing on an industrial scale may not be as good as mixing on a laboratory scale (5). In smaller-scale reactors it is easier to maintain the optimal conditions of pH, temperature, and substrate concentration required for maximum productivity of metabolites in a fermenter.

Furthermore, in fermentation systems efficient mixing is required to keep the pH within the limited range, giving maximum growth rates or maximum production of the microorganism during addition of acid or alkali for pH control. Mixing time—or the degree of homogeneity—is also very important in fed-batch fermentation, where a required component, supplied either continuously or intermittently, inhibits the microorganisms or must be kept within a particular concentration range (114,115). A large number of commercially important biological systems are operated in batch or fed-batch mode. In this operation mode, fast distribution of the incoming fluid is required, and the necessity for understanding the dynamics of mixing behavior in these vessels is obvious. Even for batch systems, good control of the operating conditions, such as pH, temperature, and dissolved oxygen, require prior es-

timation of mixing so that the addition rates can be suitably adjusted. Deviation of the pH or temperature from the permitted range may cause a damage to the microorganism, in addition to its effect on the growth and production rates. Moreover, a knowledge of the mixing characteristics is required for modeling and interpreting mass and heat transfer data.

A parameter used frequently to represent mixing in reactors is the mixing time (t_m). It has the disadvantage that it is specific to the reactor design and scale, but it is easy to measure and understand. Mixing time is defined as the time required to achieve the desired degree of homogeneity (usually 90–95%) after the injection of an inert tracer pulse into the reactor. The so-called degree of homogeneity (I), is given by:

$$I = \frac{C - C_m}{C_m} \tag{25}$$

where C is the maximum local concentration and C_m is the mean concentration of tracer at complete mixing.

A more comprehensive way of analyzing mixing, applicable to continuous systems, is a study of the residence time distribution (RTD). Although ALRs are usually operated in a batch-wise manner, at least in the laboratory, advantage is taken of the fact that the liquid circulates on a definite path to characterize the mixing in the reactor. Hence, a single-pass RTD through the whole reactor or through a specific section is usually measured. Based on the observed RTD, several models have been proposed. These models have the advantage of reducing the information of the RTD to a small number of parameters, which can later be used in design and scale-up.

The axial dispersion model, which has the advantage of having a single parameter, is widely accepted for the representation of tower reactors. This model is based on visualization of the mixing process in the tower reactor as a random, diffusion-like eddy movement superimposed on a plug flow. The axial dispersion coefficient D_z is the only parameter in the formulation:

$$\frac{\partial C}{\partial \tau} = D_z \frac{\partial^2 C}{\partial z^2} + U_L \frac{\partial C}{\partial z} \tag{26}$$

where C is the concentration of a tracer. The boundary conditions depend on the specific type of tower reactor. This model is attractive, since it has a single parameter, the Bodenstein number (Bo), which is used to describe the mixing in the reactor:

$$Bo = \frac{U_L L}{D_z} \tag{27}$$

where L is the characteristic length. When the Bo number tends to infinity, the mixing conditions are similar to those of a plug-flow reactor, and the reactor can be considered as well-mixed for low Bo numbers.

The alternative approach of Buffham and Mason states that the mixing characteristics of a piece of equipment should be expressed as the variance σ^2 of the distribution obtained by injection of a pulse of tracer without adopting any mechanistic model (116). The relationship between Bo and σ^2 depends on the reactor configuration (117). The approach of Buffham and Mason facilitates the presentation of mixing characteristics free of any modeling assumptions. The variance σ^2 is the second moment of the distribution and carries information on the spread of the distribution around the mean value (first moment). Nevertheless, most of the data on mixing in bioreactors are presented either as t_m or as overall Bo numbers, which can be obtained by relatively simple experiments of pulse injection.

Single-pass mixing in the ALR is due to mixing in the individual and interrelated sections of the reactor—riser, separator, downcomer, and bottom. Repeated passage mixing is the sum of the mixing in the subsequent passages. The latter is usually reported as the mixing time (t_m), the former as Bo or σ^2. Indeed, these parameters are interrelated, and knowledge of Bo or t_m is sufficient for calculating, theoretically, the mixing time (108,118) based on the deviation of the envelope of the maxima in the response curve to a pulse, which is a measure of the degree of inhomogeneity. Verlaan et al. (80) and Lin et al. (119) correlated their results as follows:

$$t_m = MBo \tag{28}$$

where M is a constant equal to 0.093 (80) or to 0.089 (119). The coefficient M given by Verlaan et al. is in exact agreement with the theoretical relationship derived by Murakami et al. (118) for $Bo > 50$ and a degree of inhomogeneity, $I = 0.05$.

Equation 28 shows that the circulation path, which enters in the definition of Bo, has a linear effect on the mixing time. If the mean circulation time and the axial dispersion coefficients are known, it is possible to theoretically estimate the mixing time using equation 28. Experimental details must, however, be carefully planned to avoid complications. Note that in order to simplify data processing it is important to inject the signal and to measure the response at exactly the same point (120) (often the position of the injection point is not specified despite its effect on the mixing time). In a study of the effect of the injection point on the dynamics of the mixing time, Schügerl et al. (12) concluded that the gas–liquid separator is the best choice for tracer injection for short mixing times. Fields and Slater (114) reported a marked dependence of the respiratory quotients upon the injection point of methanol during unlimited fed-batch growth of *Methylophilus methylotropus* in a concentric-tube ALR. The lines in Figure 19 show experimental data for Bo (as overall values) reported for different types of ALR (in which the reactor is considered as a single unit). The dimensions of the reactors are given in Table 4. Because of the definition of the overall Bo, the values are specific to the reactor for which they were obtained and can be used only as indication of trends and orders of magnitude.

As explained above, the ALR is, in fact, a combination of several regions having quite different fluid dynamic characteristics. The overall mixing is the result of the contributions of each of them, and the overall Bo represents

Table 4. Bodenstein Number as a Function of the Superficial Gas Velocity (Key for Fig. 19)

Curve number	Authors	Type	A_d/A_r	H/D_r	Liquid	Ref.
1	Weiland	External loop	0.25	85	Water	44
2	Weiland	External loop	0.25	85	2-propanol 1.65%	44
3	Weiland	External loop	0.25	85	CMC 50%	44
4	Lin et al.	External loop, unbaffled	0.11	20	Water	119
5	Lin et al.	External loop, baffled	0.11	20	Water	119
6	Lin et al.	External loop, unbaffled	0.11	40	Water	119
7	Bello et al.	External loop	0.69	12	Water	45
8	Bello et al.	External loop	0.69	12	Water	45
9	Bello et al.	External loop	0.11	20	Water	45
10	Moor Nagar	External loop	1.0	30	Water	122
11	Fields and Slater	Concentric tube	1.56	10.5	Water	114
12	Fields and Slater	Concentric tube	1.56	21	Water	114
13	Fields and Slater	Concentric tube	1.56	10.5	Water, antifoam	114
14	Fields and Slater	Concentric tube	1.56	10.5	1% Ethanol	114
15	Bello et al.	Concentric tube	0.13	39.65	Water	112
16	Bello et al.	Concentric tube	0.56	55.6	Water	112
17	Verlaan et al.	External loop, total *Bo* number	0.25	16.5	50 mM KCl aqueous solution	79
18	Verlaan et al.	*Bo* number in the riser	0.25	16.5	50 mM KCl aqueous solution	79
19	Verlaan et al.	*Bo* number in the downcomer	0.25	16.5	50 mM KCl aqueous solution	79
20	Verlaan et al.	External loop, total *Bo* number	0.25	16.5	50 mM KCl aqueous solution	79

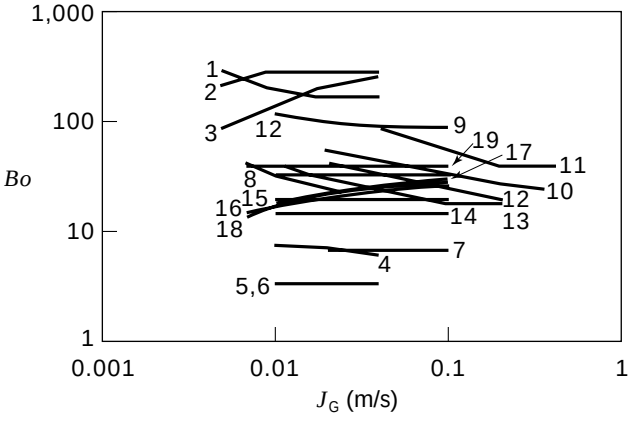

Figure 19. Global Bodenstein numbers reported for ALRs as a whole unit. See references in Table 4.

this combination for a particular reactor. This value thus has some limitations for extrapolation to other configurations or scales. Because each section has different mixing characteristics (it may have a different cross-section, flow configuration, etc.), from a strictly engineering point of view, the mixing in each of the sections of the ALR should be defined and considered separately.

One way of obtaining information on the mixing characteristics of each of the regions of the ALR is the simultaneous measurement of the response in the ALR at several points, so that after one single pulse injection the response of each section in the loop can be obtained (37,80). This method of measurement has the advantage that multiple measurements are made for the same tracer injection experiment. This enables us to check the consistency of the liquid velocity results obtained, since independent measurements can obtained in the same run, as can be seen in Figure 20.

The results for *Bo* obtained by Verlaan (80) in an external-loop ALR are shown in Figure 21 (the much higher *Bo* in the downcomer was explained by the fact that the data were obtained under conditions of complete gas disengagement so that only liquid flowed). The results indicated that most of the mixing took place in the gas separator, and both riser and downcomer could be considered as plug-flow conduits. The same conclusions were drawn for internal-loop ALRs by Merchuk et al. (37) by analysis of mixing times: the shift in results for mixing times obtained with different probes in response to the same impulse perturbation indicated that the riser and the downcomer were introducing a pure delay in the response, that is, that they behaved as plug-flow sections.

Indeed, the simplest model of an ALR, from the point of view of fluid dynamics, is a combination of two plug-flow reactors, representing the riser and the downcomer, and a perfectly stirred tank, representing the gas separator (Fig. 22) (67,123). Merchuk and Yunger (67) showed that this simple model could take into account the mixing in the ALR. The validity of using this simple model as a first approximation is supported by experimental evidence that shows that the mixing time decreases when the separator volume increases (31,124). When the volume of the separator is increased substantially without changing the reactor diameter, the gas separator becomes tall and slender and may depart from total mixing behavior. It has been reported that under such conditions the circulation time measured from two successive peaks of a probe is not influenced by changes in the top clearance (42,43). This indicates that the gas separator acts as two interconnected well-mixed regions, one of them (the lower one in Figure 23) being the link between riser and downcomer, as shown schematically in Figure 23.

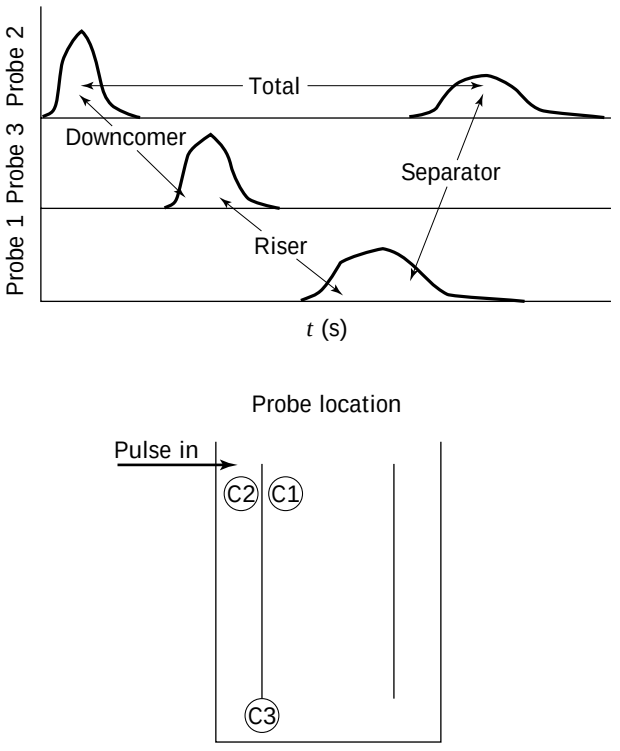

Figure 20. Response of three electrodes in the riser, separator, and downcomer to a pulse of electrolyte. The information that can be obtained from a single experiment is indicated by the *arrows*. From Merchuk et al. (37).

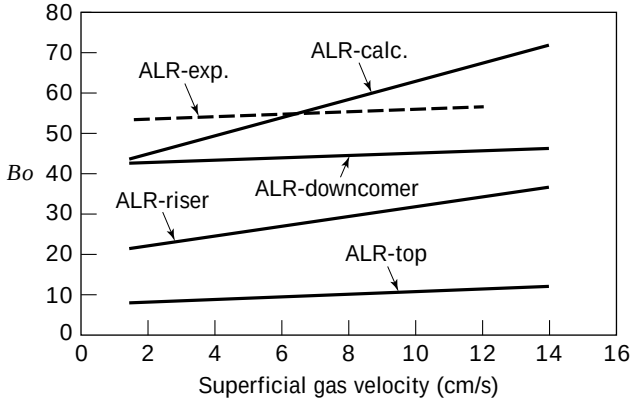

Figure 21. Bodenstein numbers as a function of the superficial gas velocity in an external-loop ALR. ALR-exp, experimental values for the whole reactor; ALR-calc, calculated values for the whole reactor. Adapted from Vorlaan et al. (80).

The extent of mixing in the gas separator of internal-loop ALRs can probably be compared to that in a bubble column of the same dimensions. In the case of external-loop ALRs, the extent of mixing depends on the geometric design. In special designs, like the channel-loop reactor (125), a different approach must be taken. However, in general, a rule of thumb may be recommended: consider that all the mixing takes place in the gas separator, and calculate the degree of mixing in it using published data for bubble columns. Correlations available for bubble columns can thus be used. Godboole and Shah (126) recommend the use of the correlation proposed by Deckwer et al. (127):

$$D_Z = 0.678 \cdot D^{1.4} \cdot J_G^{0.3} \tag{29}$$

where D_Z is the dispersion coefficient and D is the column diameter, or the relationship proposed by Joshi (128):

$$D_Z = 0.33(U_c + J_L)D \tag{30}$$

where J_L is the superficial liquid velocity and U_c is the cell circulation velocity given by:

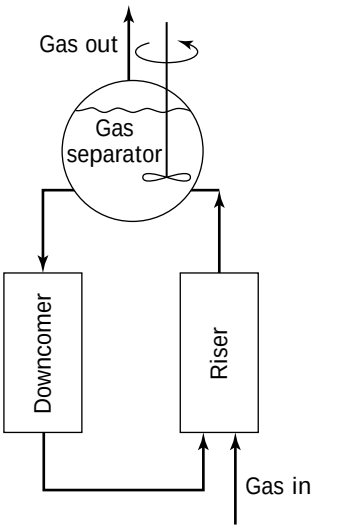

Figure 22. Simple model of an ALR representing the riser and the downcomer as plug-flow reactors and the gas separator as a perfectly mixed region. From Merchuk and Siegel (67).

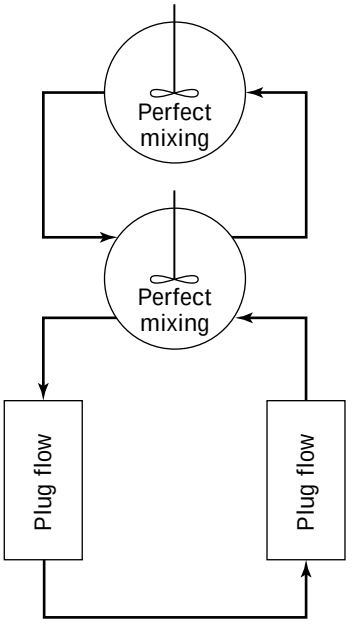

Figure 23. Schematic representation of the effect of a tall slender gas separation region in a concentric-tube ALR.

$$U_C = 1.31\left[gD\left(J_G - \frac{\varphi_G}{1 - \varphi_G} J_L - \varphi_G U_{b\infty}\right)\right] \quad (31)$$

where $U_{b\infty}$ is the terminal bubble velocity.

The liquid superficial velocity (J_L) can be easily calculated for external-loop reactors, and for internal loop reactors, J_L may be taken as half the liquid velocity in the riser. The viscosity may also play a role in the rate of mixing. An increase in liquid viscosity will increase the energy dissipation in the loop and result in an increase in mixing time and *Bo*. In non-Newtonian fluids, however, the behavior may be different, as shown in Figure 24. It has been reported that in the case of the addition of polymers that confer pseudoplastic behavior to the liquid, low concentrations produce a decrease of the mixing time (65,129). This can be explained in terms of the drag reduction due to the presence of polymers in the boundary layer near the walls. Fields et al. (129) found that the mixing time increased for concentrations of the natural polymer, xanthan gum, above the critical concentration. (The critical concentration is a theoretically calculated value at which appreciable overlapping of polymer molecules occurs and which marks the onset of a rapid increase of the apparent viscosity [130]).

Mixing in the Gas Phase

For all practical purposes, the gas in the riser of an ALR exhibits plug flow behavior. Only for extremely high J_G or hindered liquid circulation will the axial dispersion of the bubbles have some effect on the gas RTD. In the downcomer, the gas flow is almost plug-flow when the bubble recirculation is fully developed. But at the stage at which a stationary phase of suspended bubbles appears at the top of the downcomer, appreciable dispersion will occur. This zone has a large degree of mixing due to coalescence and consequent rise of larger bubbles amid smaller ones, with repeated events of breakup and coalescence. However, this type of operation has no relevance to practical applications. It is an operation mode to be avoided at all costs. Indeed, no data on mixing under these conditions have been reported. The main question related to the mixing of the gas phase is, in fact, related to gas recirculation. When a particular gas flow has developed in the downcomer, part of the gas is being recirculated (see "Liquid Velocity"). A pulse of gas tracer at the inlet would produce, as a response, a series of pulses, separated one from the other by the gas circulation time. In practice, not many of these pulses would be detected, due to dilution and disengagement of the tracer in each pass through the separator.

The only reported study on gas phase mixing in an ALR is that of Frehlich et al. (131). The distribution of the gas residence times in two reactors, one of 0.08 m^3 and the other of 4 m^3, was measured using pseudostochastic tracer signals and a mass spectrometer. The values of *Bo* were calculated from the first and second peaks, indicating the main gas stream and the recirculation. Figure 25 shows the *Bo* obtained for a laboratory-scale ALR. The values obtained in a pilot plant were of the same order.

Energy Dissipation and Shear Rate in Airlift Reactors

ALRs are being increasingly used in processes involving shear-sensitive cells (mammalian, insect, and plant cell cultures) (3,11,14,18,21,28,29). This situation has created the need for considering shear stress as one of the parameters relevant in the design of such reactors. Although the a priori evaluation of shear rates is a matter that has been studied for many years in stirred tanks, information on this subject is scanty for pneumatically stirred reactors. The first approach made in this direction in pneumatically agitated vessels was that of Nishikawa et al. (70), who were interested in the problem of heat transfer to a non-Newtonian liquid in a bubble column. This study was extended to mass transfer by Nakanoh and Yoshida (132), who proposed the expression:

$$\gamma = 5000\ J_G \quad (32)$$

This expression has been widely accepted despite the criticism sometimes leveled at it (62,68,123,133). Some modifications have thus been proposed (92,95,134), which, like the original approach, were based on data for bubble

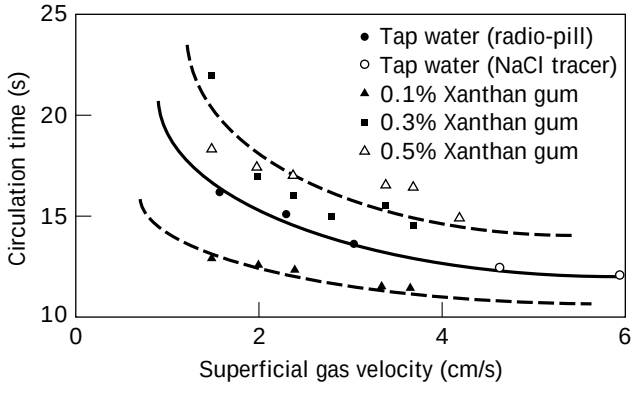

Figure 24. Variation of mean circulation times with J_G for several solutions. Adapted with permission from Fields and Slater (129).

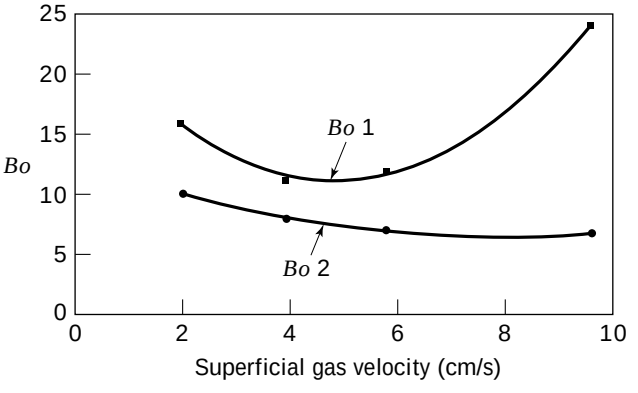

Figure 25. Bodenstein numbers of the first and second peaks of the gas residence time distribution in an 80-L internal-loop ALR, as a function of the gas superficial velocity. From Frehlich et al. (131).

column performance and therefore have limited application for ALRs. Recently, a method facilitating the prediction of the distribution of the energy dissipated in an ALR, based on a simple thermodynamic approach, has been developed (77). Energy dissipation was considered to occur in the ALR by two main mechanisms, wall friction and bubble-associated dissipation (ideal gas behavior was assumed). The work done by the gas on the liquid (and vice versa) was expressed assuming isothermal expansion of the bubbles. The energy dissipation inside the gas phase was considered negligible. The general energy balance (135) was written as:

$$\Delta(PQ) + \Delta E_p + E_D = W_S \tag{33}$$

In this equation, the first term represents the flow work lost by the system under consideration, E_D is the energy dissipated per unit of time, and W_S is the shaft work done by the surroundings on the system under consideration. The schematic representation of the concentric-tube ALR in Figure 26 indicates the different points in the reactor considered in the mathematical expressions. The expressions found for the energy dissipated in each zone were the following:

Riser

$$(E_d)_R = Q_L(P_4 - P_5) - Q_L\rho_L gh - Q_r P_4 \ln\left(\frac{P_5}{P_4}\right) \tag{34}$$

Gas separator

$$(E_d)_S = Q_L(P_5 - P_2) - Q_{in}P_4 \ln\left(\frac{P_1}{P_5}\right) - Q_d P_4 \ln\left(\frac{P_2}{P_5}\right) \tag{35}$$

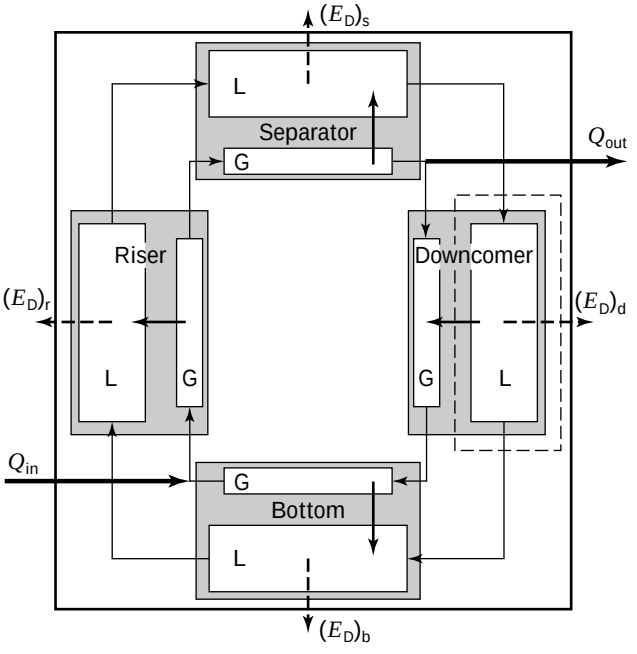

Figure 26. Schematic description of the variables in the thermodynamic model for energy dissipation distribution in an ALR. From Merchuk and Berzin (77).

Downcomer

$$(E_d)_d = Q_L(P_2 - P_3) - Q_L\rho_L gh - Q_d P_4 \ln\left(\frac{P_3}{P_2}\right) \tag{36}$$

Bottom

$$(E_d)_b = Q_L(P_3 - P_4) - Q_d P_4 \ln\left(\frac{P_4}{P_3}\right) \tag{37}$$

Results of this model of an ALR can also be used to estimate the global shear rate in each region of the reactor, according to the global approach presented Merchuk and Ben-Zvi (Yona) (96). The shear stress in the liquid of each region of the reactor can be defined as the energy dissipated divided by the mean path of circulation in the region and by the sum of the areas of all the bubbles. For the region i in the ALR

$$\tau_i = \frac{(E_d)_{bulk,i}t_i}{a_i h_i^2 A_i} \tag{38}$$

where t_i is the residence time of the liquid, h_i is the effective length, and a_i is the specific interfacial area, in the region i.

A global shear rate γ_i can be calculated for each region i as

$$\gamma_i = \frac{\tau_i}{\mu} \tag{39}$$

where μ is the effective viscosity of the fluid.

For liquids exhibiting different types of rheological behavior, the corresponding constitutive equation must be used. Such an approach has been used for the interpretation of shear effects on mammalian cells (136) and algal growth (43).

MASS TRANSFER

The volumetric mass transfer coefficient ($k_L a$) is the rate of gas transfer across the gas-liquid interface per unit of driving force (the driving force is the gas concentration gradient between the liquid and the gas). The mass transfer coefficient $k_L a$ can be seen as the product of two terms: the mass transfer coefficient k_L and the specific interfacial area a. Both terms depend on a series of variables that can be grouped into three categories: (*1*) static properties of the liquid, such a density, diffusivity, and surface tension; (*2*) dynamic properties of the liquid (related to liquid flow), such as rheological parameters; and (*3*) liquid dynamics. In general, the variables in group 1 do not change very drastically. The variables in groups 2 and 3, however, may span wide ranges.

Mass Transfer Rate Measurements

Methods for the determination of $k_L a$ in a reactor can be grossly classified as steady-state and nonsteady-state methods. In the steady-state methods, the rates of oxygen uptake in steady-state operation are evaluated, either by measurement of inlet and outlet rates of oxygen or by di-

rect analysis of a compound that reacts with the oxygen, as in the case of the sulfite method. One of the problems associated with these procedures is that the changes in oxygen concentration in the gas streams are usually small, and the errors of measurement thus have a substantial influence. When a chemical is added to the system, there is the question of whether the addition has provoked changes in the physicochemical properties, which thus become different from the properties of the original system.

Transient methods may be applied to follow the response of the dissolved oxygen concentration in the system after a step-change of oxygen concentration in the inlet gas stream. These methods have the advantage that addition of an alien material is not required and that a single concentration is measured. The correct use of this method has been analyzed in depth by Linek et al. (137).

One important point to take into account is the dynamics of the oxygen electrode. The lag in the response of the oxygen electrode makes it necessary to discern between the electrode response and the real oxygen concentration, especially when close to a sharp change in concentration. A correct analysis should also include the model of the dynamic behavior of the electrode. In order to simplify these procedures, approximations based on truncation of parts of the response curve have been proposed (133,138). These methods are based on truncating the first part of the electrode response obtained in a transient experiment. Once the error included in the value of k_La is set, the extent of truncation is fixed, allowing simplification of the analysis of the remainder of the curve. It should be kept in mind that this simplification implies the loss of part of the information, and due care should be given to statistical analysis of the results.

Variations of the method have been proposed to minimize disturbances in the system by introduction of step variations of agitation or pressure (137,139). In this way, the method can be applied to bioreactors during real operation of the system.

One problem that may appear in the measurement of mass transfer rates, especially when viscous liquids are used, is related to the presence of very small bubbles that are depleted of oxygen very rapidly but do not disengage in the gas separator, thus constituting an inert volume of gas in the reactor (134). Kawase and Moo-Young (140) analyzed the use of transient absorption of CO_2 for the determination of k_La and concluded that the error due to small bubble retention was much smaller than that in the case of O_2.

Whatever the method used for the determination of k_La, the process of data elaboration is basically the same as is shown schematically in Figure 27 (141). The measured variable (usually oxygen concentration) is compared to the value predicted by a mathematical model of the process. The model includes k_La as a parameter, and the value of k_La that gives the best fit is chosen. It is thus obvious that the choice of the model is very important, and poor assumptions on flow characteristics of gas or liquid phases may lead to errors and deviations from the true values (142). All the models are a simplified (amenable to mathematical treatment) description of the system. It should be kept in mind, therefore, that k_La is not a property of the

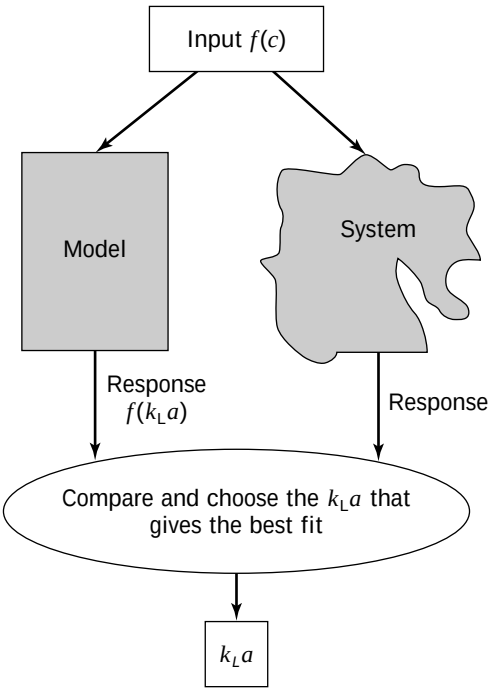

Figure 27. Steps in the determination of the mass transfer coefficient (k_La). From Merchuk et al. (141).

system, but a parameter of the model adopted. If total mixing is assumed in the model adopted, the mass transfer coefficient obtained will consequently be limited. The assumption of complete mixing is such a common practice that many reports do not even specify explicitly that this has been done, and in many texts the mass transfer coefficient k_La is defined by the equation:

$$\text{OTR} = k_1a(C^* - C) \tag{40}$$

It is often forgotten to state that this equation is valid only for perfectly mixed systems.

Strictly, the different sections of ALRs (riser, downcomer, and gas separator) have different flow characteristics, and the mass transfer coefficient may be expected to differ from one region to another. Some researchers (108) have assumed that the contribution of the downcomer to the overall mass transfer is negligible and have reported values of k_La that are, in fact, the entire mass transfer divided by the volume of the riser. The fact that the values of the mass transfer coefficient are calculated and reported in different ways introduces some ambiguity into the published data; special care should therefore be taken when comparing data or using published mass transfer coefficients for design purposes.

The assumption of perfect mixing in the liquid phase may be questionable in the case of tall reactors. One very simple method to verify this assumption is the simultaneous measurement of the response of the concentration to a step-change in the inlet. In a perfectly mixed system, the location of the probe should be irrelevant. Figure 28 (143) shows the response of three probes, one located at

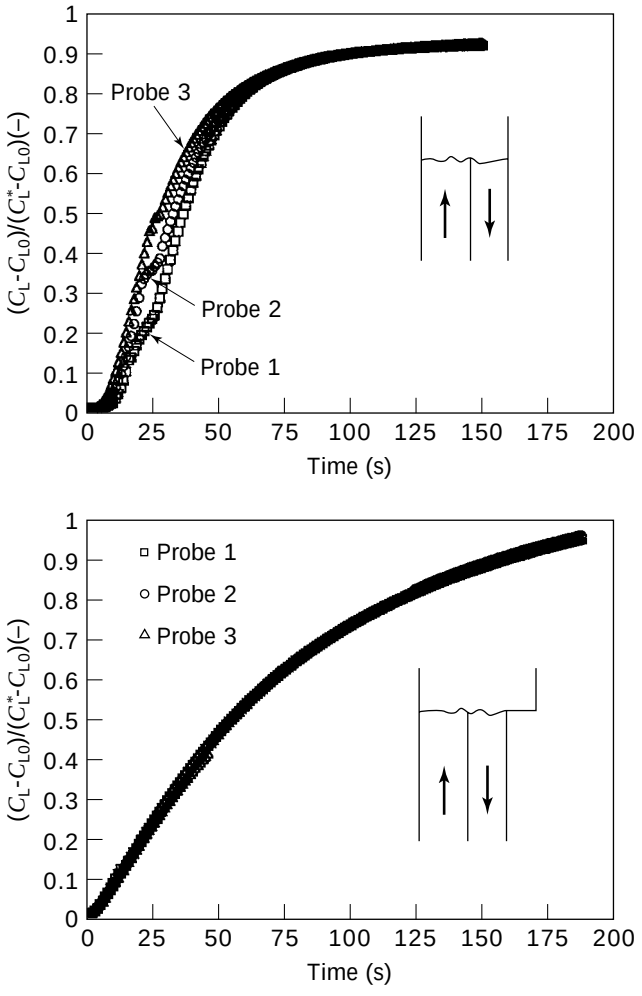

Figure 28. Response of three probes, one located at the end of the riser, one at the inlet of the downcomer, and one at the bottom of a split-cylinder ALR. From Siegel et al. (143).

the end of the riser, one at the inlet of the downcomer, and one at the bottom of a split-cylinder ALR. The difference between the figures stems from a different gas separator section, which changes the fluid dynamics in the system. In one case the system behaved as perfectly mixed, because of the large volume of the gas separator and the faster liquid circulation. In the other (closed system in the figure), the responses of the three electrodes were clearly different, calling for a different analysis. The validity of the criterion, originally proposed by Andre et al. (144), that compares the circulation time in the reactor (t_c) with the characteristic time for mass transfer, which is the inverse of the mass transfer coefficient, was thus confirmed (143):

$$t_c \cdot k_L a < 0.5 \tag{41}$$

If this condition is not fulfilled, the bioreactor cannot be considered as a perfectly mixed volume, and more sophisticated ways of analysis are required. In this case, the mathematical model, and, consequently, the analysis of the experimental data become much more complicated. Nevertheless, this approach has been used (48,122,145,146), and the mass transfer experiments render values of $k_L a$ for each of the regions of the ALR. Figure 29 shows the results reported by Hwang and Lu (146) in an internal-loop ALR. The graph shows that the mass transfer takes place at the highest rate in the riser. Values for the downcomer are 50% lower, and those for the gas separator are intermediate between the riser and the downcomer. The overall mass transfer rate is the result of the balance between the volumes and rates in the three sections.

Bubble Size and Interfacial Area

As said earlier, the interfacial area per unit volume is an important component of the volumetric mass transfer coefficient. In fact, it is the part of $k_L a$ that is most susceptible to changes in operation variables and fluid properties. The mass transfer coefficient k_L varies only within a limited range (147), but the interfacial area is the main component responsible for the changes in mass transfer rate due to variations in turbulence, initial bubble size, and liquid properties.

The methods for measurement of the interfacial area are based either on rapid chemical reactions or on direct measurement of bubble size. If a mean bubble size can be defined, then the interfacial area can be evaluated with the aid of the holdup measurement, since, in a population of homogeneous bubble size, it can be applied:

$$a = \frac{6\varphi}{d_s} \tag{42}$$

where the Sauter mean diameter (d_S) is given by

$$d_S = \frac{\sum n_i d_i^3}{\sum n_i d_i^2} \tag{43}$$

and n_i is the number of bubbles of diameter d_i

There are very few published data on bubble size applicable to ALRs. For the riser, the correlation presented by Miyahara et al. (57) for the volumetric mean diameter

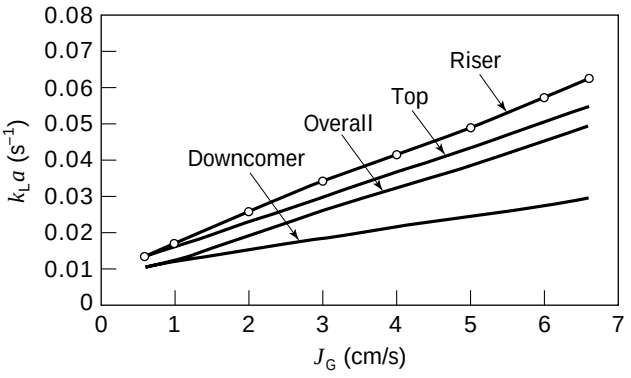

Figure 29. Influence of the superficial gas velocity on overall $k_L a$ and on the $k_L a$ in each of the regions of an ALR. Adapted from Hwang and Lu (146).

of the bubbles in the riser of a concentric-tube ALR can be used:

$$\bar{d}\left(\frac{g\rho_L}{\sigma d_0}\right)^{1/3} = f(N_W) \quad (44)$$

where d_0 is the diameter of the sparger orifice and σ the surface tension,

$$N_W = \frac{We}{Fr^{0.5}} \quad (45)$$

and the function $f(N_W)$ is different for each range of N_W:

$$\begin{aligned} f(N_W) &= 2.9 & N_W &< 1 \\ f(N_W) &= 2.9N_W^{-0.188} & 1 &< N_W < 2 \\ f(N_W) &= 2.9N_W^{-0.5} & 2 &< N_W < 4 \\ f(N_W) &= 3.6 & 4 &< N_W \end{aligned} \quad (46)$$

Data on bubble size in the downcomer of an ALR were published by Popovic and Robinson (63). No data on interfacial area measured by chemical methods have been published.

Data Correlations for Mass Transfer Rate

There are two ways of correlating experimental data from ALRs. First, the hydrodynamic point of view suggests that the movement of the fluid in the reactor determines its overall behavior; the gas superficial velocity is therefore the more appropriate independent variable. Second, the thermodynamic point of view is based on a consideration of energy balance, a more global approach to the system. This will lead to correlation of the phenomena in the system as a function of the energy input. Indeed, it is easier to compare mass transfer coefficients in ALRs with those in conventional reactors when the data are presented as a function of the total power input (both mechanical and pneumatic) per unit volume of the medium (34) (Fig. 30).

Figure 31 shows data for mass transfer coefficients as a function of specific power input (149). References and geometric characteristics can be seen in Table 5.

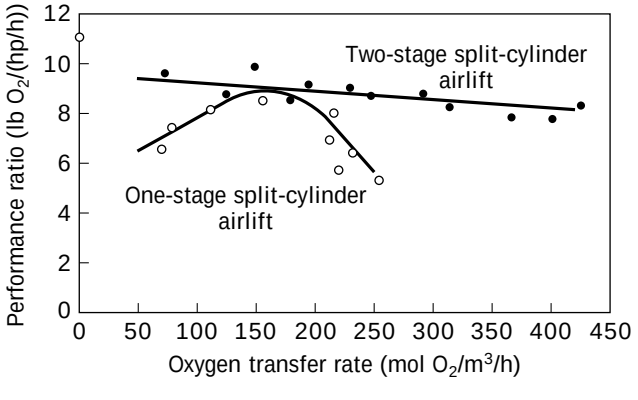

Figure 30. Performance of ALRs. Adapted from Orazem and Erickson (148).

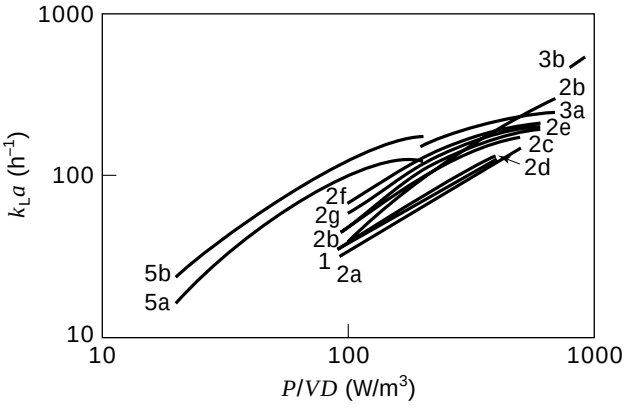

Figure 31. Mass transfer coefficients as a function of specific power input. With permission from Siegel et al. (123). See Table 5.

Selected of correlations proposed for the prediction of mass transfer coefficients are shown in Tables 6 and 7 for internal- and external-loop ALRs, respectively, and the predictions are compared in Figures 32 and 33. Among the internal-loop reactors, two correlations presented for reactors with a rectangular cross-section are shown (32,154). For external-loop ALRs, the correlation by Popovic and Robinson (88) is recommended. In the case of internal-loop ALRs, most of the correlations predict similar values. The correlation of Merchuk et al. (37) can be recommended on the basis that more geometric parameters have been taken into account, and this gives greater generality. Nevertheless, the general considerations already expressed when analyzing other correlations in this chapter are valid here as well.

HEAT TRANSFER

Because of the relatively low reaction rates of processes involving microorganisms and cells, it may—in a very general way—be said that heat-effect problems related to local variations of temperature are not common in bioreactors. Even in the case in which polymeric products are released into the medium and very high viscosity is reached, heat transfer is not the controlling step, because such viscous media will hinder the mass transfer, and heat generation will consequently be limited. In such cases the main point of focus is thus, mass, rather than heat, transfer. Reactions catalyzed by immobilized enzymes, however, may require different considerations, because of higher reaction rates.

There is a far greater body of published data on heat transfer in bubble columns than in ALRs, and some of the basic observations are valid for both types of reactor. The heat transfer rate in bubble columns is much larger than that expected from single-phase flow (155). This is a result of the bubble-driven turbulence and liquid recirculation, which are characteristic of the flow in pneumatically agitated reactors.

Several correlations have been proposed for the prediction of the heat transfer coefficient in these reactors. Recently, Kawase and Moo-Young (62) presented an expres-

Table 5. Mass Transfer in ALRs

Curve no.	Reactor type	Height (cm)	*D* Riser (cm) draught tube	*D* Downcomer (cm) reactor tube	A_d/A	Ref.
1	Concentric tube	143	21	30	1.04	150
2a	External loop	180	15.2	76 + 10.2	0.69	45
2b	External loop	180	15.2	7.6	0.25	45
2c	External loop	180	15.2	5.1	0.11	45
2d	Concentric tube	180	8.9	15.2	0.56	45
2e	Concentric tube	180	7.6	15.2	0.35	45
2f	Concentric tube	180	5.1	15.2	0.13	45
2g	Bubble column	180	0	15.2	0.00	45
3a	Rec. split vessel; all experiments, except high recirculation and two spargers	435–450	9 × 250	7 × 25	0.78	32
3b	Rec. split vessel; high recirculation and two spargers	435–450	9 × 25	7 × 25	0.78	32
4	External loop	850	10	5	0.25	78
5a	Concentric tube	170	11.7	20	1.96	44
5b	Concentric tube	170	17.6	20	0.26	44

Note: Curve numbers correspond to Figure 31.

Table 6. Mass Transfer in Internal-Loop ALRs

No.	Formula	Ref.
1	$Sh = 3 \cdot 10^4 Fr^{0.97} M^{-5.4} Ga^{0.045} \left(1 + \frac{A_d}{A_r}\right)^{-1}$	1
2	$Sh = 2.66 Sc^{0.5} Bo^{0.715} Ga^{0.25} \left(\frac{D_r}{D}\right)^{-0.429} \varphi^{1.34}$	151
3	$k_L a = 0.0343 J_{Gr}^{0.524} \mu_{ap}^{-0.255}$ $\gamma = 5000 J_{Gr}$ for $J_{Gr} \geq 0.04\ \mathrm{ms}^{-1}$ $\gamma = 5000 J_{Gr}^{0.5}$ for $J_{Gr} \leq 0.04\ \mathrm{ms}^{-1}$	48
4	$Sh = 0.68 n^{-0.72} Fr^{0.38n+0.52} Sc^{0.38-0.14n}$	59

Table 7. Mass Transfer in External-Loop ALRs

No.	Formula	Ref.
1	$K_L a = k_1 J_{Gr}^{0.8} \left(1 + \frac{A_d}{A_r}\right)^{-2}$ Water $K_L = 0.75 \mu^{-0.8} \sigma^{-0.2}$ NaCl $K_L = 0.79 \mu^{-0.8} \sigma^{-0.2}$	45
2	$k_L a = 0.5 \cdot 10^{-2} J_{Gr}^{0.52} \left(1 + \frac{A_d}{A_r}\right)^{-0.85} D_1^{0.5} \rho_1^{1.03} \sigma_1^{-0.25} \mu_{ap}^{-0.89}$ or in simplified form: $k_L a = 1.911 \cdot 10^{-4} J_{Gr}^{0.52} \left(1 + \frac{A_d}{A_r}\right)^{-0.85} \mu_{ap}^{-0.85}$ $k_L a = 0.24 J_{Gr}^{0.837} \left(1 + \frac{A_d}{A_r}\right)^{-1}$	88
3	in case of suspended solids: $k_L a = (0.349 - 0.102 C_s) J_{Gr}^{0.837} \left(1 + \frac{A_d}{A_r}\right)^{-1}$	152
4	$k_L a = 913 \left(\frac{P}{VD}\right)^{1.04} (U_L)^{-0.15}$	32
5	$k_L a = (0.349 - 0.102 C_s \left(1 + \frac{A_d}{A_r}\right)^{-1} J_{Gr}^{0.837}$	152

sion that satisfactorily fits most of the published data. The model is based on Levich's (156) three-zone concept and Kolmogoroff's (157) isotropic turbulence theory and has no empirical adjustable parameters. The model can take into consideration non-Newtonian behavior of the liquid and predicts the enhancement of the heat transfer due to the shear-thinning effect of the fluid. The dimensionless expression may be written as:

$$Nu = 0.075(10.3n^{-0.63})^{\beta} n^{1/3} (Pr^*) \frac{1}{3} Fr^{-\beta} (Re^*)^{\beta + 3(n+1)} \tag{47}$$

with

$$\beta = \frac{4 - n}{6(n + 1)}; \quad Pr^* = \frac{\kappa D^{1-n}}{\left(\frac{\kappa}{C_p}\right) J_G^{1-n}}; \quad Re^* = \frac{D^n J_G^{2-n}}{\left(\frac{k}{\rho}\right)} \tag{48}$$

where the symbols defined in "Nomenclature" have been used.

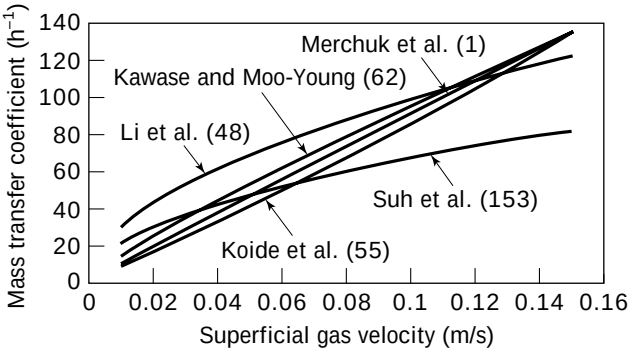

Figure 32. Mass transfer coefficient $k_L a$ as a function of gas superficial velocity for internal-loop ALRs. Correlations are presented in Table 6.

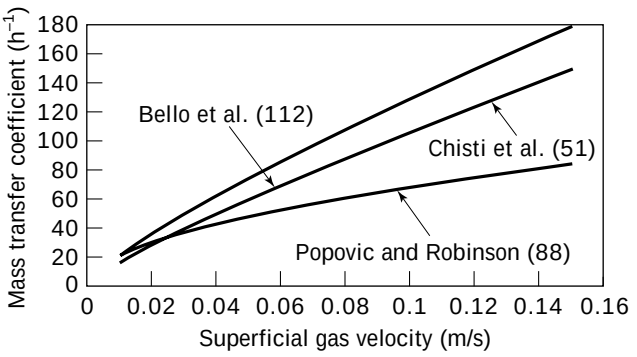

Figure 33. Mass transfer coefficient k_La as a function of gas superficial velocity for external-loop ALRs. Correlations are presented in Table 7.

For Newtonian liquids, this equation reduces to:

$$Nu = 0.134^{1/3}(Pr)^{1/3}Fr^{-1/4}(Re)^{3/4} \qquad (49)$$

Kawase and Moo-Young (140) compared their model with data and correlations published by various investigators and found satisfactory agreement for both Newtonian and non-Newtonian liquids.

For ALRs (64), the flow in the reactor may be similar to that in bubble columns if the internal recirculation is high, or it may be even closer to net two-phase flow in pipes, in which case the equations for heat transfer in pipes can be used (126).

Blakebrough et al. (158) studied heat transfer rates in an external-loop airlift fermentor used for culturing *Aspergillus niger*. They concluded that the enhancement of the heat transfer rate could be explained by disturbances in the liquid layer near the surface caused by the presence of the microorganisms.

THREE-PHASE AIRLIFT REACTORS

The special qualities of the ALR stem, as stated before, from its fluid dynamic characteristics. One such characteristic is the directionality of the liquid flow. Independently of superimposed fluctuations, a clear net flow is present in the reactor, with exception of the gas separator in internal-loop designs. Therefore, it is to be expected that the fluidization capacity of the ALR will be markedly superior to that of a bubble column. Several studies have been conducted on the suspension of solids in ALRs, particularly on the use of this type of device for catalytic processes in the chemical industry, where the solid support is usually heavy (61,159–163). In this regard, a very important point is the minimum gas superficial velocity that leads to complete solid fluidization (61,87,159,162,164–166). Hysteresis has been observed in some cases; once total fluidization has been attained, the superficial velocity can be reduced to values lower than that required to reach this state. This is due to the high pressure drop related to passage of liquid through a bed of solids, before fluidization, as compared to the drag forces required to maintain the solid in suspension after all the solids are suspended. Contradictory data on the effect of the suspended solids on the reactor performance have been reported. Fan et al. (167) claimed that the overall gas holdup increased due to the presence of the solids, whereas Koide et al. (168,169) showed the opposite effect on the gas holdup and reported a small decrease in k_La as well. It is possible that these discrepancies are due to the use of different solids. One of the properties of solids that is often overlooked is wettability. Small bubbles may adhere on wettable solids, leading to a change in the apparent density of the particle and thus changing their solid circulation velocity.

In the case of suspended solids that take an active part in the process, the mass transfer rate from the liquid to the solid may become the limiting step. The dependence of particle size on the mass transfer to the suspended solids has been studied by several authors (19,170,171).

All the comments made above relate to heavy solids. This situation is not very frequent in biological processes, with the exception of biolixiviation (172) or the special case of microbial desulfuration of coal (173). In most of the biological processes that may take place in an ALR, the solids are either cells, clumps of cells, or supports that are not much more dense than the medium. Therefore, neither fluidization nor the distribution of solids in the reactor constitutes a problem. Assa and Bar (174) found very small variations in the axial distribution of animal and plant cells suspended in an internal-loop ALR. This is due to the small free-falling velocity of the solids, which is the reason for the difference in loading between the riser and the downcomer when heavy particles are used (160–162). Because of the small difference between solid and medium density, the movement of the particles usually present in biological processes is not as dependent on gravity forces as on liquid and bubble movement. In this case, the transport of liquid in the wake of the bubbles may be considered to be the prevailing transport mechanism (175). Snape and Thomas (176) proposed a Monte Carlo algorithm for modeling particle movement by this mechanism in bubbly flow to predict distribution of circulation times in the reactor. Koide et al. (169) conducted a broad study of gas holdup and mass transfer rates in an internal-loop ALR containing Ca-alginate beads, which are often used for cell immobilization. The authors found that solid loading had a negative effect on both parameters, but the particle diameter had no influence in the range studied (1.8 mm $< d_p <$ 3.98 mm). Chang et al. (31) studied the influence of suspended pellets (cylindrical pellets of immobilized penicillin acylase) on the mixing time in an internal-loop ALR. They found mixing time increased when the solid volumetric concentration was raised up to 15%. For higher concentrations the trend inverted, and the mixing time decreased. No such effects were observed with heavier solids. Increases in gas superficial velocity and in top clearance both lead to decreases in mixing time in all cases.

AIRLIFT REACTOR—SELECTION AND DESIGN

Scale-up of Airlift Bioreactors

The problems encountered in the scale-up of bioreactors can be concentrated into two groups. The first includes the cases in which a high power input per unit volume is used

on a laboratory scale, but cannot be maintained on an industrial scale due to economic or mechanical limitations. This is not the case for plant or animal cultures, for which a very high specific power input cannot be used because of cell fragility. The second group of problems can be generalized as lack of knowledge about the hydrodynamics of large-volume vessels.

The methods available for scale-up of bioreactors have been reviewed by Oosterhuis (177), Kossen and Oosterhuis (178), Sweere et al. (179), and Sola and Godia (180), among others. Because, in general, design from first principles cannot be undertaken because of the lack of basic knowledge about the hydrodynamics of the bioreactors, one possible solution is the semifundamental method, which comprises using approximate simple models for fluid dynamics and integrating them with basic known kinetics and heat and mass transfer rates.

It does not happen very often that all this information is available with a degree of certainty that allows safe design of a large system. Thus, the designer must usually resort to dimensional analysis. This method requires a knowledge of all the variables affecting the process, which can be obtained from a qualitative, but realistic, model (181).

A simplified version of this method is to limit the number of variables to one or two and to follow rules of thumb (182), which, depending on the specific case, may be constant P/V, constant k_La, etc. The literature shows, however, many cases of inconsistency for this method. For example, design of a scaled-up bioreactor in which the oxygen transfer rate is kept constant can lead to a better performance than expected, as in the example reported by Taguchi et al. (183) for glucoamylase production by *Endomyces* sp., or worse than expected, as in the case of protease production by *Streptomyces* sp. (184). These two examples are shown in Figure 34.

The method of regime analysis and scale down, proposed by Kossen and Oosterhuis (178), combines two tools to overcome the problem posed by the complexity of biochemical reactors. Their method is based on considering the regime of the full-scale process as the objective and planning the strategy of process development from this point on. This method is therefore applicable only to conventional and well-studied bioreactors that are to be used in a new bioprocess.

Regime analysis is based on the consideration that, generally, biochemical processes involve a series of steps, some being mass or heat transfer by convection, some being diffusive mechanisms (activated or not), and others being chemical reaction steps. In the latter case, a mass-transfer mechanism is superimposed, since molecules must encounter one another in order to react, and usually a heat effect will accompany the reaction. Depending on whether these steps take place in parallel or in series and on the relaxation time for each step (185), the rate of the total process is often given as the rate of one single step. But the equilibrium between all the individual rates can be (and usually is) upset by a change in scale. This is to be expected, because a change in scale will not bring a change in the physicochemical or kinetic parameters (scale-insensitive variables), but will affect the overall convective mass and

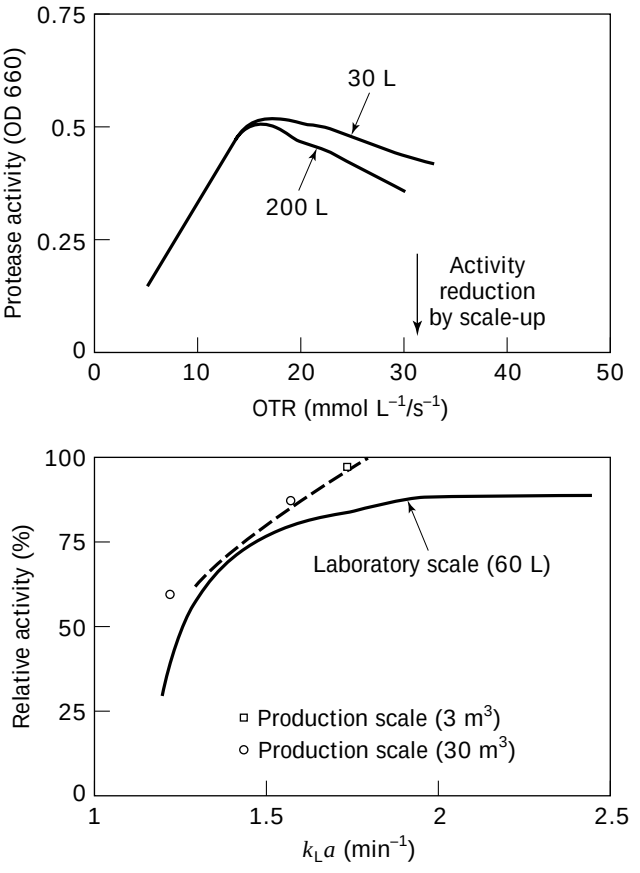

Figure 34. Results for a scaled-up bioreactor with a constant oxygen transfer rate (183,184). OD 660 is the optical density measured at wavelength of 660 nm.

heat rates (scale-sensitive variables). A new equilibrium will be established, and the interplay of all the parameters of the system may lead to a regime in which a different step becomes the step-controlling the process rate.

The method of Kossen and Oosterhuis (178) starts with an analysis of the operation of the large-scale system. Once the regime is clarified, a small-scale system is designed in such a way that it simulates the operation regime of the larger one. Optimization studies can be done on the smaller model, and conclusions will then be extrapolated to the full-scale process. This concept is depicted in Figure 35. An example of this method is given by Oosterhuis (177), in which a large-scale stirred tank reactor is simulated on a laboratory scale by two interconnected vessels, one with a small liquid volume, high agitation rate, and high rate of oxygen supply (representing the zone near the impeller-sparger in the reactor), and a second vessel, with a much larger liquid volume, oxygen consumption (simulated by nitrogen sparging), and gentle agitation. The success of this model suggests that large vessels must be carefully analyzed and their internal structure studied for proper modeling and design to be performed. The analysis starts with the definition of the characteristic time constants of the system.

In the case of low gas recirculation, the relationship between the total circulation time and the residence time in

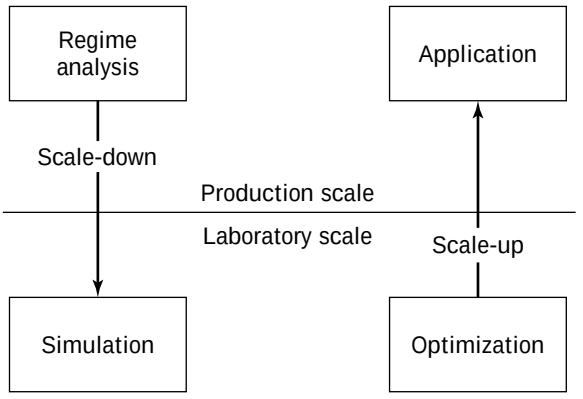

Figure 35. Schematic representation of the scale-down method. Adapted from Oosterhuis (177).

the downcomer may become very relevant. This was shown by MacNeil and Kristiansen (180,186) for the scale-up of an external-loop ALR for the production of *Aureobasidium pullulans*. The poor oxygen supply in the downcomer was reflected on the level of product synthesis, as shown in Figure 36. The smaller residence times lead to higher *A. pullulans* production.

An analysis of the time constants required for the design of an ALR for plant cell culture has recently been presented (187). Figure 37 shows the reported values of the time constants calculated for an external-loop ALR for mixing, mass transfer, and oxygen consumption at two different cell concentrations: 5 and 30 kg/m^3. These graphs exemplify the changes in the controlling mechanism that may take place as the physical properties of the broth change in the course of the bioprocess.

Details on bioreactor scale-up may be found in the recent review of Sola (180). It should be remembered, however, that the reliability of a scale-up will always be limited by the quality of the predictions of gas holdup, liquid velocity, and mass transfer rate.

Design Improvements

In the design of ALR, several modifications aiming at the improvement of some of the characteristics of the equipment have been proposed. One of the earliest modifications was the two-staged ALR, proposed by Orazem and Erickson (148). Their design was inspired by the improvement observed by them in the performance obtained with multistage sieve trays over single-stage bubble columns. They claimed that a substantially higher mass transfer coefficient was obtained, as was a better performance in terms of oxygen transferred per unit of energy invested.

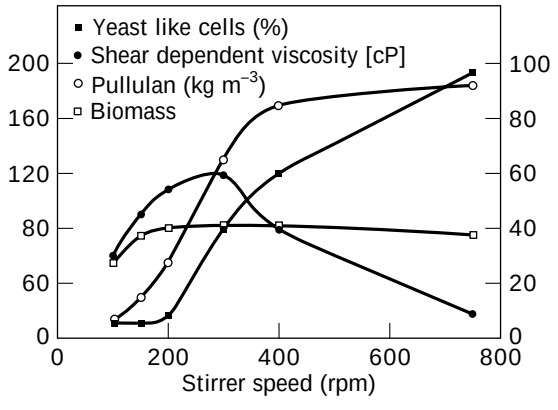

Figure 36. Influence of residence time in the poorly aerated downcomer on the production of *A. pullulans*. Adapted from McNeil and Kristiansen (186).

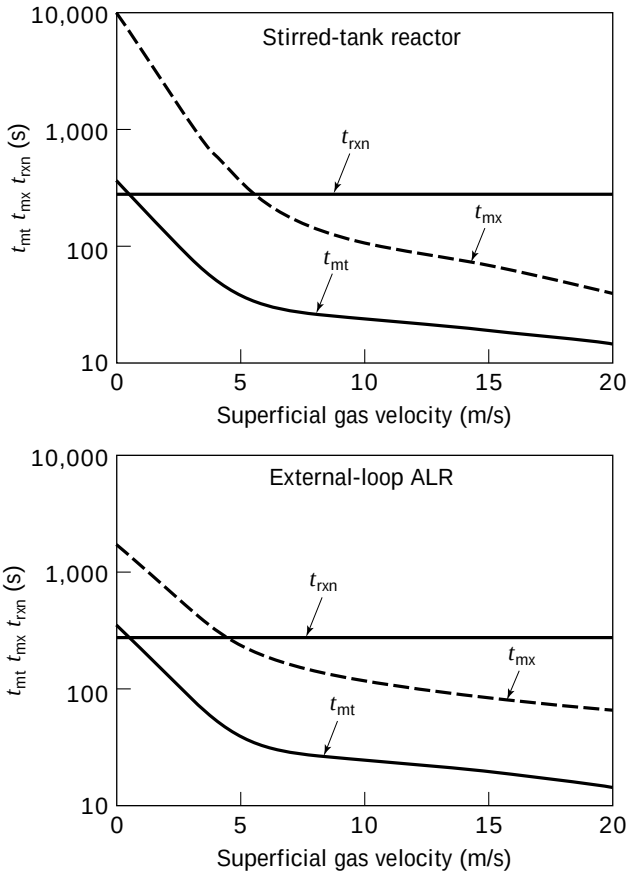

Figure 37. Time constants calculated in an external-loop ALR as a function of the superficial gas velocity (187).

The combination of a concentric-tube ALR with a marine propeller (1000 rpm) was studied by Pollard et al. (188) (Fig. 38). This modification, in which the stirrer was located near the bottom of the draft-tube, served to increase the circulation rate, which may be low for viscous liquids. This configuration showed enhanced oxygen transfer and more uniform distribution of the dissolved oxygen concentration throughout the reactor in comparison with that of the unmodified ALR. The liquid circulation was also intensified. However, the improvement was achieved at the cost of the introduction of a focus of energy input. As has been mentioned before, the absence of such a high shear region is one of the advantages of the ALR. This advantage is, in part at least, lost. It is interesting to note that a bakers' yeast culture (188) grown in the same type of modified reactor did not reveal any improvement. This may be related to the strong shear rate in the vicinity of the propeller.

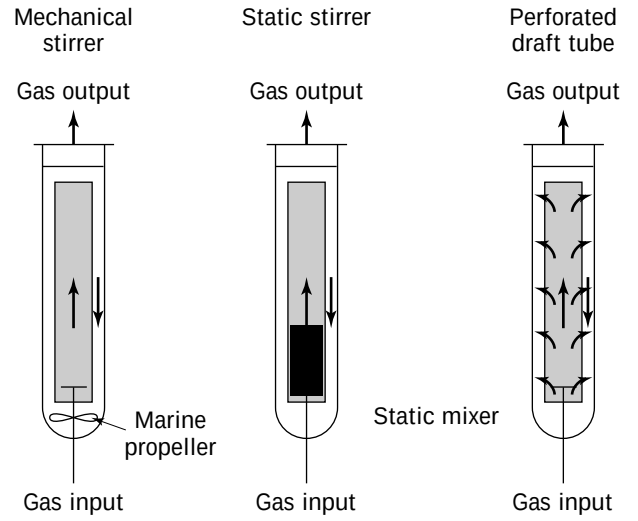

Figure 38. Modifications proposed in ALRs.

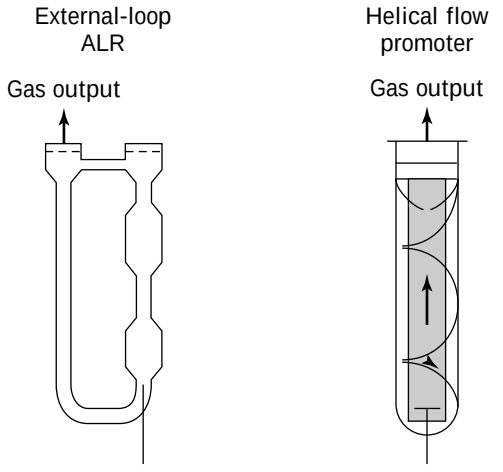

Figure 39. Comparison between a bubble column an ALR and an ALR with helical flow promotors. From Schlotelburg et al. (196).

Different types of static mixers, usually located in the riser, have also been used for enhancing the performance of ALRs (Fig. 38). Potucek (189) studied the influence of static mixers on the gas holdup and interfacial gas-liquid area in a concentric-tube ALR and found an improvement in interfacial area. Enhancement of $k_L a$ has been also obtained, especially in viscous liquids, as reported by Gaspillo and Goto (190) and Chisti et al. (191). Zhou et al. (192) showed better growth of *Cephalosporum acremonium* in an ALR with static mixers.

As mentioned above, it has been shown repeatedly that the mass transfer rate in a bubble column is usually higher than that in the conventional ALR. It therefore makes sense to try to bring into the ALR some of the characteristics of bubble columns in a controlled fashion. This was done by Bando et al. (193,194), who tested a perforated draft tube in a concentric-tube ALR. The perforations in the draft tube facilitated communication between the less-well aerated liquid in the downcomer and the better aerated riser (Fig. 38). The reported improvements in mass transfer rates were undoubtedly obtained at the cost of a reduction of circulation velocity.

Another variant tested is the converging-diverging tube ALR (195), which can be seen in Figure 38. The authors report that the changes in cross-section in the riser produced an increase in the gas holdup.

One of the advantages of the directionality of flow in ALRs is the improved fluidization capacity. The strengthening of this advantage was the aim of another modification, the helical flow promoter, proposed by Gluz and Merchuk (170). The helical flow promoter causes the fluid to flow down in the downcomer (Fig. 39) in a helical pattern. The device comprises several fins or baffles, which have the effect of modifying the flow paths; instead of going in straight lines along the axis, the flow paths move along an helix. The baffles may be installed in a small section at almost any place along the riser or the downcomer, and the effect is perceived throughout the reactor. One of the best positions for the helical flow promoter is the top of the riser. A helical flow is then generated in the downcomer to produce a swirl at the bottom and a corkscrew-like path in the riser. This has a strong potential for the culture of photosynthetic microorganisms. The helical movement causes secondary flow, which leads to enhanced radial mixing, and therefore more homogeneous distribution of light and heat among liquid elements and suspended particles. With the helical flow promoter, it is thus more likely that all the elements of the fluid get the same exposure to light and heat exchange.

One of the most important characteristics of the helical flow promoter is the enhanced capacity for fluidizing solid particles. This is due to the swirls that develop at the bottom of the reactor. Thus, this modification is especially suited to processes operating with cells immobilized on a solid. The minimal gas flow rate for complete fluidization of solids in an ALR may be reduced drastically by the use of a helical flow promoter (170). In addition, the mass transfer rate to suspended solids may be enhanced up to 50%, because of the higher relative velocity between the particles and solids.

Another interesting aspect of the performance of helical flow promoters can be seen in Figure 39 (196). Mass transfer coefficients obtained in a bubble column, an ALR, and an ALR with HFP were compared, for water and two solutions of CMC: 0.2% and 0.04%. The corresponding effective viscosities for $\gamma = 50\ s^{-1}$ are 16 and 38 mPa s respectively. It is clearly seen that although with water there is a consistent difference in favor of the bubble column, the differences diminish as the CMC concentration increases, and for the highest concentration tested the difference is negligible. This implies that under these conditions the disadvantage of the HFP in mass transfer vanishes, whereas all the advantages mentioned before subsist.

SUMMARY AND CONCLUSIONS

ALRs are popular in modern bioprocess research and development. These reactors are particularly suitable for biological processes in which a high mass transfer rate is re-

quired, but excessive power input may lead to damage of the cells due to shear effects. ALRs also have very appealing characteristics for bioprocesses for low-value products in which efficiency of energy utilization may become the key point for design. Such is the case for ALRs for wastewater treatment. The ALR is particularly effective for solid fluidization, which is important in many biological processes in which the biocatalyst is available in the form of pellets or is immobilized on a solid support.

The distinctive characteristics of ALRs are conferred by the fluid dynamics of the liquid–gas or liquid–gas–solid mixtures in it. These characteristics are expressed as gas holdup, liquid velocity, and mixing in each of the zones of the ALR. It is important to recognize the differences in the fluid dynamic characteristics of these zones: the riser, the gas separator, and the downcomer. Only a correct understanding of behavior and interconnection of these regions can make possible the correct design of a new reactor or the scale-up of a laboratory device up to pilot or industrial size.

The purpose of scale-up is to conserve and repeat on a larger scale the fluid dynamics of the reactor. Therefore, one of the most important factors in the design and scale-up of reactors is the influence of the geometric characteristics of the system on the flow of the different phases present.

The variables affecting the performance of the reactor are geometric design, operation variables, and fluid properties. Several correlations are available in the technical literature for the prediction of the fluid dynamic characteristics of the reactor (gas holdup, liquid velocity, mixing time of axial dispersion coefficient) and of the mass and heat transfer coefficients. Although attempts have been made to study all the aspects described, no single research group has managed to cover all the variables over a wide range. It is therefore extremely important that the engineer confronting scale-up or de novo design of an ALR analyzes in depth the range of validity of the correlations used for the calculations.

NOMENCLATURE

a	Interfacial area (m^{-1})
A	Cross-sectional area (m^{-2})
B	Heat transfer area (m^2)
Bo	Bond number or Bodenstein number (−)
C	Concentration (mg/L)
Co	Distribution parameter (−)
C	Clearance or fiction losses coefficient (−)
d	Mean diameter (mm)
D	Diameter (m), diffusivity, dispersion coefficient
D_L	Diffusivity, dispersion coefficient (m^2 sec^{-1})
E	Energy (J)
Fr	Froude number (−)
g	Gravitational constant (m sec^{-2})
Ga	Galileo number (−)
h	Height (m)
h_b	Overall heat transfer coefficient ($W\ m^{-2}sec^{-1}K^{-1}$)
I	Degree of homogeneity (−)
J	Superficial velocity (cm sec^{-1})
K	Saturation constant in Monod's equation mgL^{-1}
k_La	Volumetric mass transfer coefficient (hr^{-1})
K_b	Hydraulic coefficient bottom (−)
K_t	Hydraulic coefficient top (−)
L	Length (m)
M	Wetted surface parameter (−)
Ma	Bubble coalescence parameter (−)
Mo	Morton number (−)
n	Flow index (−)
N	Agitation speed (sec^{-1})
Nu	Nusselt number (−)
N_W	Parameter (−)
OTR	oxygen transfer rate
P	Pressure, power input (Pa)
Pe	Peclet number (−)
Pr	Prandtl number (−)
r	Reaction rate ($mol\ m^{-3}sec^{-1}$)
Re	Reynolds number (−)
S	Surface area (m^2)
Sc	Schmidt number (−)
Sh	Sherwood number (−)
t	Time (sec)
U	Velocity (m sec^{-1})
V	Volume (m^3)
Q	Flow rate (m^3sec^{-1})
We	Weber number (−)
Wi	Weissenberg number (−)

Greek Letters

α	Coefficient (−)
β	Flowing volumetric concentration (m^3/m^3)
γ	Shear rate (sec^{-1})
Δ	Difference
φ	Gas holdup (−)
κ	Behavior coefficient (Pa s^{n+2})
λ	Heat conductivity coefficient ($W\ m^{-1}K^{-1}$)
μ	Dynamic viscosity (Pa s), specific growth coefficient (h^{-1})
ρ	Density ($kg\ m^{-3}$)
σ	Surface tension ($N\ m^{-1}$)
τ	Shear stress (Pa)
ν	Kinematic viscosity (m^2 sec^{-1})

Indices

ab	All bubbles
ap	Apparent
b	Bottom
$b\infty$	Terminal
c	Circulation

d	Downcomer, dissipation
D	Dissipation
d	Downcomer
g	Growth
G	Gas
ht	Heat transfer
HM	Heat production by the microorganisms
HS	Heat production by stirring
i	Region of reactor
in	Input
L	Liquid
m	Mixing
max	Maximal
mt	Mass transfer
oc	Oxygen consumption
p	Potential
r	Riser
s	Gas separator
sc	Sugar consumption
sh	Shaft
sol	Solid
t	Top
T	Total
w	Water

BIBLIOGRAPHY

1. J.C. Merchuk, N. Ladwa, A. Cameron, M. Bulmer, and A. Pickett, *AIChE J.* **40**, 1105–1117 (1994).
2. K. Koide, K. Kurematsu, S. Iwamoto, Y. Iwata, and K. Horibe, *J. Chem. Eng. Jpn.* **16**, 413–418 (1983).
3. H. Tanaka, *Proc. Biochem.* **22**, 106–112 (1987).
4. W.R. Kessler, M.K. Popovic, C.W. Robinson, *Can. J. Chem. Eng.* **71**, 195–202 (1993).
5. J.Y. Oldshue, *Fluid Mixing Technology*, McGraw-Hill, New York, 1983.
6. J.C. Merchuk, *Adv. Biochem. Eng.* **44**, 65–95 (1991).
7. R.J. Weetman and J.Y. Oldshue, *Power, Flow and Shear Characteristics of Mixing Impellers, Proceedings of the 6th European Conference on Mixing*, Cranfield, 1988, p. 43.
8. H. Markl, R. Bronnenmeier, B. Wittek, *Int. Chem. Eng.* **31**, 185–197 (1991).
9. JD.a.P. Wase, Y.R., *J. Gen. Microbiol.* **131**, 725–731 (1985).
10. N. Edwards, S. Beeton, A.T. Bull, and J.C. Merchuk, *Appl. Microbiol. Biotechnol.* **30**, 190–196 (1989).
11. J. Tramper, D. Smit, J. Straatman, and J.M. Vlak, *Bioprocess Eng.* **3**, 37–41 (1988).
12. L. Yerushalmi and B. Volesky, *Biotechnol. Bioeng.* **27**, 1297–1305 (1985).
13. F.J. Petersen, V.L. McIntire and E.T. Papoutsakis, *J. Biotechnol.* **7**, 229–246 (1988).
14. D.E. Martens, C.D. de Gooijer, C.A.M. van der Velden-de Groot, E.C. Beuvery, and J. Tramper, *Biotechnol. Bioeng.* **41**, 429 (1993).
15. H.R. Millward, B.J. Bellhouse, A.M. Nicholson, S. Beeton, N. Jenkins, and C.J. Knowles, *Biotechnol. Bioeng.* **43**, 899–906 (1994).
16. H. N.a.U. Shiragami, *Bioprocess Eng.* **10**, 43–45 (1994).
17. N.A. Stathopoulos and J.D. Hellums, *Biotechnol. Bioeng.* **27**, 1021–1026 (1984).
18. H.J. Silva, T. Cortinas, and J.R. Ertola, *J. Chem. Technol. Biotechnol.* **40**, 41–49 (1987).
19. H. Tanaka, H. Semba, T. Jitsufuchi, and H. Harada, *Biotechnol. Lett.* **10**, 485–490 (1988).
20. C.G. Smith, P.F. Greenfield, and D.H. Randerson, *Biotechnol. Tech.* **1**, 39–44 (1987).
21. Z. Zhang, Y. Christi, and M. Moo-Young, *J. Biotechnol.* **43**, 33–40 (1995).
22. J.J. Meijer, H.J.G. ten Hoopen, Y.M. van Gameren, and K.Ch.A.M. Luyben, *Enzyme Microb. Technol.* **16**, 467–477 (1994).
23. G.Z. Lu, B.G. Thompson, and M.R. Gray, *Biotechnol. Bioeng.* **40**, 1277–1281 (1992).
24. H.E. Dunlop, K.N. Pradyumna, and Z.M. Rosenberg, *Chem. Eng. Sci.* **49**, 2263–2276 (1994).
25. L.D.a.L. Landau, E.M., *Fluid Mechanics*, Volume 6, Pergamon, Oxford, U.K., 1975, pp. 115–123.
26. W.S. Tan, G.C., Dai, W. Ye, and J.P. Shen, *Chem. Eng. J. Biochem. Eng. J.* **57**, B31–B36 (1995).
27. H.F. Svendsen, H.A. Jakobsen, and R. Torvik, *Chem. Eng. Sci.* **47**, 1297–1304 (1992).
28. A. Stafford, L. Smith, and M.W. Fowler, *Plant Cell Tissue Organ Culture* **4**, 83–94 (1985).
29. P.J. Wilkinson, in G.W. Moody and P.B. Baker eds., *Biotransformations*, Elsevier, London, 1992.
30. A. Gebauer, T. Scheper, K. Schugerl, *Bioprocess Eng.* **2**, 13–23 (1987).
31. C.M. Chang, W.J. Lu, K.S. Own, and S.J. Hwang, *Biotechnol. Tech.* **7**, 317–322 (1993).
32. M.H. Siegel and J.C. Merchuk, *Biotechnol. Bioeng.* **32**, 1128–1137 (1988).
33. G.A. Legrys, *Chem. Eng. Sci.* **33**, 83–86 (1978).
34. M.E. Orazem and L.E. Erickson, *Biotechnol. Bioeng.* **21**, 69–88 (1979).
35. M.H. Siegel, J.C. Merchuk, and K. Schugerl, *AIChE J.* **32**, 1585–1596 (1986).
36. H. Kubota, Y. Hosono, and K. Fujie, *J. Chem. Eng. Jpn.*, **11**, 319–325 (1978).
37. J.C. Merchuk, N. Ladwa, A. Cameron, M. Bulmer, A. Pickett, and I. Berzin, *Chem. Technol. Biol.* **66**, 174–182 (1996).
38. D. Barnea, Y. Taitel, in N.P. Cheremisinoff, ed. *Encyclopedia of Fluid Mechanics*, Gulf, Houston, Tex., 1986, pp. 403–491.
39. G.B. Wallis, *One Dimensional Two-Phase Flow*, McGraw-Hill, New York, 1969.
40. K. Wiswanathan, *Flow Patterns in Bubble Columns*, Gulf, Houston, Tex., 1986, pp. 291–308.
41. J.C. Merchuk, in K. Schügerl ed. *Biotechnology*, Springer, New York, 1990.
42. A.B. Russell, C.R. Thomas, and M.D. Lilly, *Biotechnol. Bioeng.* **43**, 69–76 (1994).
43. A.C. Gomez, Univ. of Almeria, Spain, 1996.
44. P. Weiland, *Ger. Chem. Eng.* **7**, 374–385 (1984).
45. R.A. Bello, C.W. Robinson, and M. Moo-Young, *Chem. Eng. Sci.* **40**, 53–58 (1985).
46. M.Y. Chisti and M. Moo-Young, *Chem. Eng. Commun.* **60**, 195–242 (1987).

47. K. Koide, S. Iwamoto, Y. Takasaka, S. Matsura, E. Takasashi, M. Kimura, and H. Kubota, *J. Chem. Eng. Jpn.* **17**, 611–618 (1984).
48. G.Q. Li, S.Z. Yang, Z.L. Cai, and J.Y. Chen, *Chem. Eng. J.* **56**, B101–B107 (1995).
49. J. Cai, T.J. Niewstad, and J.H. Kop, *Water Sci. Technol.* **26**, 2481–2484 (1992).
50. M. Popovic and C.W. Robinson, *Proc. 34th Can. Chem. Eng. Conf.* Quebec, Oct., 1984, pp. 258–264.
51. M.Y. Chisti, B. Halard, and M. Moo-Young, *Chem. Eng. Sci.* **43**, 451–457 (1988).
52. G. Vatai and M.N. Tekis, *Effect of Pseudoplasticity on Hydrodynamic Characteristics of Airlift Loop Contactors*, Prague, 1986.
53. K. Akita and M. Kawasaki, *Proc. 48th Meet. of Chem. Engrs. Engrs. Jpn.* Kyoto, 1983, pp. 122–126.
54. Y. Kawase, M. Tsujimura, and T. Yamaguchi, *Bioproc. Eng.* **12**, 21–27 (1995).
55. K. Koide, K. Horibe, H. Kawabata, and I. Shigetaka, *J. Chem. Eng. Jpn.* **18**, 248–254 (1995).
56. K. Koide, M. Kimura, H. Nitta, and H. Kawabata, *J. Chem. Eng. Jpn.* **21**, 393–399 (1988).
57. T. Miyahara, M. Hamaguchi, Y. Sukeda, and T. Takahashi, *Can. J. Chem. Eng.* **64**, 718–725 (1986).
58. M. Chakravarty, H.D. Singh, J.N. Baruah, and M.S. Lyengar, *Indian Chem. Eng.* **16**, 17–22 (1974).
59. Y. Kawase, M. Moo-Young, *Chem. Eng. Commun.* **40**, 67–83 (1986).
60. J.C. Merchuk, M. Bulmer, N. Ladwa, A.M. Pickett, and A. Cameron, in R. King, ed., *Bioreactor Fluid Dynamics* Elsevier, London, 1988, pp. 391–414.
61. K. Koide, K. Horibe, H. Kawabata, and S. Ito, *J. Chem. Eng. Jpn.* **17**, 368–374 (1984).
62. Y. Kawase, M. Moo-Young, *Chem. Eng. Res. Des.* **65**, 121–126 (1987).
63. M. Popovic and C.W. Robinson, *Biotechnol. Bioeng.* **32**, 301–312 (1988).
64. M. Siegel and J.C. Merchuk, *Can. J. Chem Eng.* **69**, 465–471 (1991).
65. M. Hallaile, *Biotechnology*, Ben-Gurion Univ. Beer Sheva, Israel, 1993.
66. M. Ghirardini, G. Donati, and F. Rivetti, *Chem. Eng. Sci.* **47**, 2209–2214 (1992).
67. J.C. Merchuk and R. Yunger, *Chem. Eng. Sci.* **45**, 2973–2976 (1990).
68. Y. Chisti and M. Moo-Young, *Biotechnol. Bioeng.* **34**, 1391–1392 (1989).
69. J.H. Hills, *Ind. Chem. Eng.* **52**, 1–9 (1974).
70. N.N. Clark, C.M. Atkinson, and R.L.C. Flemmer, *AIChE J.* **33**, 515–521 (1987).
71. J.C. Merchuk and Y. Stein, *AIChE J.* **27**, 377–381 (1981).
72. B. Glennon, W. Al-Masry, P.F. MacLoughlin, and D.M. Malone, *Chem. Eng. Commun.* **121**, 181–192 (1993).
73. W. Freedman and J.F. Davidson, *Trans. Inst. Chem. Eng.* **47**, 251–262 (1969).
74. N. Zuber and J.A. Findlay, *Trans. ASME J. Heat Transfer* **87**, 453–468 (1965).
75. S.G. Bankoff, *J. Heat Transfer* **82**, 252–258 (1960).
76. P. Verlaan, J. Tramper, K. van't Riet, and K. Luyben, *Chem. Eng. J.* **33**, B43–B48 (1986).
77. J.C. Merchuk and I. Berzin, *Chem. Eng. Sci.* **50**, 2225–2233 (1995).
78. P.a.O.U. Weiland, *Ger. Chem. Eng.* **4**, 174–181 (1981).
79. P. Verlaan, J. Tramper, K. van't Riet, and K.Ch.A.M. Luyben, *Hydrodynamics and Axial Dispersion in an Airlift Loop Reactor with Two and Three Phase Flow*, Cambridge, UK, 1986.
80. P. Verlaan, A.M.M. Van Eijs, J. Tramper, K. van't Riet, and K. Ch. A.M. Luyben, *Chem. Eng. Sci.* **44**, 1139–1144 (1989).
81. Y. Chisti, *Airlift Bioreactors*, Elsevier, London, 1989.
82. P. Verlaan, J.C. Vos, and K. van't Riet, in R. King ed., *Bioreactor Fluid Dynamics II*, Elsevier, London, 1988.
83. J.C. Merchuk, *Chem. Eng. Sci.* **41**, 11–16 (1986).
84. D. Posarac and D. Petrovic, *Chem. Eng. Sci.* **43**, 116–119 (1991).
85. R.A. Bello, Ph.D. Thesis, Univ. of Waterloo, Ontario, Canada, 1981.
86. Z. Kemblowski, J. Prywarski, and A. Diab, *Chem. Eng. Sci.* **48**, 4023–4035 (1993).
87. D. Posarac, D. Petrovic, A. Dudukovic, and D. Skala, *J. Serb. Chem. Soc.* **56**, 227–240 (1991).
88. M.K. Popovic and C.W. Robinson, *AIChE J.* **35**, 393–405 (1989).
89. M. Nishikawa, H. Kato, and K. Hashimoto, *Ind. Eng. Chem. Process Des. Dev*, **16**, 133–137 (1977).
90. M. Nishikawa, *Biotechnol. Bioeng.* **37**, 691–692 (1991).
91. H.J. Henzler, *Chem.-Ing.-Tech.* **52**, 643–652 (1980).
92. A. Schumpe and W.D. Deckwer, *Bioproc. Eng.* **2**, 79–94 (1987).
93. A. Zaidi, H. Bourziza, and L. Echihabi, *Chem.-Ing.-Tech.* **59**, 748–749 (1987).
94. S.A. El-Tamtamy, S.A., Khalil, A.A. Nour-El-Din, and A. Gaber, *Appl. Microbiol. Biotech.* **19**, 376–381 (1984).
95. H.J. Henzler, J. Kauling, *Scale-Up of Mass Transfer in Highly Viscous Liquids*, Wurzburg, Germany, 1985, pp. 303–312.
96. J.C. Merchuk and S. Ben-Zvi (Yona), *Chem. Eng. Sci.* **47**, 3517–3523 (1992).
97. A. Lubbert, S. Frohlich, B. Larson, and K. Schugerl, *Fluid Dynamics in Airlift Loop Reactors as Measured During Real Cultivation Processes*, London, 1988, pp. 379–394.
98. A. Lubbert, B. Larson, L.W. Wan, and S. Broring, *I. Chem. E. Symp. Ser.* **121**, 203–213 (1990).
99. C.H. Lee, L.A. Glasgow, L.E. Erickson, and S.A. Patel, *Liquid Circulation in Airlift Fermentors*, Miami Beach, 1986.
100. A.G. Jones, *Chem. Eng. Sci.* **40**, 449–462 (1985).
101. D.J. Niklin, *Chem. Eng. Sci.* **17**, 693–702 (1962).
102. M. Clark and A.G. Jones, *Chem. Eng. Sci.* **42**, 378–384 (1987).
103. Y. Chisti and M. Moo-Young, *J. Chem. Technol. Biotechnol.* **42**, 211–219 (1988).
104. S. Wachi, A.G. Jones, and T.P. Elson, *Chem. Eng. Sci.* **46**, 657–661 (1991).
105. E. Garcia Calvo, *Chem. Eng. Sci.* **44**, 321–323 (1989).
106. R.S. Richardson and D.J. Higson, *Trans. Inst. Chem. Eng.* **40**, 169–182 (1962).
107. E. Garcia Calvo and P. Leton, *Chem. Eng. Sci.* **46**, 2947–2951 (1989).
108. H. Blenke, *Adv. Biochem. Eng.* **13**, 121–127 (1979).
109. Y.C. Hsu and M.P. Dudukovic, *Chem. Eng. Sci.* **35**, 135–141 (1980).

110. P. Ayazi Shamlou, D.J. Pollard, A.P. Ison, and M.D. Lilly, *Chem. Eng. Sci.* **49**, 303–312 (1994).
111. W.J. Lu, S.J. Hwang, and C.M. Chang, *Chem. Eng. Sci.* **30**, 1301–1310 (1995).
112. R.A. Bello, C.W. Robinson, and M. Moo-Young, *Biotech. Bioeng.* **27**, 369–381 (1985).
113. J. Zahradnik, M. Fialova, F. Kastanek, K.D. Green, and N.H. Thomas, *Trans. IChE* **73A**, 341–346 (1995).
114. P.R. Fields and N.K.H. Slater, *Chem. Eng. Sci.* **38**, 647–651 (1983).
115. T. Yamane, in J.A. Asenjo and J.C. Merchuk eds., *Bioreactor System Design*, Dekker, New York, 1994.
116. G. B.A.a.M. Buffham and G. Mason, *Chem. Eng. Sci.* **48**, 3879–3887 (1993).
117. O. Levenspiel and K.B. Bishoff, *Adv. Chem. Eng.* **4**, 95–126 (1963).
118. Y. Murakami, T. Hiroshe, S. Ono, and T. Nishijima, *J. Chem. Eng. Jpn.* **15**, 121–126 (1982).
119. C.H. Lin, B.S. Fang, H.Y. Wu, T.F. Fang, T.F. Kuo, and C.Y. Hu, *Biotechnol. Bioeng.* **18**, 1557–1562 (1976).
120. J.C. Merchuk and J.A. Asenjo, *Bioreactor System Design*, Dekker, New York, 1994.
121. K. Schügerl, *Adv. Biochem. Eng.* **19**, 71–94 (1981).
122. Moor Nagar, Graduate Thesis, Ben Gurion University, Dept. of Chemical Engineering, 1992.
123. M.H. Siegel, M. Hallaile, and J.C. Merchuk, in A. Mizrahi ed., *Advances in Biotechnological Processes*, Liss, New York, 1988, pp. 79–124.
124. W.J. Lu, S.J. Hwang, and C.M. Chang, *Ind. Eng. Chem. Res.* **33**, 2180–2186 (1994).
125. M. Siegel and J.C. Merchuk, *Influence of the Gas-Liquid Separator on Air-Lift Reactor Design and Operation*, 1990.
126. S.P. Godboole and Y.T. Shah, *Design and Operation of Bubble Column Reactors*, Gulf, Houston, Tex., 1986.
127. W.D. Deckwer, R. Burckhart, and G. Zoll, *Chem. Eng. Sci.* **29**, 2177–2187 (1974).
128. J.B. Joshi, *Trans Inst. Chem. Eng.* **58**, 155–161 (1980).
129. P.R. Fields and N.K.H. Slater, *Biotechnol. Bioeng.* **26**, 719–723 (1984).
130. M.R. Makley and A. Keller, *Phylos. Trans. Roy. Soc. London*, **278**, 1276–1281 (1975).
131. S. Frehlich, M. Lotz, T. Korte, A. Lübbert, K. Schügerl, and M. Seekamp, *Biotech. Bioeng.* **38**, 43–48 (1991).
132. M. Nakanoh, F. Yoshida, *Ind. Eng. Chem. Process Des. Dev.* **19**, 190–195 (1980).
133. J.C. Merchuk, S. Yona, M.H. Siegel, and A. Ben-Zvi, *Biotech. Bioeng.* **35**, 1161–1163 (1990).
134. S.P. Godbole, A. Schumpe, Y.T. Shah, and N.L. Carr, *AIChE J.* **30**, 213–220 (1984).
135. R.B. Bird, *Chem. Eng.* **27**, 102–109 (1993).
136. E. Molina-Grima, Y. Chisty, and M. Moo-Young, *J. Biotechnol.* **52**, 195–201 (1997).
137. V. Linek, V. Vacek, and P. Benes, *Chem. Eng. J.* **34**, 11–34 (1987).
138. T. Philichi, L. Stenstrom, K. Michael, *J. Water Pollut. Control Fed.* **4**, 83–86 (1989).
139. C.F. Mignone and J. Ertola Rodolfo, *J. Chem. Technol. Biotechnol.* **34**, 121–126 (1984).
140. Y. Kawase and M. Moo-Young, *Biotechnol. Bioeng.* **30**, 345–347 (1987).
141. J.C. Merchuk, S. Ben-Zvi, and K. Niranjan, *TibTech* **12**, 501–511 (1994).
142. W.D. Deckwer, *Bubble Column Reactors*, Wiley, New York, 1991.
143. M. Siegel, S. Ben-Zvi, and J.C. Merchuk, *Measurement and Interpretation of Mass Transfer Data in Air-Lift Bioreactors*, Kuyngju, Korea, 1990, pp. 449–453.
144. G. Andre, C.W. Robinson, and M. Moo-Young, *Chem. Eng. Sci.* **38**, 1845–1854 (1983).
145. J.C. Merchuk, G. Osemberg, M. Siegel, and M. Shacham, *Chem. Eng. Sci.* **47**, 2221–2226 (1992).
146. S.-J. Hwang, W.-J. Lu, *Chem. Eng. Sci.* **52**, 853–857 (1997).
147. J.C. Merchuk, *TibTech*, **8**, 66–71 (1990).
148. M.E. Orazem and L.E. Erickson, *Biotechnol. Bioeng.* **21**, 69–88 (1979).
149. M. Siegel, M. Hallaile, and J.C. Merchuk, in A. Mizrahi ed. *Advances in Biotechnological Processes*, Liss, New York, 1988, pp. 51–75.
150. T.W. Barker and J.T. Worgan, *Eur. J. Appl. Microbiol. Biotechnol.* **13**, 77–82 (1981).
151. K. Koide, K. Horibe, H. Kawabata, and S. Ito, *J. Chem. Eng. Jpn.* **18**, 248–254 (1985).
152. Y. Chisti, K. Fujimoto, and M. Moo-Young, *Biotechnol. Prog.* **5**, 72–76 (1988).
153. I.S. Suh., A. Schumpe, and W.D. Deckwer, *Can. J. Chem. Eng.* **69**, 506–512 (1991).
154. M.Y. Chisti and M. Moo-Young, *Biotechnol. Bioeng.* **31**, 487–494 (1988).
155. Y.T. Shah, B.G. Kelkar, S.P. Godbole, and W.D. Deckwer, *AIChE J.* **38**, 353–359 (1982).
156. V.G. Levich, *Physicochemical Hydrodynamics*, Prentice Hall, Englewood Cliffs, N.J., 1962.
157. A.N. Kolmogoroff, *Dokl. Akad. Nauk SSSR* **66**, 1949.
158. N. Blakebrough, I.A. Fatile, W.J. McManamey, and G. Walker, *Chem. Eng. Res. Des.* **61**, 383–387 (1983).
159. K. Koide, M. Terasawa, and H. Takekawa, *J. Chem. Eng. Jpn.* **19**, 341–344 (1986).
160. R.S. Douek, G.F. Hewitt, and A.G. Livingston, *Trans. Inst. Chem. Eng.* **73A**, 336–340 (1995).
161. A.G. Livingstone and S.F. Zhang, *Chem. Eng. Sci.* **48**, 1641–1654 (1993).
162. J.C. Merchuk and M. Herskowitz, *Can. J. Chem. Eng.* **64**, 57–62 (1986).
163. L.S. Fan, S.J. Hwang, and A. Matsuura, *Chem. Eng. Sci.* **39**, 1677–1681 (1984).
164. D. Petrovic, D. Posarac, and D. Skala, *Chem. Eng. Sci.* **44**, 997–998 (1989).
165. D. Petrovic, D. Posarac, A. Dudukovic, and D. Skala, *Chem. Eng. Sci.* **45**, 2967–2970 (1990).
166. M. Immich and U. Onken, *Chem. Eng. Sci.* **47**, 3379–3386 (1992).
167. L.S. Fan, K. Fujie, and T.R. Long, *AIChE Symp. Ser.* **80C24T**, 102–107 (1984).
168. K. Koide, K. Horibe, H. Kawabata, and S. Ito, *J. Chem. Eng. Jpn.* **18**, 248–254 (1985).
169. K. Koide, K. Shibata, H. Ito, S.Y. Kim, and K. Ohtaguchi, *J. Chem. Eng. Jpn.* **25**, 11–16 (1992).
170. M.D. Gluz and J.C. Merchuk, *Chem. Eng. Sci.* **51**, 1920–1925 (1996).
171. K.B. Kushalkar and V.G. Pangarkar, *Chem. Eng. Sci.* **49**, 139–144 (1994).

172. G. Rossi, *Biohidrometallurgy*, McGraw-Hill, Hamburg, Germany, 1990.
173. B.C. Smith and D.R. Skidmore, *Biotechnol. Bioeng.* **35**, 483–491 (1990).
174. A. Assa and R. Bar, *Biotechnol. Bioeng.* **38**, 1325–1330 (1991).
175. J. Schmidt, R. Nassar, and A. Lubbert, *Chem. Eng. Sci.* **47**, 2295–2300 (1992).
176. J.B. Snape and N.H. Thomas, *Biotechnol. Bioeng.* **40**, 337–345 (1992).
177. N.M.G. Oosterhuis, Ph.D. Thesis, Dept. of Chemical Technology, Univ. of Technology, Delft, The Netherlands, 1984.
178. N.W.F. Kossen and N.M.G. Oosterhuis, in N.J. Rhem and J. Reed eds. *Biotechnology* VCH, Weinheim, Germany, 1985.
179. A.P.J. Sweere, K.C.A.M. Luyben, and N.W.F. Kossen, *Enzyme Microb. Technol.* **9**, 386–392 (1987).
180. C. Sola and F. Godia, in J.A. Asenjo, J.C. Merchuk eds., *Bioreactor System Design*, Dekker, New York, 1994.
181. F.H. Johnson, H. Eyring, and M.J. Polissar, *The Kinetic Basis of Molecular Biology*, Wiley, New York, 1954.
182. D.G. Jordan, *Chemical Process Development*, Volume 6, Wiley, New York, 1968.
183. H. Taguchi, T. Imanaka, S. Teramoto, M. Takatsu, and M. Sato, *J. Ferment. Technol.* **46**, 823–830 (1986).
184. H. Takei, K. Misusawa, and F. Yoshida, *Ferment. Technol.* **53**, 151–156 (1975).
185. J.A. Roels, *Energetics and Kinetics in Biotechnology*, Elsevier, Amsterdam, 1983.
186. B. McNeil and B. Kristiansen, *Biotechnol. Lett.* **9**, 101–107 (1987).
187. P.M. Doran, *Adv. Biochem. Eng. Biotechnol.* **48**, 115–168 (1993).
188. D.J. Pollard, A.P. Ison, P. Ayazi Shamlou, and M.D. Lilly, *The Examination of Bioreactor Heterogeneity with Rheological Different Fermentation Broths*, Kluwer, Dordrecht, The Netherlands, 1994, pp. 163–170.
189. F. Potucek, *Collect. Czech. Chem. Commun.* **55**, 981–986 (1990).
190. P.D. Gaspillo and S. Goto, *J. Chem. Eng. Jpn.* **24**, 680–682 (1991).
191. Y. Chisti, M. Kasper, and M. Moo-Young, *Can. J. Chem. Eng.* **68**, 45 (1990).
192. S.Q. Zhou, L.M. Tang, and K. Schugerl, *J. Biotechnol.* **28**, 165–177 (1993).
193. Y. Bando, M. Nishimura, H. Sota, S. Suzuki, and N. Kawase, *Chem. Eng. Sci.* **47**, 3371–3378 (1992).
194. Y. Bando, M. Nishimura, A. Hayaashi, S. Hiura, S. Indo, and A. Idota, *J. Chem. Eng. Jpn.* **28**, 225–227 (1995).
195. T.K. Ghosh, B.R. Maiti, and B.C. Bhattacharyya, *Biotechnol. Tech.* **7**, 301–307 (1993).
196. C. Schlotelburg, M. Gluz, M. Popovic, and J.C. Merchuk, *Int. Symp. on Bubble Columns*, Kyoto, Nov. 1997.

See also BIOREACTORS, CONTINUOUS STIRRED-TANK REACTORS; BIOREACTORS, FLUIDIZED-BED; BIOREMEDIATION; ENZYMES, IMMOBILIZATION METHODS; FERMENTATION MONITORING, DESIGN AND OPTIMIZATION; MASS TRANSFER; RHEOLOGY OF FILAMENTOUS MICROORGANISMS, SUBMERGED CULTURE; SCALE-UP, STIRRED TANK REACTORS.

BIOREACTORS, CONTINUOUS STIRRED-TANK REACTORS

MICHAEL E. LASKA
CHARLES L. COONEY
Massachusetts Institute of Technology
Cambridge, Massachusetts

KEY WORDS

Chemostat
Continuous culture
Continuous stirred-tank reactor (CSTR)

OUTLINE

INTRODUCTION

Definitions

A continuous stirred-tank reactor (CSTR) is defined as an agitated vessel with continuous addition and removal of material and energy. The CSTR is one of the basic continuous reactor types widely used in the chemical process industries because of its amenability to process control and scale-up, although in biotechnology applications the CSTR is used more often as a research tool than as a production technology. An idealized, well-mixed CSTR can be modeled as having no spatial variations in temperature, concentration, fluid properties, or reaction rates. Thus, the properties of the exit stream may be considered the same as those throughout the vessel. Although such ideal mixing is never observed, the vessel is designed to provide good mixing through selection of operating conditions and vessel, baffle, and impeller geometries. The stirred tank used in continuous bioprocesses is similar to that used in batch bioprocesses, with the exception that the CSTR likely has an overflow or other level control device. Oxygen can be introduced into the vessel by sparging through inlets at the base of the vessel, where impellers then disperse the bubbles. Vessel jacketing or internal cooling coils provide a means for heat transfer. Continuous systems that are not agitated vessels often are modeled as CSTRs when their behavior

approximates that of the ideal CSTR. CSTRs are also known as backmix reactors, continuous-flow stirred-tank reactors (CFSTRs), or chemostats, when used for cell growth.

Strategy for CSTR Analysis

The performance and analysis of a CSTR is based on the material and energy conservation balances and the underlying processes governing the reaction kinetics. Because of the large variety of CSTR applications and limited space for discussion in this article, a brief outline of the steps in systems analysis will be beneficial in understanding any CSTR-based process.

The strategy for analyzing CSTR performance first requires defining the problem statement and goals. The second step is system identification, which includes defining the system boundaries and the interactions between the system and its environment across the system boundaries. The system could be a cell, the fluid in the reactor, or an entire bioprocessing plant. The third step is to identify the state variables that characterize the system. During the course of the analysis, new state variables may be identified and added to the original list. The fourth step is to characterize the state of the system using material and energy balances that account for the accumulation of mass and energy. In a general balance for a particular quantity, the rate of accumulation of that quantity in the system is equal to the net influx of the quantity across the system boundaries plus the rate at which the quantity is generated. Separate material balances are written for the reactants, products, and the catalyst (e.g., cells or enzymes). The final step is to calculate performance metrics and revisit the assumptions to determine the conditions under which they are valid.

REACTION KINETICS

This section discusses the theory governing ideal CSTR performance in two important bioprocess applications (cell growth and enzyme reactions), the underlying assumptions of the theory, and some practical aspects associated with CSTR operation.

Cell Growth

Introduction. Cell growth occurs in response to the environment. It is useful to classify growth in four mechanistic categories and identify those features relevant to the analysis of CSTRs. These classes are fission, budding, mycelial, and viral growth. The modes of growth serve to highlight the impact of morphology on bioprocessing considerations.

Bacteria grow by a process of binary fission yielding two identical daughter cells with doubling times typically between 0.5 and 3.0 h. The high specific growth rates of bacteria make them especially suitable for many CSTR applications; however, high O_2 requirements and metabolic heat generation become important considerations in bioprocess scale-up. Animal cells (5 to 20 μm) are much larger than bacteria ($\sim$1 μm) and yeast (5 to 10 μm) cells but grow more slowly, with typical doubling times between 18 and 48 h. Because of their larger size and lack of a protective cell wall, mammalian cells are particularly sensitive to the fluid shear in the vessel as well as to the osmotic pressure of the medium. Mammalian cells grow over a narrow range of osmotic/pressures and pH and typically have more complex nutritional requirements than bacteria and yeasts do.

Cell division in yeast occurs primarily by budding, with typical doubling times between 1 and 3 h. The budding process leads to a mother and a daughter cell, each having different growth rates and cell surface characteristics. Unlike bacterial cultures, yeast cell populations have a broad and time-varying distribution of ages and properties that may influence the formation of a desired product.

Mycelial growth occurs in molds, actinomycetes, and some yeasts by a process of hypha chain elongation and branching. Mycelial cultures also are characterized by a distribution of ages, with younger cells located at the hyphal tips. The hyphae form intertwined cellular strands, or mycelia, that increase the broth viscosity and lead to nonideal fluid mixing. High broth viscosity can be problematic for process monitoring and control, cell separation and recycle, and oxygen and heat transfer. Furthermore, fluid shear in the vessel can cause hyphal breakage and the formation of denser, more highly branched pellets or flocs. Cells in these pellets may be exposed to different microenvironments because of mass transfer limitations, which can vary with culture conditions and influence important cell properties.

Viral growth initially requires the infection of a host cell, which occurs by attachment of the virus to the cell surface and injection of viral nucleic acids into the cell interior. New viruses are constructed from biological molecules synthesized by the host cell under the direction of the viral genome. Viral nucleic acid is replicated many times (e.g., $>$500) and encapsulated in coat proteins to form a large number of new viral particles. Viral growth can proceed to one of two phases. In the lytic cycle, the host cell will lyse or break open and release infectious viral particles, whereas in the lysogenic cycle, the viral DNA will be integrated into the host cell DNA and the host cell will continue to reproduce normally.

CSTRs used for cell growth are commonly referred to as chemostats or turbidostats, depending on the strategy used to control the vessel environment. The most common arrangement is the chemostat (1–3), in which the medium fed to the vessel is designed so that all but a single nutrient essential for growth are present in excess of the cells' requirements. Any nutrient necessary for growth can be used to control the size of the cell population in the vessel, making the chemostat a flexible tool to study cellular behavior under different nutrient limitations. In a turbidostat, the cell concentration in the vessel is maintained constant by monitoring the optical density of the culture and modulating the medium feed rate to achieve a set point optical density. When the optical density rises above the set point, the feed rate is increased and, because the fluid volume is maintained constant by an overflow device, the well-mixed culture is diluted and the optical density approaches the set point value. The turbidostat is less commonly used because of difficulties in continuously monitoring the cell con-

centration. Its main utility is to control the growth rate near the maximum growth rate, an operating region in which the chemostat is less stable.

Material Balances. Cell mass is most often used to quantify microbial growth and usually is proportional to cell number under conditions of balanced growth, in which cellular chemical and physical properties are preserved in subsequent generations. Material balances based on cell number may have particular utility for some applications, such as mammalian cell culture, where number rather than mass is the conventional method of analysis. One may need to be wary of variations in cell size and morphology that may not be apparent from measurements of cell mass or number. The material balance for a uniform cell population in a CSTR can be written as shown in equation 1, in which $\mu[h^{-1}]$ represents the specific growth rate and $\alpha[h^{-1}]$ represents the specific rate of cell lysis and/or endogenous metabolism (i.e., resulting in a decrease in cell mass). The specific growth and death rates differ among organisms and are functions of the cell environment (e.g., pH, temperature, nutrients).

$$\underbrace{F \cdot X_0}_{\text{CELLS IN}} - \underbrace{F \cdot X}_{\text{CELLS OUT}} + \underbrace{V \cdot \mu \cdot X}_{\text{CELL GROWTH}} - \underbrace{V \cdot \alpha X}_{\text{CELL LYSIS}} = \underbrace{\frac{d(V \cdot X)}{dt}}_{\text{ACCUMULATION}} \tag{1}$$

It may be necessary to reformulate the cell balance if the cell population is significantly differentiated; examples include mixed cultures, mammalian cell culture, and recombinant fermentations with plasmid instability (see "Selection/Mutation and Contamination"). If we assume the system is operating at steady state and there is no accumulation of fluid or cells in the vessel, then the time derivative can be set to zero. Under normal bioprocessing conditions, cell death is assumed to be negligible (i.e., $\mu \gg \alpha$). Bacterial and yeast cells maintain approximately complete viability except in suboptimal environments and at very low dilution rates, whereas in mammalian cell culture, viability and cell lysis may vary significantly with time.

Assuming that the feed to the reactor is sterile ($X_0 = O$), the material balance reduces to equation 2, in which the specific growth rate is equal to the liquid flow rate from the vessel divided by the liquid volume. This quantity is called the dilution rate D (the inverse residence time for the CSTR) and has units of h^{-1}.

$$\mu = \frac{F}{V} = D \tag{2}$$

Equation 2 illustrates one of the most important attributes of the chemostat: that the specific growth rate can be controlled by manipulating the dilution rate. Control of the specific growth rate, combined with the ability to maintain a constant, defined cell environment, makes the chemostat a powerful experimental tool with which to investigate the many factors that influence cell growth, metabolism, and product formation. It is as an investigative tool, rather than as a production technology, that continuous culture has found its widest and most successful application.

A second material balance can be written for the growth-limiting substrate (S) using an *allocation model* for substrate utilization, in which substrate uptake is divided into cell growth, cell maintenance, and product formation components.

$$\underbrace{F \cdot S_0}_{\text{SUBSTRATE IN}} - \underbrace{F \cdot S}_{\text{SUBSTRATE OUT}} - V \cdot \left(\underbrace{\frac{\mu \cdot X}{Y_{X/S}}}_{\text{GROWTH}} + \underbrace{m \cdot X}_{\text{MAINTENANCE}} + \underbrace{\frac{q_P \cdot X}{Y_{P/S}}}_{\text{PRODUCT FORMATION}} \right) = \underbrace{\frac{d(V \cdot S)}{dt}}_{\text{ACCUMULATION}} \tag{3}$$

In this equation, $Y_{X/S}$ is the cell yield (or dry cell weight, DCW) on substrate (g DCW/g substrate), m is the cell maintenance coefficient (g substrate/g DCW $\times$ h), q_P is the specific product formation rate (g product/g DCW $\times$ h), and $Y_{P/S}$ is the mass yield of product on substrate (g product/g substrate). Each specific yield coefficient describes the allocation of substrate to cells, product, or maintenance. Depending on whether the fermentation goal is to produce cells (biomass) or a metabolic product, it may be possible to simplify the substrate balance by assuming that some uptake terms are dominant. The following sections describe the analysis of biomass production and product formation.

Biomass Production. In the case of biomass production, in which the goal of the fermentation is to produce cells, the large majority of nutrient uptake goes toward cell growth. The rate of substrate uptake for growth is assumed to be much greater than that for maintenance (i.e., $\mu/Y_{X/S} \gg m$) and product formation (i.e., $\mu/Y_{X/S} \gg q_P/Y_{P/S}$). Assuming the system is at steady state, the substrate balance (equation 3) can be rewritten and solved for the cell concentration using equation 2.

$$X = Y_{X/S} \cdot (S_0 - S) \tag{4}$$

To determine the relationship between the specific growth rate and the cell environment, a suitable growth model must be adopted. The simplest and most common relationship used is the unstructured Monod growth model, in which cell growth is a function of a single limiting substrate, usually the carbon source. Alternative unstructured growth models are given in Table 1. These unstructured growth models are empirically derived from observations of chemostat behavior, and their applicability to dynamic-batch or fed-batch processes should not be assumed. Some unstructured models (e.g., substrate inhibition) can have more than one solution, making different steady states possible depending on the starting conditions. Structured models, which typically account for either changes in cell composition, intracellular concentra-

Table 1. Common Unstructured Growth Models

Monod		
$\mu = \frac{\mu_{max} \cdot S}{K_S + S}$		
Modified monod		
$\mu = \frac{\mu_{max} \cdot S^{\lambda}}{K_S + S^{\lambda}}$ where λ is an adjustable parameter		
Inhibition models	**Noncompetitive**	**Competitive**
Substrate inhibition	$\mu = \frac{\mu_{max} \cdot S}{(K_S + S) \cdot \left(1 + \frac{S}{K_I}\right)}$	$\mu = \frac{\mu_{max} \cdot S}{K_S + S + \left(\frac{K_S}{K_I}\right) \cdot S}$
Product inhibition	$\mu = \frac{\mu_{max} \cdot S}{(K_S + S) \cdot \left(1 + \frac{P}{K_P}\right)}$	$\mu = \frac{\mu_{max} \cdot S}{K_S + S + \left(\frac{K_S}{K_P}\right) \cdot P}$

tions (4), or cell morphology (5), have been proposed in varying degrees of complexity (6,7). Structured models can have utility when such properties significantly influence the kinetics and are required to accurately describe behavior (such as in dynamic process modeling).

$$\mu = \frac{\mu_{max} \cdot S}{K_S + S} = D \tag{5}$$

In the Monod model, μ_{max} is the maximum specific growth rate of the organism, and K_S, called the saturation constant, is inversely proportional to the cell's affinity for the substrate. The value of K_S is typically quite low (1 to 5 mg/L for *Escherichia coli* on glucose), which means that $\mu \approx \mu_{max}$ when $S > 10K_S$ and that μ only becomes a strong function of the substrate concentration when $S < 10K_S$.

Note that the maximum specific growth rate of the organism limits the extent to which the dilution rate can be increased.

$$\mu_{max} = D_C \tag{6}$$

This threshold dilution rate is called the critical dilution rate (D_C), and increasing the dilution rate beyond D_C results in "washout"; cells are removed from the vessel at a rate faster than their growth rate. This can limit the productivity of the simple CSTR and motivates cell retention or recycle strategies that enable operation at higher throughputs.

Rearranging the growth model to solve for the substrate concentration in the vessel gives

$$S = \frac{D \cdot K_S}{\mu_{max} - D} \tag{7}$$

At dilution rates above D_C, cells have been washed out of the vessel, and the substrate concentration equals the inlet concentration (S_O). By substituting equation 7 into equation 4, the cell concentration becomes an explicit function of D and S_O.

$$X = Y_{X/S} \cdot \left(S_0 - \frac{D \cdot K_S}{\mu_{max} - D}\right) \tag{8}$$

The biomass productivity of the CSTR (R_{CSTR}), defined as the cell output per reactor volume, is calculated as

$$R_{CSTR} = \frac{F \cdot X}{V} = (D \cdot X) = D \cdot Y_{X/S} \cdot \left(S_0 - \frac{D \cdot K_S}{\mu_{max} - D}\right) \tag{9}$$

Figure 1 shows the steady-state cell and substrate concentrations and biomass productivity for the ideal chemostat. Note that the substrate is almost completely utilized

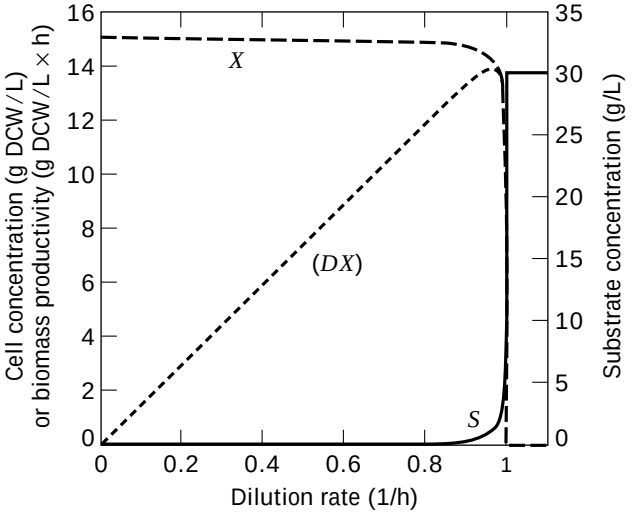

Figure 1. Ideal chemostat performance: $\mu_{max} = 1.0\ h^{-1}$, $K_S = 0.05$ g/L, $S_0 = 30$ g/L, $Y_{X/S} = 0.5$ g DCW/g substrate.

over most of the operating dilution rates. This high conversion of substrate is a key attribute of the ideal CSTR system, improving the economics of processes that depend on efficient substrate utilization and minimizing the effects of substrate inhibition. Also shown in Figure 1 is the high concentration of cells in the vessel until washout at the critical dilution rate. The maximum biomass productivity is located close to the washout point, making operation at the maximum productivity point very sensitive to deviations in dilution rate.

The dilution rate associated with maximum biomass productivity for a fixed limiting nutrient concentration in the feed (D_M) can be calculated by setting the derivative of (DX) with respect to D to zero and solving for the dilution rate. D_M is then given as

$$D_M = \mu_{max}\left(1 - \sqrt{\frac{K_S}{K_S + S_0}}\right) \tag{10}$$

By substituting D_M into equation 8, we can solve for X_M, the cell concentration corresponding to D_M.

$$X_M = Y_{X/S}\left[S_0 + K_S - \sqrt{K_S(S_0 + K_S)}\right] \tag{11}$$

Considering the limiting nutrient concentration (S_0) as an independent design variable, equation 11 suggests that the substrate concentration in the feed can be increased arbitrarily to achieve extraordinary cell densities and productivities. In reality, the productivity of an aerobic reactor system is ultimately limited by the rates of heat and/or mass transfer when the reaction kinetics are fast (i.e., high X and D) (see "Mass Transfer"). Oxygen transfer, and not the carbon substrate, is often growth limiting because oxygen is an essential nutrient for aerobic metabolism. It is poorly soluble in the medium (typically around 7 mg/L for air at 1 atm), and its transfer rate is restricted by the physical capabilities of the oxygenation system. Oxygen-limited growth may be expressed as a steady-state balance between the oxygen uptake rate (OUR) and the oxygen transfer rate (OTR). Oxygen transfer is usually limited by transfer from the gas to liquid phases, leading to the steady-state balance:

$$\underbrace{\left(\frac{\mu \cdot X}{Y_{X/O_2}} + m_{O_2} \cdot X\right)}_{OUR} = \underbrace{k_L a(C^* - C_L)}_{OTR} \tag{12}$$

in which Y_{X/O_2} is the cell yield on oxygen (g DCW/g O_2), m_{O_2} is the maintenance coefficient for oxygen (g O_2/g DCW $\times$ h), k_L is the liquid phase mass transfer coefficient (cm/h) a is the specific interfacial area for mass transfer (cm^2/cm^3), $k_L a$ is the mass transfer coefficient (h^{-1}), and ($C^* - C_L$) is the driving force for mass transfer where C^* is the equilibrium oxygen concentration (mmol/L) and C_L is the dissolved oxygen concentration (mmol/L). Typical values for Y_{X/O_2} are located in Table 2. The ability of the heat transfer system to remove heat generated during microbial growth can also limit R_{CSTR}, as discussed in "Energy Balance". These limitations will be important in evaluating and comparing CSTR performance.

Table 2. Yield Coefficients for Bacteria on Different Carbon Substrates

Substrate (i)	$Y_{X/S}$ [g DCW/g substrate]	Y_{X/O_2} [g DCW/g O_2]	Y_{HI} [g DCW/kcal]
Acetate	0.36	0.70	0.21
Glucose	0.51	1.5	0.42
Methanol	0.40	0.44	0.12
Ethanol	0.68	0.61	0.18
n-Paraffins	1.0	0.50	0.16
Methane	0.62	0.20	0.061

Source: From Ref. 16.

The biomass productivity of the CSTR can be compared to the productivity of a batch fermentor (R_{BATCH}) by defining a relevant batch productivity. The batch fermentation cycle consists of a lag phase, an exponential growth phase, cell harvest, and a batch turnaround time associated with cleaning, sterilizing, and filling the vessel. The lag, harvest, and turnaround activities can be grouped into a term $t_{TURNAROUND}$ in order to determine the batch cycle time (t_{CYCLE}) using equation 13, in which X_i is the concentration of cells in the vessel following inoculation (typically $X_i \sim 0.1 \times X$).

$$t_{CYCLE} = \frac{1}{\mu_{max}} \ln\left(\frac{X}{X_i}\right) + t_{TURNAROUND} \tag{13}$$

Cell growth can be calculated from the cell yield on the growth-limiting substrate and the initial concentration of substrate, again assuming cell maintenance and product formation are negligible.

$$X - X_i = Y_{Y/S} S_0 \tag{14}$$

Subsequently, the ratio of biomass productivities in the CSTR at D_M, $(R_{CSTR})_M$, and in the batch fermentor is given by equation 15, in which it is assumed that $S_0 \gg K_S$ (as it often is).

$$\frac{(R_{CSTR})_M}{R_{BATCH}} = \frac{(D_M \cdot X_M)}{\left(\frac{X - X_i}{t_{CYCLE}}\right)} = \ln\left(\frac{X}{X_i}\right) + \mu_{max} \cdot t_{TURNAROUD} \tag{15}$$

Equation 15 often appears as a measure of relative biomass productivity, in which the CSTR is favored over batch operation at high growth rates and long turnaround times. However, equations 10 and 11, associated with maximum productivity, do not reflect the ultimate limitation posed by heat and mass transfer in industrial aerobic processes. Given that productivity has a limit dictated by the system, the independent parameters, D and S_0, can be adjusted so that the maximum productivity is attained during operation. Recognizing that (R_{CSTR}) is ultimately limited by the maximum oxygen transfer rate, equation 12 can be rearranged to give the biomass productivity.

$$(D \cdot X) = \frac{D \cdot Y_{X/O_2} \cdot OTR_{MAX}}{(D + m_{O_2} \cdot Y_{X/O_2})} \tag{16}$$

Notice that the cell concentration is fixed once an operating

dilution rate is specified. Solving equation 16 for X and substituting into equation 4 yields

$$S_0 = \frac{Y_{X/O_2} \cdot OTR_{MAX}}{Y_{X/S} \cdot \delta_S \cdot (D + m_{O_2} \cdot Y_{X/O_2})} \quad (17)$$

where δ_S is the fractional substrate conversion. High substrate conversion leads to lower raw materials costs and reduces the burden of residual substrate on downstream purification and waste treatment operations. When operating near the maximum reactor productivity (i.e., maximum OTR), the dilution rate and the inlet substrate concentration can be adjusted independently to achieve target levels of cell concentration and/or substrate conversion, as shown in Figure 2.

For biomass production when O_2 transfer is not limiting productivity, the CSTR is favored over batch operation when the specific growth rate is high and the batch turnaround time is long. However, most industrial processes will be operating at or near the oxygen or heat transfer limitation. The desirability of enhanced O_2 transfer has motivated the development of novel bioreactor designs (e.g., bubble columns, loop or airlift reactors). For therapeutic products, however, the overwhelming majority of fermentations are batch or fed-batch processes. In these applications, the choice of operating mode is not based on biomass productivity. Performance metrics such as volumetric productivity of the product, product yield, and product concentration become more important in evaluating potential operating strategies than simply the biomass concentration.

Product Formation. When the goal of the fermentation is to produce a product other than biomass, the criteria used to evaluate alternative operational modes are less straightforward than biomass productivity. In order to evaluate process alternatives, a proper set of performance metrics must be identified that relate to overall process economics. When process economics are dominated by fermentation costs (e.g., fuel alcohol or gluconic acid production), volumetric productivity and conversion yields are especially relevant criteria as they relate to the size and cost of the reactor system and the cost of raw materials. In processes where recovery costs dominate (e.g., antibiotics), however, the size and operational costs of the recovery system are proportional to the fluid volume processed and inversely proportional to the product concentration (8). As a result, the final product concentration, or titer, is more important than biomass productivity.

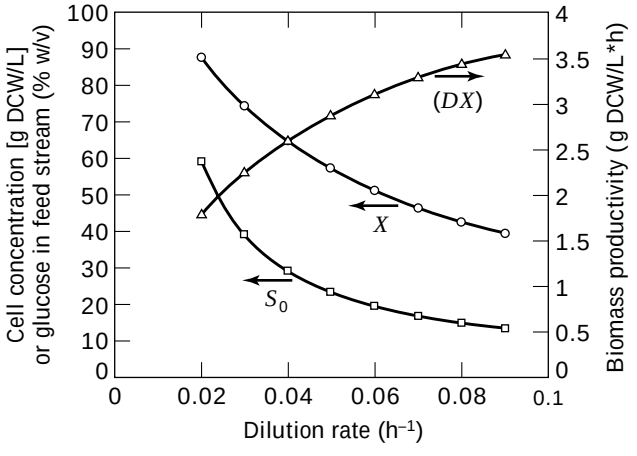

Figure 2. Chemostat operating at maximum oxygen transfer rate: OTR^{max} = 100 mmol O_2/L × h, μ_{max} = 0.09 h^{-1}, Y_{X/O_2} = 1.56 g DCW/g O_2, m_{O_2} = 0.024 g O_2/g DCW × h, $Y_{X/S}$ = 0.45 g DCW/g substrate, 95% substrate conversion.

The material balance on the product can be written as shown below, in which product formation is expressed using a specific product formation rate q_P (g product/g DCW × h), and product degradation by a specific rate constant $k_P(h^{-1})$.

$$\underbrace{q_P \cdot X}_{\text{PRODUCT FORMATION}} - \underbrace{k_P \cdot P \cdot D}_{\text{PRODUCT DEGRADATION}} - \underbrace{D \cdot P}_{\text{PRODUCT OUT}} = \underbrace{\frac{dP}{dt}}_{\text{PRODUCT ACCUMULATION}} \quad (18)$$

Product formation can be characterized in relation to growth, being growth (primary metabolites) or nongrowth (secondary metabolites) associated. Examples of growth-associated products are direct catabolic products of the carbon substrate, such as ethanol and citric or acetic acid. Nongrowth-associated products, comprising many antibiotics, are metabolites that are not necessary for cell growth and typically are only produced during slow or stationary growth phases. Some products, such as xanthan gum and lactic acid, are mixed growth associated in that they are produced during slow and stationary growth phases. Numerous models of product formation have been proposed, taking into account variables such as hyphal morphology, cell age, surface area, metabolic carbon flux, and plasmid copy number. A simple model expresses the growth dependence of q_P as (9)

$$q_P = \underbrace{\alpha \cdot \mu}_{\text{GROWTH ASSOCIATED}} + \underbrace{\beta}_{\text{NONGROWTH ASSOCIATED}} \quad (19)$$

The steady-state product balance can be rewritten and solved for P.

$$P = \frac{q_P \cdot X}{D} = \frac{(\alpha \cdot \mu + \beta)}{D} \cdot X = \left(\alpha + \frac{\beta}{D}\right) \cdot X \quad (20)$$

For growth-associated products (i.e., $\alpha \gg \beta$) product concentration is proportional to biomass and is independent of the dilution rate when X is approximately constant. Increasing the dilution rate results in increased product formation up to the region near D_C. The growth dependence of product formation and intracellular metabolic fluxes can be determined using a chemostat (10). An example of growth-associated product formation is shown in Figure 3 (11), in which product concentration is proportional to biomass and the growth dependence of q_P is evident.

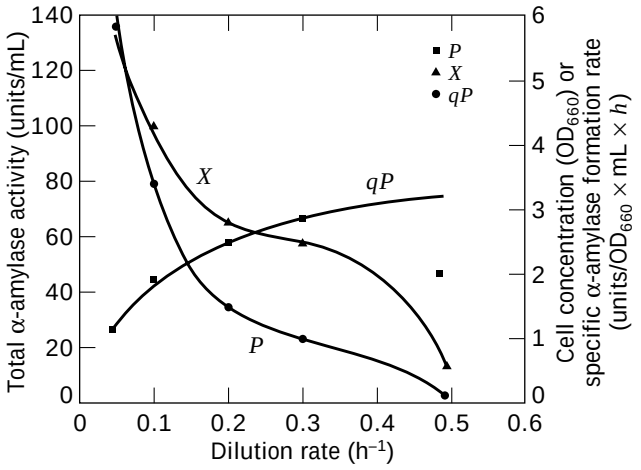

Figure 3. Production of α-amylase in a chemostat by recombinant *Escherichia coli*. The authors (11) used a modified Leudeking–Piret model, $q_P = (\alpha\mu + \beta)(1 + k\mu)^{-1}$, to describe α-amylase kinetics. The term $(1 + k\mu)^{-1}$ accounts for an observed increase in plasmid copy number with decreasing growth rate. Model parameters were regressed from data: $\alpha = 34.12$ units/mL $\times$ OD_{660}, $\beta = 4.2 \times 10^{-10}$ U/mL $\times$ OD_{660} $\times$ h, and $k = 8.63$ h. Experimental data are depicted as points, model predictions as solid lines, and trend lines as dotted lines.

In the case of secondary metabolites (i.e., $\alpha \ll \beta$), product concentration is inversely proportional to the dilution rate, and the productivity ($D \times P$) is independent of dilution rate. The low dilution rates favorable for secondary metabolite production approach batch operation, which is generally favored over the CSTR in such instances.

Other issues can impact the decision between batch and continuous culture. The ability of the CSTR to maintain an ideal environment for product formation may offer a competitive advantage over the batch fermentation, with its time-varying environment and prolonged lag and stationary growth phases. Regulatory and market factors also play an important role in deciding on the operating mode. The CSTR is a dedicated manufacturing system used to produce a single product. Such a system may not be well suited for the production of specialty chemicals and pharmaceuticals because it can neither adapt to variable market demand nor satisfy demand for multiple products.

Energy Balance. Heat transfer is an important consideration in fermentor design, scale-up, operation, and sterilization. The energy balance is used to determine the time–temperature profile of the fermentation broth by accounting for the transfer and accumulation of energy. The heat transfer rate limits the ability to reduce the cycle time for sterilization (12). More importantly, the rate of heat removal from the broth during cell growth can constrain volumetric productivity, an issue in very large reactors with reduced area-to-volume ratios. Because considerable heat generation accompanies rapid cell growth, the high specific growth rates favored in industrial CSTR applications will exacerbate the problem of heat transfer in large reactors. The steady-state energy balance for the fluid in the CSTR is written as

$$Q_{AGIT} + Q_{MET} + \Delta Q_{SENS} - Q_{LOSS} - Q_{EVAP} - Q_{EXCH} = 0 \quad (21)$$

in which Q_{AGIT} is the mechanical energy imparted to the fluid through impeller agitation (equal to the gassed power input), Q_{MET} is the metabolic heat generated by cell growth, ΔQ_{SENS} is the net sensible heat added to the system by streams entering and leaving the system, Q_{LOSS} is the sum of the heat losses from the system to the surroundings, Q_{EVAP} is the latent heat removed by evaporation, and Q_{EXCH} is the heat removed from the system by an appropriate heat exchanger system (13). In some cases, the heats of solution and mixing must be accounted for, but in most cases they are negligible. The terms ΔQ_{SENS}, Q_{LOSS}, and Q_{EVAP} are comparatively small, leading to the simplified energy balance

$$Q_{EXCH} = Q_{MET} + Q_{AGIT} \quad (22)$$

For fast-growing microorganisms, the heat exchanger duty can be as high as 7.7 to 23.2 kW/m^3, of which Q_{MET} and Q_{AGIT} typically represent about 75% and 25% of the total, respectively (14).

Approximately 40 to 50% of the energy contained by a substrate is converted into useful chemical energy, whereas the balance is released as heat. If this metabolic heat is not removed from the fermentation broth, the temperature will rise and possibly hinder performance. Metabolic heat generation is a function of the growth rate of the organism, the cell concentration, the fluid volume, and the efficiency of cell growth on a particular substrate (i), which can be expressed as the metabolic heat released per gram of cell produced ($1/Y_{Hi}$) (kcal/g DCW).

$$Q_{MET} = V\frac{\mu \cdot X}{Y_{Hi}} \quad (23)$$

In aerobic fermentations, oxygen is the final electron acceptor in substrate metabolism, enabling a correlation between the rates of oxygen uptake and heat generation. The following empirical correlation (15) gives Q_{MET} (kcal/h) as a function of specific oxygen consumption, q_{O_2} (mmol O_2/L $\times$ h), and V(L):

$$Q_{MET} = 0.12 \cdot V \cdot q_{O_2} \quad (24)$$

where the oxygen demand during exponential growth can be expressed using the cellular yield on oxygen, Y_{X/O_2} (g DCW/g O_2).

$$Q_{O_2} = \frac{\mu \cdot X}{Y_{X/O_2}} \quad (25)$$

Table 2 gives values of Y_{Hi} and Y_{X/O_2} for bacterial growth that can be used to estimate oxygen demand and metabolic heat generation. Notice that the more reduced substrates result in greater O_2 demand and heat generation and subsequently a larger burden on the O_2 transfer and heat exchange system.

Heat exchange systems are chosen based on the expected heat exchanger duty, influence on fluid mixing, im-

pact on cleaning and sterilization, utility economy, and maintenance, operating, and capital costs. Heat exchangers for fermentors commonly consist of a jacket or shell around the vessel, internal coolant coils, or occasionally an external heat exchanger. The rate of heat removal by a heat exchanger system can be described using a Fourier's law expression:

$$Q_{\mathrm{EXCH}} = U \cdot A \cdot (T - Tc) \tag{26}$$

in which A is the surface area available for heat transfer, U is an overall heat transfer coefficient accounting for all heat transfer resistances, and $(T - Tc)$ is the driving force for heat transfer, where T is the bulk temperature of the fermentation broth and T_{C} is the temperature of the cooling fluid used in the heat exchanger. Typical values of the heat transfer coefficient are 50 to 150 BTU/ft^2 $\times$ h $\times$ °F (280 to 850 W/m^2 $\times$ K). An important consequence of fermentor scale-up is a decreasing surface-area-to-volume ratio (A/V): at increasing scale the capacity for heat removal relative to heat generation diminishes and often becomes limiting at larger volumes.

The rate of heat removal can be increased by increasing the temperature driving force, increasing the heat transfer surface area, or reducing resistance to heat transfer (increasing U). Water is primarily used as the coolant fluid because of its availability and low cost relative to a refrigerated coolant system. The temperature of the cooling water increases as it passes through the heat exchanger, so an arithmetic or logarithmic mean Tc may give a more representative measure of the coolant temperature. Increasing the coolant flow rate can decrease the mean coolant temperature but with a subsequent increase in utility consumption. Furthermore, the pressure drop of the exchanger and pump capacity limit the extent to which coolant flow rate can be increased. The heat exchanger area is dictated by the size and type of heat exchange system chosen during process scale-up. The overall heat transfer coefficient and constituent resistances are thoroughly discussed elsewhere. In general, poor mixing contributes to decreased heat transfer (see "Nonideal Mixing"). It is sufficient to focus on the convective heat transfer coefficient on the fermentation broth side, h[W/m^2 $*$ K], which is often the dominant heat transfer resistance. The convective heat transfer coefficient is a function of the Reynolds number (Re), Prandtl number (Pr), viscosity ratio (Vi), and the system geometry (F_{GEOMETRY}). In many cases $Vi \approx 1$, and the exponents a and b have typical values of 0.8 and 0.3, respectively.

$$Nu = C_1 \cdot Re^{\mathrm{a}} \cdot Pr^{\mathrm{b}} \cdot Vi^{\mathrm{c}} \cdot F_{\mathrm{GEOMETRY}}$$

$$\frac{h \cdot D_{\mathrm{T}}}{k} = C_1 \cdot \left(\frac{D_{\mathrm{i}}^2 N \rho}{\mu}\right)^{\mathrm{a}} \left(\frac{Cp\mu}{k}\right)^{\mathrm{b}} \left(\frac{\mu}{\mu_{\mathrm{w}}}\right)^{\mathrm{c}} F_{\mathrm{GEOMETRY}} \tag{27}$$

Economic Considerations. Operating costs are those costs associated with maintaining a given production level dictated by the scale and scheduling of the process, typically grouped as raw materials, direct expenses, and indirect expenses. Although the focus here will be on raw materials and direct expenses (e.g., utilities, maintenance, operating supplies, and labor) associated with the CSTR, it is important to view the reactor system in the context of the entire process. The process flow diagram will form the basis for determining not only the reactor operating costs but also the capital and operating costs of air compressors, pumps, holding tanks, and various downstream units. It is important to remember that the relative costs associated with the reactor system, batch or continuous, may not have a significant impact on the total process economics if product recovery costs are dominant (see "Product Formation"). Raw materials costs include the material and handling costs of components added to the system to satisfy metabolic (e.g., C, N, O sources) or process (e.g., acids or bases and antifoam agents) requirements. Direct expenses include the cost of utilities, maintenance, operating supplies, operating labor, direct supervision, laboratory charges, and patent royalties. Continuous systems are easier to automate and offer the potential of lower labor costs than batch production systems, with their labor intensive start-up and shut-down operations. Indirect expenses include taxes and depreciation, usually expressed as a percentage of the plant cost.

Media. The selection of bioprocess media typically involves a trade-off between media cost and the product yield and titer. It is an important stage of development that can influence the design and performance of the entire process. Selecting an apparently cheap media, for example, may result in more expensive downstream recovery and waste treatment operations. In general, media selection includes a number of technical and economic considerations: yield or titer of desired and undesired products; cost; variability in composition and price; availability; effect on downstream processes; need for pretreatment or supplements; shipment, storage, and handling, and need for testing and validation.

Media can be classified as defined or undefined with respect to chemical composition. Laboratory-scale chemostat investigations commonly use defined media to allow precise control over the growth-limiting nutrient and medium composition. Small bioreactors (1 to 4 L) are preferred for continuous operation in the laboratory because media preparation and storage are less of a burden. Industrial microbial fermentations predominantly use undefined media because they generally are less costly and perform better than defined media. Undefined microbial media often contain agricultural by-products (e.g., molasses or corn steep liquor) and thus are subject to source market fluctuations in quality and price. Processes that have been validated with a variety of media may change the production media to take advantage of market changes. The costs of raw materials as a percentage of operating costs for primary metabolites can range from 40% for citric acid to 70% for ethanol from sugar cane (17), whereas for secondary metabolites media costs can be around 10 to 20%. At small scale (less than 10 m^3), mammalian cells are often grown in undefined serum, an expensive and sometimes scarce media derived from mammalian plasma. Viral contamination and the presence of serum proteins can complicate cultivation, product recovery, and quality control and quality assurance (QA–QC) in industrial processes. These complications, combined with regulatory pressure to safeguard

against viral contamination, are a driving force toward the development of defined, serum-free media in order to avoid use of animal-derived media components.

Utility Expenses. Steam, cooling water, and power requirements comprise the majority of utility expenses. Process demand for water-for-injection (WFI) must also be determined for clean-in-place (CIP) systems. Steam usage occurs predominantly during media and equipment sterilization and can be calculated using knowledge of the sterilization cycle. Continuous reactors readily lend themselves to the use of continuous, as opposed to batch, media sterilization systems, offering advantages in reduced thermal degradation of heat-sensitive media, reduced sterilization time, more efficient fermentor use, and greater steam economy (about 20 to 25% of the steam used by batch sterilization) (12). The cooling water requirement, w_{H_2O} (kg/h), can be calculated knowing the heat exchanger duty from the energy balance (equation 21):

$$w_{H_2O} = \frac{Q_{EXCH}}{C_p \cdot (T_{out} - T_{in})} \tag{28}$$

where C_p is the heat capacity of water [$\sim$1 kcal/kg $*$ K] and T_{out} and T_{in} are the outlet and inlet cooling water temperatures, respectively. The availability of abundant low-temperature water can reduce cooling water requirements and possibly allow the use of larger reactors because of the improved ability to remove metabolic heat.

Oxygen demand and mixing requirements drive power consumption by agitators and compressors, whereas larger volumes, higher cell densities, higher specific O_2 uptake rates, and higher broth viscosities result in increased power requirements. Total power consumption for agitated vessels is typically in the range of 2 to 10 kW/m^3. Centrifugal pumps are predominantly used in bioprocesses for their relatively low cost and ability to handle suspended solids. Although pumps represent only a small fraction of power consumption, they can be a significant percentage of overall maintenance costs. In addition, the performance of continuous processes is particularly susceptible to pump failure and may warrant additional capital investment toward the installation of backup pumps in parallel.

Actual vs. Ideal Behavior. In this section, the assumptions used in the development of the ideal CSTR theory are revisited in order to determine when they are invalid and to gauge the impact of nonidealities on performance.

Nonideal Mixing. The major assumption of the ideal CSTR is that there are no spatial variations of properties inside the vessel. Such ideal mixing is never observed in actual systems and even deteriorates on scale-up, although it can be a good approximation of behavior. The challenge is to determine when nonidealities can be expected and how they will influence performance.

Equipment design, operating conditions, and broth properties all influence the quality of fluid mixing in the vessel. Agitated tanks are designed to provide good mixing through selection of tank geometry, baffle placement, and impeller design, although mixing quality decreases with increasing scale. Agitator power input and gas sparging rates, although typically associated with oxygen transfer, are critical to mixing. High broth viscosities, typical of mycelial fermentations, contribute to poor mixing. Poor mixing can affect oxygen transfer (18), product formation (19), heat transfer, process monitoring and control, and the distribution of components added to the system (20,21).

Nonideal mixing in continuous systems is typically characterized by either the residence time distribution, the distribution of fluid residence times around the ideal residence time (τ) (22), or the mixing time (t_M), the time required for a system to respond to a feed disturbance. The ideal mixing time is equal to zero (instantaneous), and the mean value of the residence time distribution is τ (or D^{-1}). Residence time distributions are typically measured by pulse or step addition of a tracer into the reactor feed and tracking the appearance of the tracer in the exit stream as a function of time. Correlations obtained from dimensional analysis can be used to predict mixing times, which increase with scale and broth viscosity (23). Small vessels ($<$500 L) are generally well mixed ($t_M \sim$ s), but large fermentors ($>$5,000 L) typically have poor mixing ($t_M \sim$ min). Compartmental mixing models, in which the bulk fluid is modeled as discrete CSTRs and plug flow reactors (PFRs) with fluid interchange, have been used to describe heterogeneity in large vessels (24).

Wall growth is a special case of nonideal mixing in which cells adhere and proliferate on vessel surfaces (25), where they are hidden from cell mass measurements obtained from samples of the bulk fluid. The system, in addition to being heterogeneous, is no longer at steady state because cells are accumulating in the vessel. This can pose serious problems if the accumulating organism is a contaminant or otherwise undesirable organism. The metabolism and growth of wall-bound cells can be quite different from the suspended population because of mass transfer limitations. Wall growth can reduce heat transfer, create sterilization and cleaning problems, and corrupt measurements in experimental systems. It can be a significant factor when the surface-area-to-volume ratio (A/V) is high (e.g., laboratory-scale systems and vessels with internal cooling coils) and may require modifications to chemostat design or operation (26). For example, the glass walls of laboratory vessels are sometimes treated with organosilane compounds to minimize wall growth. Yeast and mycelial cells with a propensity to form pellets are prone to wall growth under the same conditions that favor flocculation. A discrete washout point does not exist with wall growth, because cells are effectively immobilized in the vessel even past D_C.

Substrate Assumptions. Deviations from ideal chemostat behavior may arise when assumptions regarding the magnitudes of nutrient uptake, the consistency of cell composition, or the identity of the growth-limiting nutrient become invalidated. Substrate uptake for growth in equation 3 was assumed to be much larger than that for maintenance and product formation. At low dilution rates (i.e., low growth rates) the maintenance term becomes significant ($m \sim \mu/Y_{X/S}$) and less substrate goes toward cell growth, causing the actual X to be less than predicted by the ideal theory at low D. Similarly, at high dilution rates, the production and accumulation of growth-related prod-

ucts and intermediates can become significant, leading to a reduced cell yield at higher D.

The ideal chemostat derivation assumes that cell composition does not change over the operating region. In actuality, cell composition varies with pH, temperature, growth rate (27), and medium composition. As cell composition changes, the demand for essential nutrients will change in ways that were not accounted for in the derived equations. Proper evaluation of experimental data from a chemostat may require consideration of the variation of nutrient uptake and cell composition with environment and growth rate.

When using complex and undefined media or an organism with complex nutritional requirements (e.g., mammalian cells), it is often difficult to identify the growth-limiting nutrient. In addition, the limiting nutrient itself may change because the nutrient demand, and subsequently the media composition, may change with operating conditions. The cell concentration profile in these situations likely would be constantly decreasing with dilution rate, unlike the ideal chemostat where X is approximately constant over the majority of $0 < D < D_C$. More complicated, structured growth models would be required to account for such behavior.

Non-Steady-State Behavior. The potential sources of process variability and non-steady-state behavior are perhaps too numerous to mention. However, typical instances include chemostat start-up, execution of control actions, induced disturbances (e.g., pulse and shift methods [28]), variations in feed composition, culture degeneration (e.g., plasmid loss or apoptosis), wall growth, or equipment failures. Steady state often is declared when the measurable process states are maintained constant for 3 to 5 residence times. Sustained oscillations are sometimes observed in continuous culture and often are the result of growth inhibition resulting from either an accumulated product (29) or the burden of product formation (30).

Selection/Mutation and Contamination. By controlling the culture conditions in the CSTR, a highly selective environment for the selection and proliferation of certain microorganisms can be created. Cells in this selective environment with growth rates less than the dilution rate will be washed out of the reactor, leaving only those cells with the properties that have been selected for. In this way, continuous culture can be used as a strain improvement tool to select organisms that possess a desirable trait, such as yeast with higher ethanol tolerance (31).

Because of the metabolic burden imposed by high levels of product formation, the production strain has a growth disadvantage relative to unproductive strains that are present in the reactor. Without selection pressure in favor of the production strain, a gradual decline in productivity will be observed over time as nonproductive cells dominate the culture. Examples include the reversion of specially selected antibiotic strains to low productivity mutants or the domination of recombinant protein processes by plasmid-free cells. The configuration of CSTRs in series can be used to circumvent this problem by providing separate environments for growth and product formation (see "CSTRs in Series"). Selective pressure in favor of the production strain (and against contaminants) may be exerted through the application of elevated temperatures, extremes of pH, the use of narrowly defined or modified media, and the use of specially selected cultures (e.g., antibiotic-resistant strains).

The prolonged operating periods of continuous culture increase the probability of contamination by a foreign organism. The threat posed by contamination depends on the ability of the undesirable microorganism to complete and thrive in the CSTR environment. Consider the case of two types of microorganisms with concentrations X (the desired strain) and Z (the contaminant) competing for the same limiting substrate in a CSTR. The material balances on cell mass, neglecting cell lysis, can be written as

$$\frac{dX}{dt} = \mu \cdot X - D \cdot X \tag{29}$$

$$\frac{dZ}{dt} = \mu_z \cdot Z - D \cdot Z \tag{30}$$

Subtracting equation 30 from equation 29 and rearranging leads to equation 31:

$$\frac{d \ln[X/Z]}{dt} = \mu - \mu_z \tag{31}$$

which shows that the growth rates and their dependence on the limiting substrate will determine the fate of the culture (32). The contaminant (Z) could be washed out ($\mu > \mu_z$), remain at a stable level ($\mu = \mu_z$), or dominate ($\mu < \mu_z$) the culture. This simple analysis of selection can be complicated if the contaminant has properties that prevent it from being washed out (e.g., adhesion to reactor surfaces), if the contaminant competes for a different substrate than the production strain, or if there are interactions from inhibitory cellular products. For example, lactobacilli are often a persistent contaminant of continuous ethanol production processes because of their intimate association with flocculant yeast aggregates and ability to adapt to high ethanol concentrations (33). Selective recycle of desirable organisms back to the vessel has been used to prevent domination of the culture by undesirable strains (34–36).

Enzymes

Introduction. Enzymes are biological catalysts with high selectivity toward reactants and products, making them attractive for use in a number of industrial applications. Enzyme activity is strongly influenced by the environment (e.g., pH, temperature, metal ions). Loss of activity or denaturation can be reversible or irreversible, depending on the type, strength, and duration of an unfavorable interaction. A benefit of using the CSTR for enzyme reactions is that the constant, controlled reactor environment can be designed for maximum enzyme activity and life.

Material Balances. Assuming that the inlet and outlet flow rates are approximately equal (i.e., solutions are dilute), the steady-state material balance on the substrate can be written as

$$F \cdot (S_0 - S) = v \cdot V \tag{32}$$

where F is the volumetric flow rate, v is the rate of substrate consumption by reaction, V is the fluid volume in the reactor, and S_0 and S are the substrate concentrations in the feed and vessel, respectively. Rewriting equation 32 in terms of the fluid residence time (τ) and the fractional substrate conversion (δ_S) yields the CSTR design equation

$$\tau = \frac{V}{F} = \frac{S_0 \cdot \delta_S}{v} \tag{33}$$

Using a valid rate expression for v, the design equation can be used to determine the reactor volume required to yield a given conversion rate ($S_0 \times \delta_S \times F$). Fast reaction kinetics are obviously favorable because reactor cost scales with reactor size. Enzyme loading in the reactor can be increased beyond the solubility limit by immobilization on inert support particles, which increases v, reduces the necessary reactor volume, facilitates enzyme retention and recycle, and may improve enzyme stability.

Enzyme Reaction Kinetics. Numerous mechanistic models have been developed to describe enzyme reaction rates as a function of enzyme and substrate concentrations. Some of the more common models appear in Table 3 accompanied by the corresponding solution to the design equation (equation 33).

Unlike a plug flow reactor (PFR), in which the substrate enters at a high concentration and leaves at a lower concentration, the substrate concentration in a CSTR is at a uniform, low concentration. The reduced substrate concentration leads to a slower reaction rate, so that the CSTR requires more of the active enzyme than the PFR to attain the same substrate conversion rate. Substrate inhibition is less problematic in a CSTR than in a PFR because of the lower substrate concentration in the bulk fluid, whereas product inhibition is generally more of a problem in CSTRs than PFRs. Arranging CSTRs in series can reduce the effects of product inhibition (approaching PFR behavior) while taking advantage of the good mixing characteristics of the CSTR to provide optimal pH control (37).

Temperature Effects. Like many chemical reactions, increasing the temperature enhances the rate of enzyme reactions. Higher temperatures also result in increased rates of thermal denaturation and loss of the active biocatalyst. Process economics often depend on optimal temperature control to maintain high substrate conversion and long catalyst life (38–40). The effects of temperature on the catalytic rate constant (k_2) can be described using an Arrhenius expression

$$k_2 = A \cdot e^{-Ea/RT} \tag{34}$$

where A is the Arrhenius constant, E_a is the activation energy, R is the gas constant, and T is the absolute temperature. The activation energy of enzyme-catalyzed reactions ranges from 4 to 20 kcal/mol, with most reactions near 11 kcal/mol.

Thermal denaturation usually can be described as a first-order decay reaction:

$$\frac{dE}{dt} = -k_d \cdot E \text{ or } E = E_0 e^{-k_d t} \tag{35}$$

where k_d is the thermal denaturation constant, which also follows an Arrhenius temperature dependence. For thermal denaturation, E_a varies from 40 to 130 kcal/mol, with most in the vicinity of 70 kcal/mol. Increasing temperature has a greater effect on the rate of denaturation than catalysis. For a typical enzyme (i.e., 11 and 70 kcal/mol), an increase in temperature from 30 to 40 °C results in a 1.8-fold increase in the rate of catalysis, but a 41-fold increase in the denaturation rate.

Energy Balance. An optimal temperature control strategy requires good heat removal because most industrial enzyme reactions are exothermic. Although heat transfer is generally good for soluble enzymes in agitated tanks, the high enzyme concentrations attained with immobilization can result in fast reaction rates and appreciable heat generation. Heat transfer resistance within the catalyst pellet can reduce heat removal rates, resulting in higher pellet temperatures and shorter catalyst life. Catalyst degradation from insufficient heat removal is more of a concern in packed beds with high enzyme loading, where heat transfer resistances can be significant. The steady-state energy

Table 3. Some Common Enzyme Kinetic Expression

	Rate expression $v =$	Design equation $\tau =$
Michaelis–Menten	$\frac{v_{max} \cdot S}{K_m + S}$	$\frac{1}{v_{max}}\left[S_0 \cdot \delta_S + K_m \cdot \frac{\delta_S}{1-\delta_S}\right]$
Substrate inhibition	$\frac{v_{max} \cdot S}{S + K'_m + \frac{S^2}{K'_S}}$	$\frac{1}{v_{max}}\left[S_0 \cdot \delta_S + K'_m \cdot \frac{\delta_S}{1-\delta_S} + \frac{S_0^2}{K'_S} \cdot (\delta_S - \delta_S^2)\right]$
Competitive product inhibition	$\frac{v_{max} \cdot S}{K'_m\left(1 + \frac{P}{K_P}\right) + S}$	$\frac{1}{v_{max}}\left[S_0 \cdot \delta_S + K'_m \cdot \frac{\delta_S}{1-\delta_S} + \frac{K'_m}{K_P} \cdot \left(\frac{S_0 \cdot \delta_S^2}{1-\delta_S}\right)\right]$
	Where $v_{max} = k_2 \times E_0$	Where the product concentration (P) is related to converted substrate; $P = \delta_S \times S_0$

balance for an exothermic ($\Delta H_{RXN} < 0$) enzyme reaction in a well-mixed CSTR is

$$F\rho c_P(T_F - T) + v' \cdot E \cdot V(-\Delta H_{RXN}) - Q_{EXCH} = 0 \quad (36)$$

where F is the volumetric flowrate (m^3/h), ρ is the fluid density (kg/m^3), c_P is the fluid heat capacity (kJ/kg × K), v' is the specific reaction rate (kmol substrate/kg enzyme × h), E is the enzyme concentration (kg enzyme/m^3), ΔH_{RXN} is the heat of reaction (kJ/kmol substrate), Q_{EXCH} is the heat removed by the heat exchanger (kJ/h) from equation 26, and T_F and T are the feed and bulk fluid temperatures (K), respectively.

Economic Considerations. For enzyme CSTRs, the primary operating costs are associated with enzyme replacement. Prolonged catalyst activity and marked reductions in raw materials costs can be achieved by maintaining an optimal environment for the enzyme during operation. Preserving enzyme activity reduces the number and frequency of labor-intensive cleaning and changeovers, facilitating downstream operations by consistently providing a constant-quality product stream. With multiple reactors installed in parallel, changeovers can be scheduled to minimize production variations and downtime. Industrial enzymes are often sold as a crude mixture containing only a fraction of active enzyme. Selecting enzymes among different vendors may involve a trade-off between cost and purity (percent active enzyme) and a consideration of how the impurities may affect the process.

MASS TRANSFER

Introduction

The rate of mass transfer ultimately will limit the maximum aerobic reactor performance. Oxygen transfer to the fermentor broth, for example, can limit both the extent and rate of cell growth. Mass transfer limitations to microbial flocculants and immobilized catalyst pellets can result in reduced reaction rates and inefficient conversion. Liquid–liquid mass transfer rates from hydrocarbon substrates to suspended cells may limit productivity in two-phase systems (41). To determine the rate-controlling regime, it is useful to characterize the relative rates of mass transfer and reaction using the dimensionless Damkohler number (Da):

$$Da = \frac{\text{Maximum rate of reaction}}{\text{Maximum rate of diffusion}} \quad (37)$$

The observed reaction rate may be limited by the rate of diffusion depending on the value of the Damkohler number: if $Da \gg 1$ the diffusion rate is limiting, if $Da \ll 1$ the reaction rate is limiting, and if $Da \sim 1$ then the reaction and diffusion rates are comparable. As with all dimensionless numbers, the Damkohler number is only meaningful if it is calculated using the proper time and length scales for a given system. Consider spherical pellets ($r = 400\,\mu$m) of *Penicillium chrysogenum*, assuming a pellet cell density of 0.1 g/cm^3, an effective oxygen diffusivity ($D_{O_2}^{eff}$) of 1×10^{-6} cm^2/s, a particle size of 400 μm, an oxygen concentration (c_{O_2}) of 7 mg/L, and the following cell parameters (42): $\mu = 0.075\ h^{-1}$, $Y_{X/O_2} = 1.56$ g DCW/g O_2, and $m_{O_2} = 0.024$ g O_2/(g DCW × h). The Damkholer number shows that internal mass resistance is considerable and that cell growth in the pellet is likely to be limited by oxygen transfer.

$$Da = \frac{\overbrace{\left(\frac{\mu}{Y_{X/O_2}} + m_{O_2}\right)}^{O_2\ DEMAND} \cdot \overbrace{\bar{X}}^{PELLET\ CELL\ DENSITY} \cdot \overbrace{\left(\frac{4\pi r^3}{3}\right)}^{PELLET\ VOLUME} \cdot}{\underbrace{\left(D_{O_2} \cdot \frac{c_{O_2}}{r}\right)}_{DIFFUSIVE\ FLUX} \cdot \underbrace{(4 \cdot \pi \cdot r^2)}_{PELLET\ SURFACE\ AREA}} =$$

$$\frac{\left(\frac{0.075\ h^{-1}}{1.56\ \text{g DCW/g } O_2} + \frac{0.024\ \text{g } O_2}{\text{g DCW} \cdot \text{h}}\right) \cdot \frac{0.1\ \text{g DCW}}{cm^3} \cdot (4 \times 10^{-2}\ cm)^2}{3 \cdot (1 \times 10^{-6}\ cm^2/s) \cdot (7 \times 10^{-6}\ g/cm^3)}$$

$$\cong 5.5 \times 10^5 \quad (38)$$

Gas–liquid mass transfer is often rate-limiting for gases that are sparingly soluble in the broth, such as oxygen and methane. Although highly soluble, carbon dioxide exhibits pH-dependent partitioning between gaseous and dissolved forms (CO_2, H_2CO_3, HCO_3^-, CO_3^{2-}) that is influenced by the rates of both reaction and mass transfer. Proper interpretation of the respiratory coefficient (RQ) in fermentations operated at neutral pH requires consideration of CO_2 dynamics. The OTR has already been used to determine the productivity limit of a CSTR used for biomass production in equation 12. In general, the rate of mass transfer from the gas to the liquid phase is given as

$$N_A = k_L a(C^* - C_L) \quad (39)$$

where N_A is the rate of gas transfer (mmol/l × h) and the remaining terms have the same definitions as in equation 12. For sparged, agitated tanks, $k_L a$ has typical values in the range from 50 to 1,400 h^{-1}. Several correlations have been developed for $k_L a$ as a function of the gassed power input per unit volume and the superficial gas velocity for Newtonian broths in a variety of fermentors (43). The correlations can offer wide variability in mass transfer estimates and should be used in conjunction with knowledge from past experience or empirical measurements of $k_L a$ (e.g., dynamic or sulfite oxidation methods). Oxygen transfer to shear-sensitive mammalian cells requires gentle agitation combined with surface or membrane aeration, or light sparging, as opposed to the large power inputs and high rates of gas sparging in microbial fermentations. This limitation is somewhat offset by the fact that mammalian cells have lower O_2 requirements (0.05 to 0.5 mmol/10^9 cells × h) (44) and grow to lower cell densities (10^6 to 10^7 cells/mL) than microbial cultures.

VARIATIONS ON THE SINGLE CSTR

Single CSTR with Recycle

Volumetric productivity is related to the concentration of active catalyst. Cell or enzyme concentrations greater than

the steady state obtained from the simple CSTR can be achieved by separating cells from the effluent stream and recycling them to the vessel (27,45) or by retaining them within reactor. Higher catalyst concentrations enhance substrate conversion and reduce the reactor size necessary to attain a given conversion. Recycle operation improves system stability in the face of feed disturbances by retaining cells in the vessel even under conditions that would cause washout in the simple CSTR. Recycle systems can be operated at dilution rates, or throughputs, greater than the specific growth rate of the organism. Productivity improvements achieved with cell recycle are demonstrated in Table 4 for *Saccharomyces cerevisiae* ATCC 4126 and *Zymomonas mobilis* ATCC 10988 at 100 g/L glucose feed.

Cell Recycle Methods. Cell recycle is implemented through a cell separation step, often by a unit operation commonly used in the initial stages of downstream processing. Typical methods of continuous cell separation include centrifugation, filtration, and sedimentation. Cell separation can be viewed as having two often equally important purposes: (*1*) the recovery or retention of cells for reuse and (*2*) the removal of potentially inhibitory byproducts or products from the culture environment. The separation step often has to satisfy additional performance requirements such as handling of shear- or temperature-sensitive materials, selectivity in rejection or recovery, containment, maintenance of asepsis, corrosion resistance, brief retention time, and ease of cleaning, sterilization, maintenance, and validation. Recycle operation is standard for reactors using stable enzymes, because discarding expensive active catalyst is economically unfeasible. Cell separation operations are discussed elsewhere in the context of downstream processing, although a brief description is presented here in relation to cell recycle.

Sedimentation. Sedimentation is the settling of particles in a gravitational field. With low energy requirements and simple equipment, sedimentation is a relatively inexpensive way of separating a dilute cell phase. Waste treatment is by far the largest application of sedimentation-based cell recycle, in which cells are typically separated in large sedimentation tanks using lime or clay to enhance flocculant formation. The settling velocity (u_0) for an isolated spherical particle can be described using Stoke's law:

$$u_0 = \frac{d_P^2(\rho_P - \rho_F)g}{18\eta} \tag{40}$$

in which d_P is the particle diameter, ρ_P is the particle density (the specific gravity of a typical cell is 1.05), ρ_F is the fluid density, g is the gravitational acceleration constant, and η is the fluid viscosity. The functional dependence of Stoke's law suggests ways of increasing the settling velocity. The easiest and most common method is to increase the effective cell size by promoting flocculation (cell aggregation) through physiological, chemical, and physical factors: selection of flocculant strains; modification of cell wall structure or surface charge; changing the pH, temperature, or shear stress; addition of inorganic salts (e.g., Ca^{2+} and Mg^{2+} salts) or clays; controlling the concentration of certain nutrients or products (e.g., extracellular polysaccharides); and controlling the cell age or growth phase. Selective cell recycle has been implemented using the differential sedimentation properties of a desired and unwanted microorganism (34–36). The properties of a particular broth are generally unchangeable and will probably only impede particle settling.

Although equation 40 holds for dilute suspensions of cells, the interactions among settling particles in concentrated slurries results in hindered settling. The hindered particle velocity (u_h) is influenced by the particle concentration and can be expressed with the following correlation (49):

$$\frac{u_h}{u_0} = \frac{1}{1 + \lambda \cdot \epsilon_P^{1/3}} \tag{41}$$

in which ϵ_P is the volume fraction of particles and λ is an empirical function of ϵ_P. For dilute suspensions, $\epsilon_P < 0.15$, whereas in slurries $0.15 < \epsilon_P < 0.50$.

The limiting settling velocity for a system has a strong influence on equipment design and operation. Consider the case of a continuous sedimentation tank with volumetric throughput (F) and constant cross-sectional area (A). The sedimentation tank performance can then be described by equation 42, in which throughput is directly proportional to A and independent of tank depth:

$$F = u_{lim} \cdot A \tag{42}$$

The throughput and limiting settling time will thus dictate equipment size and costs. Another design consideration is the residence time of cells in the settling tank, which must be considered in the context of nutrient depletion (particularly for oxygen) and its potential effects on performance.

Sedimentation at laboratory scale may be implemented with an external settling column (47,50,51). Similar devices may be used at bioprocessing scales, whereas large open-air tanks must be used in high-volume wastewater treatment. Internal sedimentation has been implemented

Table 4. Ethanol Productivity Enhancements for *S. cerevisiae* and *Z. mobilis*

		Dilution rate (h^{-1})	Ethanol productivity g/(L × h)	Cell density (g DCW/L)	Reference
S. cerevisiae	CSTR	0.17	7	12	46
	CSTR with recycle	0.68	29	50	47
Z. mobilis	CSTR	0.175	8	2.5	29
	CSTR with recycle	2.7	120	38	48

in tower fermenters, in which immobilized cells and enzymes or microbial flocculants are retained in the vessel by a sedimentation zone within the vessel. Unlike the ideal CSTR, tower fermenters may exhibit spatial variations in nutrient concentrations and broth properties along the height of the tower that can significantly influence reactor performance. In addition, the productivity in these reactors may be limited by the need to maintain low upward velocities (e.g., low aeration or CO_2 evolution) to allow adequate cell sedimentation.

Centrifugation. The operating principle behind centrifugation is the same as that of sedimentation; however, much higher settling velocities than in sedimentation may be obtained in the centrifugal field. Centrifugal separators enable high-volume continuous processing of fluids containing many particles, with short retention times and small space requirements. To determine the unhindered particle velocity in a centrifugal field (u_{0C}), equation 40 is multiplied by the centrifugal coefficient (C), also known as the G-value, which describes the increase in sedimentation rate due to centrifugation relative to gravitational settling:

$$u_{0C} = \frac{d_P^2 g(\rho_P - \rho_F)}{18\eta} \underbrace{\left(\frac{r\omega^2}{g}\right)}_{C} \tag{43}$$

where r is the radial distance from the axis of rotation and ω is the angular velocity.

Industrial centrifuges are most often classified by internal structure (e.g., disk stack, tubular bowl) and mode of operation (e.g., solids retaining, continuous or intermittent solids ejecting). The selection of sturdier construction and materials will enable higher rotation speeds for separation of smaller particles. The equation describing throughput in a centrifuge is analogous to equation 42, except that the centrifuge area is expressed using the Σ value, which is the area equivalent for a given centrifuge and rotation speed. Centrifuge manufacturers will often provide machine-specific Σ values, although the Σ value for simple disk-stack and tubular-bowl centrifuges can be calculated directly.

Filtration. Filtration is separation based on size, allowing retention of molecules larger than the pore size of the filter and passage of smaller molecules. Membrane filtration thus offers the twin benefits of cell retention and inhibitory by-product removal. In cell recycle systems, the most common arrangements are internal filters for cell and enzyme retention (52,53) or external membrane filters (54,55) in plate and frame, spiral cartridge, and hollow fiber configurations. In all these configurations, flow patterns tangential to the membrane surface can reduce fouling and improve the filtrate flux across the membrane. Compared to internal filters, external filters have higher surface-area-to-volume ratios and may be easier to maintain; however, they may be less easily sterilized (particularly for some polymer membranes) and could introduce problems of nutrient depletion in the external recycle loop. Membrane selection depends primarily on the critical particle size, with other criteria being cost, mechanical stability, and susceptibility to plugging and fouling. Because membranes have the potential for complete cell recycle, a purge or bleed stream is typically split from the recycle stream to prevent accumulation of inert particles and debris in the vessel.

Material Balances. A schematic of a CSTR with recycle of cells is shown in Figure 4. A material balance on cell mass for the CSTR with recycle system, neglecting cell death, may be written

$$\underbrace{F \cdot X_0}_{\text{CELLS IN FEED}} + \underbrace{\alpha \cdot F \cdot C \cdot X_1}_{\text{CELLS IN RECYCLE STREAM}} - \underbrace{(1+\alpha) \cdot F \cdot X_1}_{\text{CELLS OUT}} + \underbrace{V \cdot \mu \cdot X_1}_{\text{CELL GROWTH}} = \underbrace{\frac{d(V \cdot X_1)}{dt}}_{\text{CELL ACCUMULATION}} \tag{44}$$

where α is the recycle ratio equal to the recycle volume divided by the feed volume, C is the concentration factor (cell concentration in the recycle divided by the effluent concentration) related to the efficiency of the separation step, and X_0, X_1, and X_2 are the cell concentrations in the feed, recycle, and separator effluent streams, respectively. Note that the low substrate concentrations in waste treatment create suboptimal growth environments in which cell death cannot be neglected.

Assuming the system is at steady state ($dX_1/dt = 0$) and that the feed is sterile ($X_0 = 0$), equation 44 yields

$$\mu = (1 + \alpha - \alpha \cdot C) \cdot D \tag{45}$$

The dilution rate is no longer equal to the specific growth rate; in fact, because C > 1 and $\alpha < 1$, the dilution rate is greater than the specific growth rate.

A material balance on the limiting substrate, again neglecting maintenance and product formation, may be written

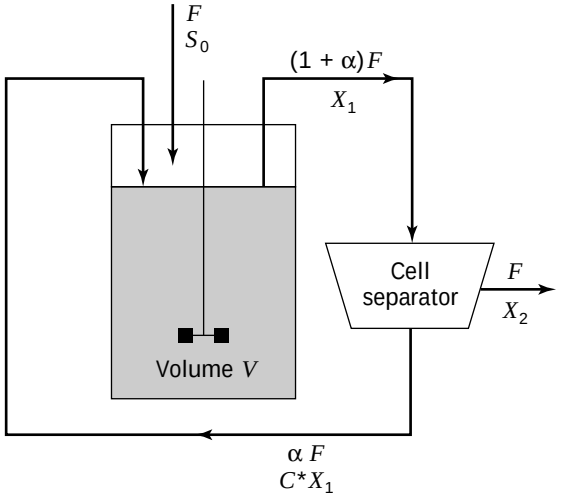

Figure 4. CSTR with recycle. Cell separation can be achieved through centrifugation, sedimentation, or filtration.

$$\underbrace{F \cdot S_0}_{\text{SUBSTRATE IN FEED}} + \underbrace{\alpha \cdot F \cdot S}_{\text{SUBSTRATE IN RECYCLE}} - \underbrace{(1 + \alpha) \cdot F \cdot S}_{\text{SUBSTRATE OUT}} - \underbrace{\frac{\mu \cdot X}{Y_{X/S}} \cdot V}_{\text{SUBSTRATE CONSUMED}} = \underbrace{V \cdot \frac{dS}{dt}}_{\text{SUBSTRATE ACCUMULATION}} \quad (46)$$

Solving equation 46 for the cell concentration, assuming steady-state ($dS/dt = 0$) operation, yields

$$X_1 = \frac{Y_{X/S} \cdot (S_0 - S)}{[1 + \alpha(1 - C)]} \quad (47)$$

in which the steady-state cell concentration with recycle is greater than that in the simple CSTR by a factor of $1/[1 + \alpha(1 - C)]$. By adopting a suitable expression for cell growth, the substrate concentration can be determined. Using the Monod expression, as before, and solving for the substrate concentration gives

$$S = K_S \frac{\mu}{\mu_{max} - \mu} = K_S \frac{D(1 + \alpha - \alpha C)}{\mu_{max} - D(1 + \alpha - \alpha C)} \quad (48)$$

Substituting equation 48 into equation 47 yields

$$X_1 = \frac{Y_{X/S}}{(1 + \alpha - \alpha C)} \left[S_0 - K_S \frac{D(1 + \alpha - \alpha C)}{\mu_{max} - D(1 + \alpha - \alpha C)} \right] \quad (49)$$

A material balance on cell mass around the separator gives the cell concentration in the outlet:

$$X_2 = (1 + \alpha - \alpha \cdot C) \cdot X_1 \quad (50)$$

Figure 5 shows the cell mass and biomass productivity of a CSTR with recycle compared to a simple CSTR. The higher biomass productivity of the recycle system results from a dilution rate higher than the specific growth rate and the increased cell concentration in the vessel.

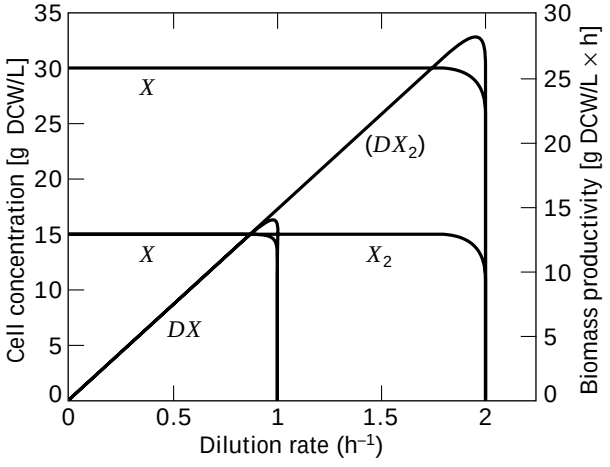

Figure 5. Comparison of steady-state behavior of a chemostat (*solid lines*) and a chemostat with recycle (*dotted lines*) using the following parameters: $Y_{X/S} = 0.5$ g DCW/g substrate, $\mu_{max} = 1.0$ h^{-1}, $K_S = 0.02$ g/L, $S_0 = 30$ g/L, $C = 2$, and $\alpha = 0.5$.

Implementation of a recycle system is often critical to the economic viability of processes using expensive biocatalysts (e.g., enzymes). Typically, this is accomplished by immobilizing the enzymes on inert support particles to facilitate either internal or external recycle. The potential use of cell recycle in an industrial process involves weighing the effectiveness and economics associated with the cell separation step against the marginal improvement in process performance. It should also be noted that higher cell densities exacerbate the oxygen transfer and heat removal burden of the system.

CSTRs in Series

In the single CSTR, the constant, controlled environment gives the advantage of being able to control the cellular–enzyme environment for maximum utility. Sometimes, however, a particular cell system will exhibit multiple properties of interest that can only be realized in different environments. The optimal environments for cell growth and product formation, for example, may be characterized by different temperatures, pH, and limiting nutrients. The configuration of CSTRs in series lends itself to those applications in which multiple environments are required.

Cell Growth. Bacterial growth in the presence of multiple carbon substrates often results in diauxic growth, in which cells preferentially metabolize a single substrate over all others. In a waste treatment application, the preferred substrate would be consumed by the microorganisms and the remaining substrates would pass through the system untreated. Configuring CSTRs in series provides a partitioning of cell metabolism so that less-favored substrates are consumed in subsequent stages.

CSTRs in series have been used to improve recombinant protein fermentations in which performance is threatened by plasmid instability (56,57) and lethal protein overproduction (30). Cells are grown to high density in the first stage without inducer so that plasmid-free cells have little growth advantage over plasmid-containing cells. Induction in the second stage results in higher productivity than the simple CSTR because the continuous introduction of plasmid-containing cells from the first stage reduces the ability of nonproductive cells to dominate the culture.

Consider the two-stage system for biomass production in Figure 6, in which a separate feedstream can be added to the second stage. The steady-state material balances for cells and substrate in the first reactor are identical to the single CSTR case (equations 1 and 3), with steady-state solutions as equations 5 and 8 for Monod growth. Considering the case without the second feedstream, the material balances on cell mass and growth-limiting substrate in the second stage can be written as

$$\underbrace{\frac{F \cdot X_1}{V_2}}_{\text{CELLS IN}} - \underbrace{\frac{F \cdot X_2}{V_2}}_{\text{CELLS OUT}} + \underbrace{\mu_2 \cdot X_2}_{\text{CELL GROWTH}} = \underbrace{\frac{dX_2}{dt}}_{\text{ACCUMULATION}} \quad (51)$$

and

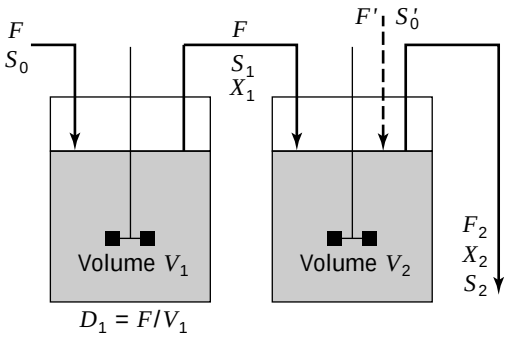

Figure 6. Two-stage chemostat system with possibility of a separate feed to second reactor.

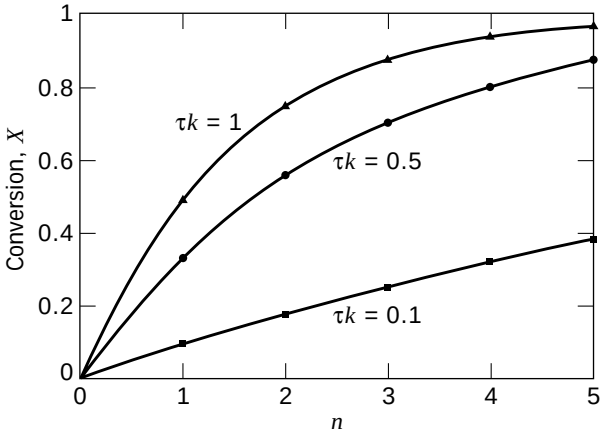

Figure 7. Substrate conversion for first order reaction in n CSTRs in series.

$$\underbrace{\frac{F \cdot S_1}{V_2}}_{\text{SUBSTRATE IN}} - \underbrace{\frac{F \cdot S_2}{V_2}}_{\text{SUBSTRATE OUT}} - \underbrace{\frac{\mu_2 \cdot X_2}{Y_{X/S}}}_{\text{CONSUMPTION FOR GROWTH}} = \underbrace{\frac{dS_2}{dt}}_{\text{ACCUMULATION}} \tag{52}$$

with steady-state solutions shown in Table 5. A growth model on the limiting substrate must be adopted to further complete the system description. Minimal cell growth will occur in the second stage if no additional substrate is added, because the majority of substrate is consumed in the first stage. Thus, non-growth-related cellular behavior and product formation could be studied in the second CSTR.

Adding an additional feedstream to the second stage (Fig. 6) provides the opportunity to introduce more of the limiting nutrient, other nutrients required for growth or product formation, inducers, or inhibitors. The material balances on cell mass and substrate on the second stage can be written as equations 53 and 54, respectively, with steady-state solutions given in Table 5. In equation 53, F' is the volumetric flow of the second feedstream, which is assumed to be sterile ($X' = 0$).

$$\underbrace{\frac{F_1}{V_2} X_1}_{\substack{\text{CELLS IN}\\ \text{FROM}\\ \text{STAGE 1}}} - \underbrace{\frac{F_1 + F'}{V_2} X_2}_{\substack{\text{CELLS}\\ \text{OUT}}} + \underbrace{\mu_2 \cdot X_2}_{\substack{\text{CELL}\\ \text{GROWTH}}} = \underbrace{\frac{dX_2}{dt}}_{\text{ACCUMULATION}} \tag{53}$$

The dilution rate for the second stage is given by $D_2 = (F_1 + F')/V_2$, and the concentration of the limiting nutrient in the second feed is S'_0.

$$\underbrace{\frac{F_1}{V_2} S_1}_{\substack{\text{SUBSTRATE}\\ \text{IN FROM}\\ \text{STAGE 1}}} + \underbrace{\frac{F'}{V_2} S'_0}_{\substack{\text{SUBSTRATE}\\ \text{IN FROM}\\ \text{SECOND FEED}}} - \underbrace{\frac{F_1 + F'}{V_2} S_2}_{\substack{\text{SUBSTRATE}\\ \text{OUT}}} - \underbrace{\frac{\mu_2 \cdot X_2}{Y_{X/S}}}_{\substack{\text{CONSUMPTION}\\ \text{FOR GROWTH}}} = \underbrace{\frac{dS_2}{dt}}_{\text{ACCUMULATION}} \tag{54}$$

Feeding additional substrate to the second stage allows for more growth to occur. In addition, the dilution rate in the second stage is larger than the maximum specific growth rate of the organism because the second stage has a continuous feed of cells.

Enzyme Reaction. Enzyme reactions may also be carried out in multiple CSTRs. The performance of CSTRs in series approaches that of a single PFR while maintaining the good mixing characteristics of the stirred-tank reactor (37). Considering a first-order enzymatic reaction for substrate conversion ($v = k \times S$), the reactor design equation for a single CSTR can be written as

Table 5. Steady-State Solutions to Material Balances for a Two-Stage Chemostat

	Cell mass	Substrate
First stage	$\mu_1 = D_1$	$X_1 = Y_{X/S}(S_0 - S_1)$
Second stage	$\mu_2 = D_2\left(1 - \frac{X_1}{X_2}\right)$	$X_2 = \frac{D_2}{\mu_2} Y_{X/S}(S_1 - S_2)$
Second stage with additional feedstream	$\mu_2 = D_2 - \frac{F_1 \cdot X_1}{V_2 \cdot X_2}$	$X_2 = \frac{Y_{X/S}}{\mu_2}\left(\frac{F_1}{V_2} S_1 + \frac{F'}{V_2} S' - D_2 S_2\right)$
	where $D_2 = D_1 = F/V_1$	where $D_2 = (F_1 + F')/V_2$

$$\tau = \frac{S_0 - S}{k \cdot S} \tag{55}$$

Assuming that there is no volume change upon reaction, the conversion in the single CSTR is given by

$$X = \frac{\tau \cdot k}{1 + \tau \cdot k} \tag{56}$$

Then for a system of n CSTRs in series with equal volumes and reactor conditions (constant k) the conversion in the nth CSTR is given by equation 57 and depicted in Figure 7.

$$X_n = 1 - \frac{1}{(1 + \tau \cdot k)^n} \tag{57}$$

NOMENCLATURE

Abbreviations

CER	Carbon dioxide evolution rate
CIP	Clean-in-place
CSTR	Continuous stirred-tank reactor
OTR	Oxygen transfer rate
OUR	Oxygen uptake rate
PFR	Plug flow reactor
RQ	Respiratory quotient, RQ = CER/OUR
WFI	Water-for-injection

Symbols

ΔH_{RXN}	Heat of reaction, >0 endothermic, <0 exothermic, kJ/mol
ΔQ_{SENS}	Net sensible heat input, W
$(R_{CSTR})_M$	Biomass productivity at X_M and D_M, g DCW/m^3 × h
A	Area, m^2
C	Concentration factor in cell recycle system
C^*	Equilibrium dissolved oxygen concentration, g/m^3
C_L	Dissolved oxygen concentration, g/m^3
Cp	Heat capacity, J/kg × K
D	Dilution rate, h^{-1}
Da	Dimensionless Damkohler number
D_C	Critical dilution rate, h^{-1}
D_M	Dilution rate associated with maximum R_{CSTR} at fixed S_0, h^{-1}
d_P	Particle diameter, m
E	Enzyme concentration
E_0	Initial enzyme concentration
Ea	Activation energy, kJ/mol
F	Volumetric flow rate, m^3/h
g	Gravitational acceleration, 9.8 m/s^2
k_2	Catalytic rate constant, h^{-1}
k_d	Thermal denaturation constant, h^{-1}
k_La	Overall mass transfer coefficient, h^{-1}
k_P	Specific product degradation constant, h$_{-1}$
K_S, K_I, K_P	Model parameters for cell growth
K_m, K_S, K'_m, K'_S	Model parameters for enzyme kinetics
m	Maintenance coefficient g/g DCW × h
N_{discs}	Number of discs in a disk-stack centrifuge
OD_{660}	Optical density at 660 nm; measure of cell concentration
P	Product concentration, g/m^3
Q_{AGIT}	Agitation heat input, W
Q_{EVAP}	Heat loss by evaporation, W
Q_{EXCH}	Heat removal by heat exchanger, W
Q_{LOSS}	Heat loss to surroundings, W
Q_{MET}	Metabolic heat generation, W
q_{O_2}	Specific oxygen uptake rate, g O_2/g DCW ∗ h
q_P	Specific product formation rate, g/g DCW ∗ h
R	Ideal gas constant, J/mol ∗ K
r_2, r_1	Outer and inner radii for centrifuge, m
R_{BATCH}	Biomass productivity for batch fermentation, g DCW/m^3 × h
R_{CSTR}	Biomass productivity for CSTR, g DCW/m^3 × h
S	Substrate concentration, g/m^3
S_0	Inlet substrate concentration, g/m^3
T	Bulk fluid temperature, K
T_C	Coolant temperature, K
t_{CYCLE}	Batch cycle time, h
t_M	Mixing time, h
$t_{TURNAROUND}$	Lumped batch turnaround time, h
U	Overall heat transfer coefficient, W/m^2 × K
u	Particle velocity, m/h
u_{lim}	Limiting particle velocity for a separator, m/h
V	Fluid volume, m^3
v	Reaction rate,
v_{max}	Maximum reaction rate
w_{H_2O}	Mass flow rate of water, kg/h
X	Cell concentration, g DCW/m^3
X_0	Inlet cell concentration, g DCW/m^3
Xi	Inoculum cell concentration, g DCW/m^3
X_M	Cell concentration associated with D_M, g DCW/m^3
Y_{Hi}	Cell mass produced per heat evolved, g DCW/kcal
$Y_{P/S}$	Product yield on substrate, g/g
Y_{X/O_2}	Cell yield on oxygen, g DCW/g O_2

$Y_{X/S}$	Cell yield on substrate, g DCW/g
Z	Concentration of contaminant microorganism, g DCW/m^3

Greek Symbols

μ	Specific growth rate, h^{-1}
α	Specific rate of cell lysis or endogenous metabolism, h^{-1}
λ	Adjustable parameter
τ	Residence time, h
Σ	Σ Factor, area equivalent for a centrifuge
ω	Angular velocity
α	Recycle ratio
ρ	Density, kg/m^3
η	Viscosity, kg/m $\times$ s
λ	Empirical function of ϵ_P
α, β	Product formation parameters, g product/g DCW and g product/g DCW $\times$ h, respectively
μ_{max}	Maximum specific growth rate, h^{-1}
ϵ_P	Volume fraction of particles
δ_S	Fractional substrate conversion

BIBLIOGRAPHY

1. J. Monod, *Ann. Rev. Microbiol.* **3**, 371 (1949).
2. A. Novick and L. Szilard, *Proc. Nat. Acad. Sci. Wash.* **36**, 708 (1950).
3. D. Herbert, R. Elsworth, and R.C. Telling, *J. Gen. Microbiol.* **14**, 601–622 (1956).
4. M.L. Shuler and M.M. Domach, in H.W. Blanch, E.T. Papoutsakis, G. Stephanopoulos eds., *Foundations in Biochemical Engineering*, American Chemical Society, Washington, D.C., 1983, p. 93.
5. J. Nielsen, *Biotechnol. Bioeng.* **41**, 715–727 (1993).
6. A. Harder and J.A. Roels, *Adv. Biochem. Eng.* **21**, 55–107 (1982).
7. J. Nielsen and J. Villadsen, *Chem. Eng. Sci.* **47**, 4225–4270 (1992).
8. N.M. Fish and M.D. Lilly, *Biotechnology* **2**, 623–627 (1984).
9. R. Luedeking and E.L. Piret, *J. Biochem. Microbiol. Tech. Eng.* **1**, 431–459 (1959).
10. R.D. Kiss and G. Stephanopoulos, *Biotechnol. Bioeng.* **39**, 565–574 (1992).
11. P. Yu and K.-Y. San, *Biotechnol. Prog.* **9**, 587–593 (1993).
12. G.K. Raju and C.L. Cooney, in H.-J. Rehm, G. Reed, A. Puhler, P. Stadler eds., *Biotechnology*, 2nd ed., vol. 3, VCH, Weinheim, Germany, 1993, pp. 159–184.
13. M.F. Edwards and W.L. Wilkinson, *Chem. Eng.* **265**, 310 (1972).
14. M. Charles, *Trends Biotechnol.* **3**, 134–139 (1985).
15. C.L. Cooney, D.I.C. Wang, and R.I. Matales, *Biotechnol. Bioeng.* **11**, 269–281 (1968).
16. B.J. Abbott and A. Clamen, *Biotechnol. Bioeng.* **15**, 117–127 (1973).
17. B.L. Maiorella, H.W. Blanch, and C.R. Wilke, *Biotechnol. Bioeng.* **26**, 1003–1025 (1984).
18. A.P.J. Sweere, L. Mesters, L. Janse, K.Ch.A.M. Luyben, and N.W.F. Kossen, *Biotechnol. Bioeng.* **10**, 567–578 (1988).
19. F. Vardar and M. Lilly, *Eur. J. Appl. Microbiol. Biotechnol.* **14**, 203–211 (1982).
20. C.G. Sinclair and D.E. Brown, *Biotechnol. Bioeng.* **12**, 1001–1017 (1970).
21. P.J. Senior and J. Windass, *Biotechnol. Lett.* **2**, 205–210 (1980).
22. O. Levenspiel, *Chemical Reaction Engineering*, 2nd ed., Wiley, New York, 1972, pp. 253–325.
23. M. Charles, in T.K. Ghose, A. Fiechter, N. Blakebrough eds., *Advances in Biochemical Engineering*, vol. 8, Springer-Verlag, New York, 1978, pp. 1–62.
24. N.M.G. Oosterhuis and N.W.F. Kossen, *Biotechnol. Bioeng.* **26**, 546–550 (1984).
25. J.A. Howell, C.T. Chi, and U. Pawlowsky, *Biotechnol. Bioeng.* **14**, 253–265 (1972).
26. R.C. Righelato and S.J. Pirt, *J. Appl. Bacteriol.* **30**, 246–250 (1967).
27. D. Herbert, in *Continuous Culture of Microorganisms*, Monograph no. 12, Society of Chemistry and Industry, London, 1961, pp. 21–53.
28. H. Kuhn, U. Friederich, and A. Fiechter, *Eur. J. Appl. Microbiol.* **6**, 341–349 (1979).
29. K.J. Lee, D.E. Tribe, and P.L. Rogers, *Biotechnol. Lett.* **1**, 421–426 (1979).
30. J. Fu, D.B. Wilson, and M.L. Shuler, *Biotechnol. Bioeng.* **41**, 937–946 (1993).
31. S.W. Brown and S.G. Oliver, *Eur. J. Microbiol. Biotechnol.* **16**, 119–122 (1982).
32. D.E. Dykhuizen and D.L. Hartl, *Microbiol. Rev.* **47**, 150–168 (1983).
33. M. Nagashima, in H. Verachtert, and R.D. Mot eds., *Yeast: Biotechnology and Biocatalysis*, Dekker, New York, 1990, pp. 57–84.
34. R.H. Davis and C.S. Parnham, *Biotechnol. Bioeng.* **33**, 767–776 (1989).
35. K.L. Henry and R.H. Davis, *Biotechnol. Prog.* **6**, 7–12 (1990).
36. K.L. Ogden and R.H. Davis, *Biotechnol. Bioeng.* **37**, 325–333 (1991).
37. S.W. Carleysmith and M.D. Lilly, *Biotechnol. Bioeng.* **21**, 1057–1073 (1979).
38. L.Y. Ho and A.E. Humphrey, *Biotechnol. Bioeng.* **12**, 291–311 (1970).
39. S.H. Park, S.B. Lee, and D.Y. Ryu, *Biotechnol. Bioeng.* **23**, 1237–1254 (1981).
40. C. Kim, H.S. Kim, and D.D. Ryu, *Biotechnol. Bioeng.* **24**, 1889–1896 (1982).
41. M. Moo-Young, *Can. J. Chem. Eng.* **53**, 113–118 (1975).
42. R.C. Righelato, A.P.J. Trinci, S.J. Pirt, and A. Peat, *J. Gen. Microbiol.* **50**, 399–412 (1968).
43. M. Moo-Young and H.W. Blanch, *Adv. Biochem. Eng.* **19**, 1–69 (1981).
44. R.J. Fleischaker and A.J. Sinskey, *Eur. J. Appl. Microbiol. Biotechnol.* **12**, 193–197 (1981).
45. S.J. Pirt and W.M. Kurowski, *J. Gen. Microbiol.* **63**, 357–366 (1970).

46. G.R. Cysewski and C.R. Wilke, *Biotechnol. Bioeng.* **18**, 1297–1313 (1976).
47. G.R. Cysewski and C.R. Wilke, *Biotechnol. Bioeng.* **19**, 1125–1143 (1977).
48. P.L. Rogers, K.J. Lee, M.L. Skotnicki, and D.E. Tribe, *Adv. Biochem. Eng.* **23**, 37–84 (1982).
49. J.E. Bailey and D.F. Ollis, *Biochemical Engineering Fundamentals*, 2nd ed., McGraw-Hill, New York, 1986, pp. 733–734.
50. T.K. Ghose and R.D. Tyagi, *Biotechnol. Bioeng.* **21**, 1387–1400 (1979).
51. D. Gold, A. Mohagheghi, C.L. Cooney, and D.I.C. Wang, *Biotechnol. Bioeng.* **23**, 2105–2116 (1981).
52. A. Margaritis and C. Wilke, *Biotechnol. Bioeng.* **20**, 727–754 (1978).
53. H.N. Chang, W.G. Lee, and B.S. Kim, *Biotechnol. Bioeng.* **41**, 677–681 (1993).
54. Y.L. Lee and H.N. Chang, *Biotechnol. Bioeng.* **36**, 330–337 (1990).
55. H.N. Chang, I.-K. Yoo, and B.S. Kim, *Biotechnol. Adv.* **12**, 467–487 (1994).
56. R. Siegel and D.D.Y. Ryu, *Biotechnol. Bioeng.* **27**, 28–33 (1985).
57. S.B. Lee, D.D.Y. Ryu, R. Seigel, and S.H. Park, *Biotechnol. Bioeng.* **31**, 805–820 (1988).

See also BIOREACTORS, AIR-LIFT REACTORS; BIOREACTORS, FLUIDIZED-BED; FERMENTATION MONITORING, DESIGN AND OPTIMIZATION; MASS TRANSFER; SCALE-UP, STIRRED TANK REACTORS.

BIOREACTORS, FLUIDIZED-BED

FRANCESC GÒDIA
CARLES SOLÀ
Universitat Autònoma de Barcelona
Barcelona, Spain

OUTLINE

KEY WORDS

Bioreactors
Fluidized-bed
Hydrodynamics
Immobilized biocatalysts

INTRODUCTION

Fluidized-bed bioreactors are directly linked to the use of biocatalysts (cells or enzymes) for transformations in an immobilized form. The solid particles of the immobilized biocatalyst are maintained in fluidization by means of the circulation of a fluid phase (either liquid, gas, or a mixture of both) that compensates their weight. In this way, good liquid mixing and mass transfer between the solid and the liquid phases can be obtained with low attrition. Also, fluidized-bed bioreactors can accommodate a gas phase and can be used to feed solids in suspension. High productivities can be achieved in these systems, but their hydrodynamic complexity and operational stability have to be well defined for a proper operation.

THE FLUIDIZATION CONCEPT: GENERAL CONSIDERATIONS

The term *fluidized-bed* is used to define those physical systems composed of a solid phase in the form of individual particles that move within a fluid phase and are not in continuous contact with each other. Fluidization of the solid particles is reached when the flow of fluid through the bed is high enough to compensate their weight. On the other hand, in order to be kept in the fluidized-bed reactor and not be washed out (elutriated), the superficial velocity of the fluid in the bed (that is, the ratio between the flow rate and the bed cross-sectional area) has to be lower than the settling velocity of the particles. These two extreme situations are outlined in Figure 1. When the flow rate of a fluid through a packed bed of solid particles steadily increases, the pressure drop increases proportionally to the flow rate, as long as the bed height remains constant. When the drag force of the fluid equilibrates the weight of

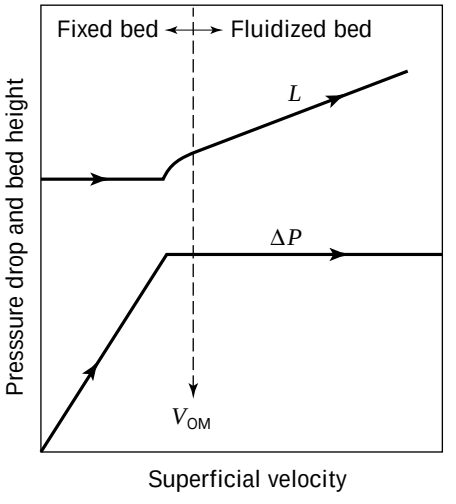

Figure 1. Illustration of the basic concept of fluidization. Variation of the pressure drop (ΔP) and the height of the solid particles in a bed (L), with increasing fluid superficial velocity. v_{OM}, minimum fluidization velocity.

the particles, the bed starts to expand and, after a transition period, reaches fully developed fluidization. At this point, further increments in the flow rate do not produce an increase in pressure drop, but instead lead to an increase of the height occupied by the solid particles in the reactor. If the flow rate is increased significantly, the elutriation of the solid particles occurs when the fluid's superficial velocity is higher than the solid's settling velocity. The fundamentals of the fluidization phenomena are discussed comprehensively in the chemical engineering literature (1,2).

Figure 2 represents the basic scheme of a fluidized-bed bioreactor. Although various configurations are possible (3), the most extensively used is the gas–liquid cocurrent up-flow reactor. In it, liquid usually comprises the continuous phase and is fed from the reactor bottom. Its flow upward in the reactor promotes fluidization of the solid particles. Usually, the reactor will have two or three phases. In addition to the liquid and solid phases, the occurrence of a gas phase is quite common in those systems using cells as biocatalysts, either for aeration requirements (in which case, an air or oxygen stream is fed to the reactor, as shown in Fig. 2) or because cell metabolism produces a gas product (for example, CO_2, CH_4). In systems using enzymes as biocatalysts, the most common situation is two-phase fluidization, without any gas phase. Very often, due to the low reaction rates of most biological transformations, long liquid residence times are needed for the completion of the reaction, and therefore the drag force created by the low liquid flow rate in a single pass reactor is not enough to promote fluidization of the solid particles. Fluidization is obtained either by external liquid recirculation or by the gas loaded to the reactor, as depicted in Figure 2. In systems where a gas is produced by cell metabolism, the gas can also be an additional factor contributing to solid particle fluidization, although other effects are also observed in this case, such as internal liquid recirculation patterns. Fluidization at relatively low liquid flow rates is also favored in tapered fluidized-bed configurations; the liquid superficial velocity at the bottom of the reactor is higher due to the reduced cross-sectional area. In general, one can distinguish three main sections in fluidized-bed bioreactors: *(1)* the bottom section, where feed (liquid, gas, or both) and recirculation are provided; *(2)* the central main section, where most of the reaction takes place; *(3)* and the top section, with a wider diameter that serves to decelerate the movement of the particles by decreasing the superficial velocity of the liquid, thus enhancing the retention of the solid phase and at the same time allowing gas disengagement from the liquid phase. It is a common trend for fluidized-bed bioreactors to use biocatalysts, either cells or enzymes, in the form of immobilized preparations. In general, the particles can be of three different types: *(1)* inert cores on which a biofilm is created by cell attachment, or in the case of enzymes, by adsorption or covalent binding immobilization; *(2)* porous particles in which the biocatalysts are entrapped; *(3)* cell aggregates obtained by self-immobilization caused by the ability of some cell strains to form flocs, pellets, or aggregates. Fluidized-bed bioreactors are usually differentiated from air-lift bioreactors by the fact that the latter do not specifically require the use of immobilized biocatalysts. Indeed, they were developed for free cell suspensions. In addition, air-lift bioreactors have different compartments, created by physical internal divisions, with different degrees of aeration.

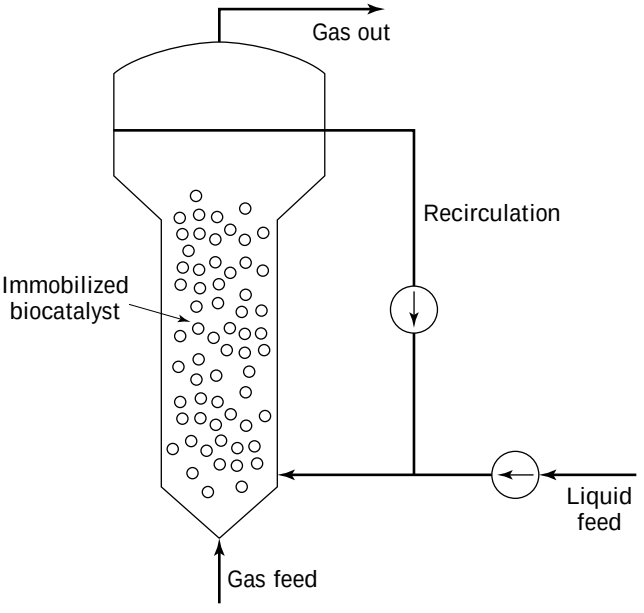

Figure 2. General scheme of a fluidized-bed reactor.

CHARACTERISTICS AND POTENTIAL OF FLUIDIZED-BED BIOREACTORS

The use of fluidized-bed bioreactors can provide a number of advantages that makes them an interesting alternative for bioprocesses, especially for continuous operation. In comparison with conventional mechanically stirred bioreactors, fluidized-bed bioreactors provide a much lower attrition of solid particles, and almost any kind of immobilized biocatalyst preparation can be used without physical disruption. Biocatalyst concentration can be significantly higher because of immobilization, and the typical wash-out limitations of continuous bioreactors operating with free cells are overcome because the solid particles are physically retained in the reactor vessel; operation at flow rates higher than the maximum growth rate of the cells can be achieved. As a consequence, the final productivity of the bioreactor can be increased substantially. Compared with packed-bed reactors, fluidized-bed bioreactors can be operated with smaller-size particles and without the drawbacks of clogging, creation of preferential flowpaths, or particle compression due to bed weight. Moreover, the smaller particle size minimizes the internal diffusional resistances, and the higher level of mixing enhances external mass and heat transfer from liquid to solid phase.

The degree of internal mixing in a fluidized bed can vary to a great extent, and it depends on various factors: density

and diameter of the solid particles, liquid and gas flow rates at the reactor inlet, endogenous gas production by cell metabolism, and recirculation rate. For some operational conditions, high gas, liquid, or recirculation flow rates, the internal mixing will be very high, and the reactor will approach the behavior of a complete mixed tank. On the other hand, operation with low gas, liquid, or recirculation rates will provide a flow pattern close to plug flow, with some degree of axial mixing. This implies that reaction kinetics is an important factor to consider in the analysis and design of fluidized-bed bioreactors. Configurations favoring liquid mixing will be more appropriate for substrate-inhibited reactions, and configurations approaching plug flow will be indicated for product-inhibited reactions. Another advantage of fluidized-bed bioreactors is the ease of separation of the gas produced in most transformations involving cells (i.e., CO_2), or the feed of a gas stream to the reactor, for example, for aeration purposes. Also, fluidized-bed reactors make biocatalyst replacement easy, without disruption of the operation, enabling good control of the overall activity of the reactor. For example, one may replace particles with deactivated enzyme or removing an excess of biomass created by biofilms. On the other hand, solids attrition is higher in fluidized-bed than in packed-bed bioreactors. From the productivity point of view, the advantages of the fluidized bed, especially with respect to mass transfer rates, make it possible to obtain higher levels of overall productivity than in packed-bed reactors, in spite of the fact that the fraction of immobilized biocatalyst particles is lower for a fluidized bed.

Fluidized-bed bioreactors are complex with regard to hydrodynamic aspects, especially taking into account that the properties of the biocatalyst particles may change considerably during the operation time and in the presence of three different phases (solid, liquid, gas) in many cases. In fact, the nature of the particles (for example, their density and size, or their evolution with time, which are especially important with respect to certain kinds of immobilized cells), the liquid and gas flow rates employed, the type of reaction kinetics, and the kinetics of cell growth or enzyme deactivation influence each other and have a direct effect on the reactor design and performance (4).

Using the biocatalyst in immobilized form also contributes to the complexity of a fluidized-bed bioreactor. The behavior of the immobilized biocatalyst, especially when cells are used, can be substantially different than that of free suspensions (5). The behavior must be determined at the kinetic level, the physiological level, and the genetic level, and the biocatalyst's relationship with the diffusional restrictions in the particles and the possible direct effects associated with the immobilization itself must be well understood and correctly described in order to build appropriate and reliable models of for reactor design, control, and scaling up.

The potential of fluidized-bed bioreactors can be further exploited by considering multistage units and using two solid particles with different properties. Figure 3 gives an example of the concept of multistage operation, in particular, a countercurrent multistage fluidized bed working with immobilized enzymes (6). The main characteristic of this bioreactor is the continuous transport of the solid particles of immobilized enzymes from one stage to another in a downward direction. The overall catalytic activity of the reactor remains constant as the exhausted enzyme is removed from the reactor bottom stage while fresh biocatalyst is added at the top stage. A second advantage of dividing the reactor into compartments is the very low degree of back-mixing of the biocatalyst, and the plug-flow regime attained in the liquid phase. The use of two solid particles with different properties, particularly with different densities, can be used in a fluidized bed to achieve the in situ separation of a product of the reaction; this is a clear advantage in systems with product inhibition or when unfavorable thermodynamic equilibria limit the conversion rate for a reaction. For example, Davison and Scott (7) have proposed a system based in two different types of particles with different densities. As one type of particle, containing the biocatalysts (in this particular example, cells of *Lactobacillus delbreuckii*), remains fluidized in the bioreactor, the second type, which is heavier and contains no cells, is introduced from the top of the bioreactor and collected at the bottom. This second type of particle is selected to selectively remove the inhibitory product of the fermentation, for example, lactic acid. Another possibility is to combine both approaches, that is, to design a multistage fluidized bed working with two types of particles to achieve a selective in situ removal of the product. Van der Wielen et al. (8) have used this approach to enhance the enzymatic deacylation of benzylpenicillin, providing the desired product, 6-aminopenicillanic acid, and as a byproduct, phenylacetic acid, by means of light particles of immobilized enzymes and heavy particles of an adsorbent of the acidic by-product. Figure 4 presents a scheme of two different possibilities for the design of a two-solid-phase fluidized-bed bioreactor: semicontinous multistage pulsed flow and continuous trickle flow. In the first, the movement of the heavier solid particles downward in the reactor is obtained by periodic pulsations; in the second, the denser particles move continuously from the top to the bottom of the reactor.

MAIN ASPECTS FOR THE DESIGN AND OPERATION OF FLUIDIZED-BED BIOREACTORS

As already described, the design and operation of a fluidized-bed bioreactor has to take into account a number of aspects regarding both physical characteristics and reaction performance. These aspects include the hydrodynamics of the bioreactor (usually with three phases), characterization of the type of flow, degree of mixing for each phase and the heat transfer, mass transfer between phases, mass balancing of the species taking part in the reaction, intrinsic kinetics of the immobilized biocatalyst, diffusion transport of the species inside the solid particles, enzyme deactivation, and cell growth. Accurate knowledge concerning these points will allow complete characterization of a fluidized-bed reactor and the development of reliable mathematical models describing its performance. Next, we discuss the conceptual aspects intrinsically related to fluidized beds. For more detailed information, including mathematical formulation of the models and their

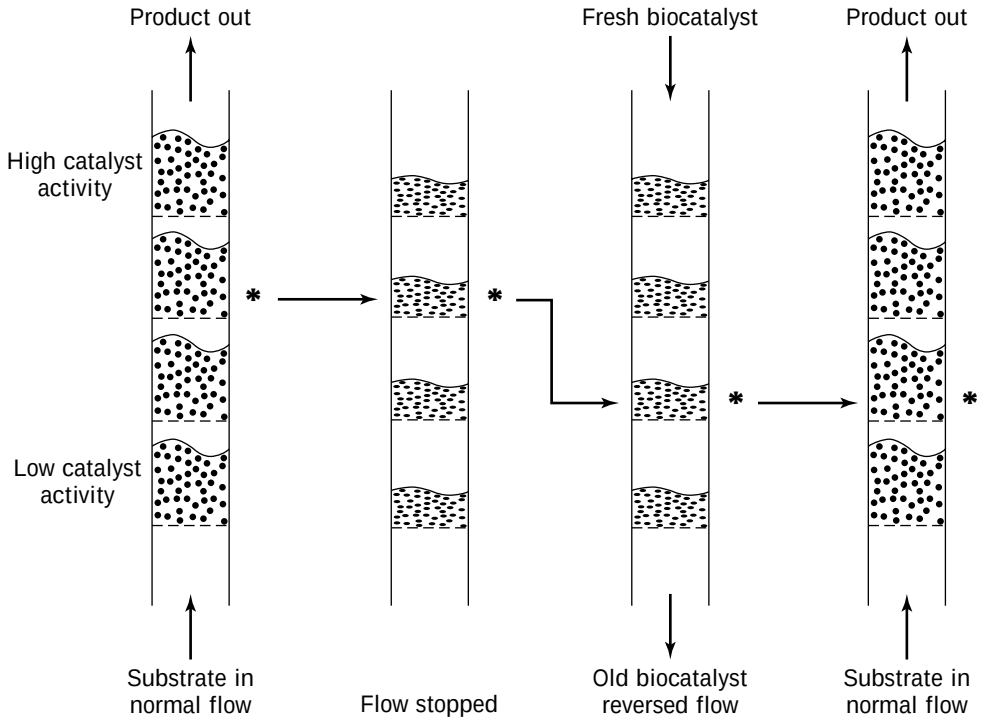

Figure 3. Operation phases of a multistage fluidized-bed reactor for a deactivating biocatalyst *Source*: From Ref. 6.

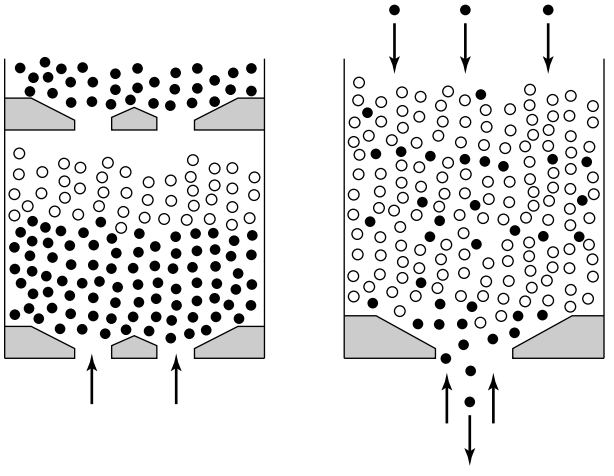

Figure 4. Schemes corresponding to two types of operation of a fluidized-bed as countercurrent adsorptive reactors, with two types of solid particles: light/small immobilized biocatalyst (○) and dense/large sorbent (●). Left: one compartment of the semicontinuous, multistage pulsed flow. Right: continuous trickle flow mode. *Source*: From Ref. 8.

application, the reader is referred to Refs. 6, 9–12 as well as general reviews in Refs. 13 and 14.

The first step in hydrodynamic characterization requires a determination of the fraction of the total volume to be occupied by the different phases (gas, liquid, solid). This is known as *phase hold-up* and can be determined using different techniques (3,15). Strictly speaking, phase hold-up may not be uniform for the whole reactor, especially with low axial dispersion. However, in systems with appreciable mixing, phase hold-up can often be considered uniform.

With respect to mixing behavior, most attention is generally paid to characterizing the liquid phase because this is, in most cases, the continuous phase in bioreactors, that is, the one in which substrates are fed and products of the reaction accumulate. For a three-phase fluidized-bed bioreactor with cocurrent up-flow circulation of liquid and gas, the type of flow pattern is very much dictated by the value and the ratio of the liquid and gas superficial velocities in the reactor (3,16). Three main regimes are possible: *(1)* the dispersed flow regime occurs at high ratios of liquid velocity to the gas velocity and is characterized by the homogeneous dispersion of small gas bubbles in the liquid; *(2)* the coalesced bubble flow regime occurs at increased gas flow rates and is characterized by the formation of bigger bubbles as a result of the coalescence of smaller ones; the coalesced bubbles have a nonuniform distribution in the liquid; *(3)* the slug-flow regime is the consequence of a further increase of gas flow rates, occurs at high ratios of gas velocity to liquid velocity, and is characterized by the formation of large gas bubbles that, in small-diameter bioreactors, tend to completely occupy their cross-sectional area. Slug formation breaks the bed continuity and causes great instability. Figure 5 gives an example of experimental data in a fluidization chart, showing these different regimes. If the gas flow rate is increased dramatically, it will eventually become the continuous phase in the bioreactor. A very detailed study on the characteristics of these dif-

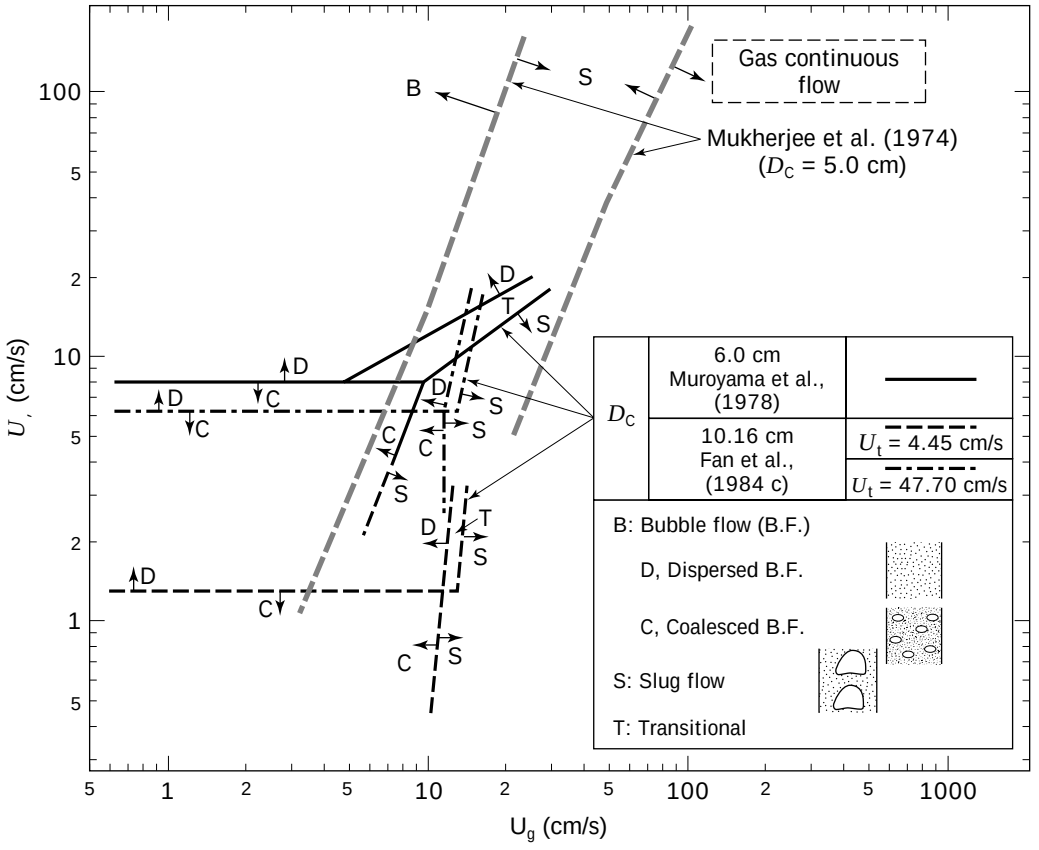

Figure 5. Flow regime diagram for the concurrent gas–liquid–solid fluidized-bed, U_g, gas superficial velocity. U_l, liquid superficial velocity. *Source*: From Ref. 3.

ferent regimes and the effect of the density and size of the solid particles on the regime transitions has been conducted by Zhang et al. (17). The liquid flow pattern in the bioreactor is directly influenced by the degree of mixing associated with these different regimes, as well as by other factors such as internal gas generation, bead size distribution, and external liquid recirculation. Basically, the flow will approach plug flow in systems with high velocity in the liquid phase. Quite often, bioreactors experience different degrees of mixing, and complete mixed flow can be observed in fluidized-bed bioreactors.

The influence of the gas phase on the liquid and solid mixing in a fluidized-bed bioreactor has been studied by Gommers et al. (18), considering two extreme situations: a reactor operating without gas and a reactor to which gas was introduced artificially from the bottom. The results showed that the gas phase greatly influences the degree of liquid mixing in the reactor, and that this effect increases sharply with the bed diameter. Another fact to consider is that in systems with gas generation associated with the reaction progress (for example, in most fermentations), the gas flow will change from the bottom to the top of the reactor, proportionally to the substrate consumption, and the axial dispersion will change with reactor height (19). An important aspect to consider in the study of the influence of the gas produced in a fluidized bed on the degree of liquid mixing is that the results will be affected by the experimental system used for gas injection, as discussed in detail by Buffière et al. (20). When liquid recirculation is used to promote fluidization because of the slow reaction rate and the long liquid-residence time required, plug flow is usually disrupted, and completely mixed flow is usually achieved.

Other factors influencing the hydrodynamic behavior of fluidized-bed bioreactors are the properties of the solid and liquid phases. In general terms, the weight and size of the solid particles will directly influence the liquid and gas flow rates required for bed fluidization. If the liquid residence time is fixed by criteria of substrate conversion, for example, then the heavier particles will require higher L/D ratios to increase liquid superficial velocity and enhance fluidization, or as an alternative, they will require high recirculation rates. In absence of recirculation, and when particles with a certain distribution in size and weight are used, solid-particle stratification is commonly found. Under stratification conditions, movement of the solid particles in the bed is very limited, and the particles are ordered by decreasing settling-velocities, from the bottom to the top of the bed. One of the consequences of this situation is that, in liquid plug-flow regimes, the particles at different reactor heights will experience different environments. For cells growing as biofilms around a solid particle, it is typical for the particles at the bottom of the bed to provide better conditions for cell growth (for example, substrate

availability), and as a consequence, they will decrease their overall density and therefore migrate to the upper part of the reactor. Removal of excess biofilm may require external treatment of the particles. The operation of a stratified fluidized bed is illustrated in Figure 6, where the stratification of a bed with activated carbon as a solid support for cell growth is combined with the capacity to absorb the product of the reaction and, therefore, remove it selectively (21). The crucial effect of particle size and density distribution, as well as gas and liquid superficial velocities, on the phenomena of solid-particle stratification is discussed in detail in various recent studies (22–24). In general, solids mixing has been studied less comprehensively than liquid mixing, and it is less well understood. The possibility of using new experimental techniques (25) has enabled researchers to propose new models for the interpretation of the solids mixing, for example, trajectory length distribution (26,27), in contrast to more classical models that assume that solids mixing can be defined by means of an axial dispersion model (28).

Another important aspect to be considered from the hydrodynamic point of view is that fluidization properties depend on the difference in densities of the solid and liquid phases in the fluidized bed, and these values change during the operation time. This situation is of particular relevance for those systems where the absolute values for the liquid and solid densities are relatively close, such as for cells immobilized in natural origin polymers (alginate, agarose, etc.) or self-aggregated cells (pellets, flocs, etc.). In this case, relatively low variations in the absolute value of the solid density (usually associated with cell growth or the accumulation of CO_2 gas in the particles) and the liquid density (usually associated with substrate consumption) may cause an important percentile variation in the density difference between both phases, producing a relevant impact on the reactor hydrodynamics, as the regime changes from dispersed to coalescing (29), and on reactor stability. This problem can be of particular relevance at the start-up of a bioreactor operation, when the density values may change to a greater extent.

A second aspect to be addressed in the characterization of a fluidized-bed reactor is the definition of the flux model. As mentioned previously, most of the attention is focused on the liquid phase, and the flux model is closely connected to the hydrodynamic conditions in the reactor that will generate a given degree of internal mixing, which is somewhere between the two extreme situations of perfectly mixed or plug flow. The determination of the real liquid flux model in the bioreactor is a necessary step for the application of the mass balance equations for the species taking part in the reaction. Stimulus–response techniques are commonly used for such a purpose and are based on the introduction of an inert tracer at the reactor inlet and the analysis of the response curve obtained at the outlet, which reflects the type of flux (30). The models that describe the liquid flux in a real reactor (31) can be *(1)* an axial dispersion model, in which axial dispersion is superimposed on the liquid convective flux; *(2)* a tank-in-series model, in which the bioreactor is considered as a series of CSTR reactors of the same volume; and *(3)* a compartmented model, in which the flux model in the bioreactor is described as the combination of different ideal compartments. For fluidized-bed bioreactors, especially when fermentation gas is produced, some interesting contributions have been proposed, such as the consideration of a variable dispersion coefficient, which increases its value in proportion to the fermentation gas generated in the reactor, up to a given point (10).

In addition to hydrodynamic and mixing characteristics, another relevant aspect of a fluidized-bed bioreactor is its biocatalytic activity. Because immobilized biocatalysts are always used, the definition of the problem must simultaneously include the reaction characteristics (kinetics, stoichiometry, equilibrium) and transport characteristics, including both the transport between the liquid and the solid phase and the transport within the solid phase. When the general situation of a solid biocatalyst particle immersed in a liquid phase, as shown in Figure 7, is studied, different phenomena have to be considered. First, substrate is transported from the liquid phase to the solid ex-

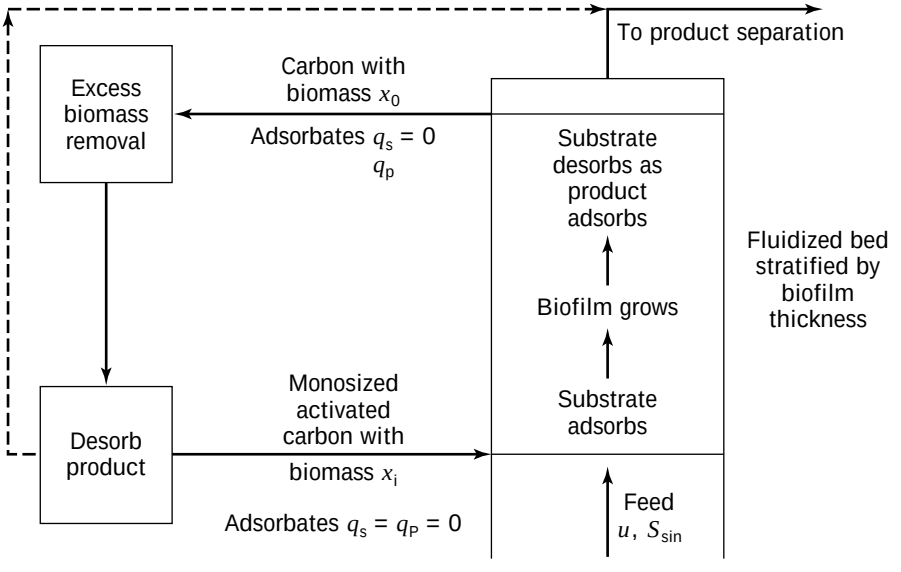

Figure 6. Operation diagram of a fluidized-bed bioreactor with simultaneous bioconversion and adsorption/desorption of substrate and product. *Source*: From Ref. 21.

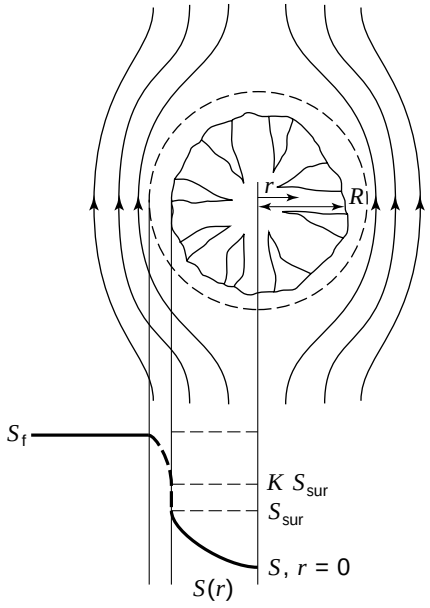

Figure 7. Inter and intraparticle mass transfer of a single porous spherical bead of radius R. Substrate concentration profiles across the stagnant liquid film and inside the solid particle, $S(r)$. S_f, concentration on the bulk liquid; S_{sur}, concentration on the solid surface; K, partition coefficient. *Source*: From Ref. 11.

ternal surface. This external mass transfer is usually modeled by means of a hypothetical liquid film that creates resistance to the transport, and it is characterized by the external mass transfer coefficient. The value of the coefficient, and thus of the external mass transfer velocity, depends on the physical properties of the liquid and the superficial velocity of the liquid around the solid; thus beds with more mixing will present better conditions for external mass transfer. When external mass transfer resistance is negligible, the concentration at the surface of the particle is the same as in the fluid phase ($S_f = S_{sur}$, according to Figure 7). An additional possibility is the occurrence of partitioning phenomena in the substrate, between the particles and the liquid, as a result of the material properties. In that case, the ratio between the substrate concentration at both sides of the solid–liquid interface will be given by the partition coefficient, K. Equally, partitioning phenomena can be determined for the product. Once in the solid particle, the substrate will diffuse inside the solid, following Fick's law, and simultaneously the reaction will take place. Therefore the corresponding equations of kinetic reaction and diffusion in the solid have to be solved simultaneously (10,11) in order to obtain the internal concentration profiles. To define this part correctly, the values for the intrinsic kinetic parameters of the reaction (that is, in absence of mass transfer limitations) and the effective diffusivities for the substrate and the product of the reaction in the solid have to be known. Moreover, the substrate conversion implies product generation, and this can affect the kinetics (for example, by product inhibition); usually the diffusion and reaction analysis is made simultaneously for both substrate and product. The overall activity of the biocatalytic particles will be dictated by the relative velocities of the two phenomena taking place inside them: reaction and diffusion. Systems with low diffusion rates with respect to the reaction rates will be diffusion controlled; on the other hand, systems with high diffusion rates with respect to the reaction rate will be controlled by the reaction. In the first case, the low diffusion will limit the efficiency of the particle because the reaction potential of the immobilized biocatalyst will not be fully used. Usually, this is reflected in terms of the efficiency factor, which is defined as the ratio between the actual reaction rate occurring in the system, and the reaction rate that would occur if no diffusional limitations existed, that is, when all solid particles would present a uniform concentration, equal to that of their surface. The relationship between the effectiveness factor and some moduli, such as the observable modulus, being proportional to the ratio between reaction and diffusion rates, is given in Figure 8. One of the interesting properties of such graphs is that they are very similar for different types of geometries and kinetics. Therefore they enable a direct analysis of the degree of diffusional limitations in a given type of particle in a fluidized bed and also suggest quantitative modifications to be performed to avoid such limitations, for example, changes in the particle size or diffusion conditions. In general terms, fluidized beds are interesting with regard to these aspects because since they require comparatively small-diameter particles for better fluidization, the potential diffusion limitations are reduced.

As mentioned at the beginning of this section, the combination of the different aspects we discussed allows the elaboration of mathematical models describing the behavior of fluidized-bed bioreactors. The reliability of these models depends greatly on the accuracy of the determination of the various parameters involved in the definition of the reactor and the reaction system (flux model, intrinsic kinetic parameters, external mass and heat transfer coefficients, internal effective diffusivities), and they will serve for various purposes such as conceptualization and understanding of the bioreactor itself (an important aspect required for building the model), design of similar bioreactors (especially in the case of scaling-up), simulation of the bioreactor operation at different conditions, and bioreactor control. As an example of how the output of a mathematical model can describe the internal concentration profiles in a fluidized-bed bioreactor, the data corresponding to a continuous fermenter for the production of ethanol from glucose by the bacteria *Zymomonas mobilis* immobilized in carrageenan beads (10) are given in Figure 9.

INDUSTRIAL APPLICATIONS OF FLUIDIZED-BED BIOREACTORS

Fluidized-bed bioreactors have been studied in a wide spectrum of applications as a consequence of the different advantages that they offer (14,33). Nevertheless, this interest has been translated with relatively low intensity into the industrial scale of operation. Possible reasons for this may be the greater complexity of the reactor compared with conventional types (especially regarding long-term

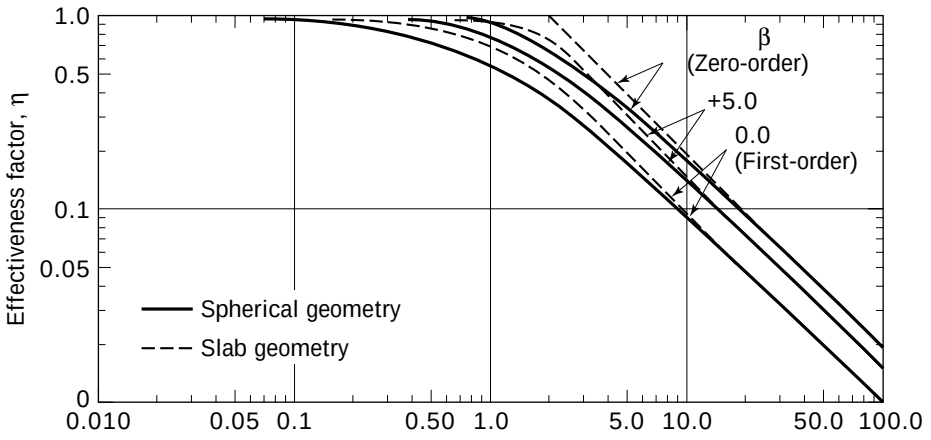

Figure 8. Variation of the effectiveness factor values for immobilized enzymes with Michaelis–Menten intrinsic kinetics with respect to the observable modulus, Φ. *Source*: From Ref. 32.

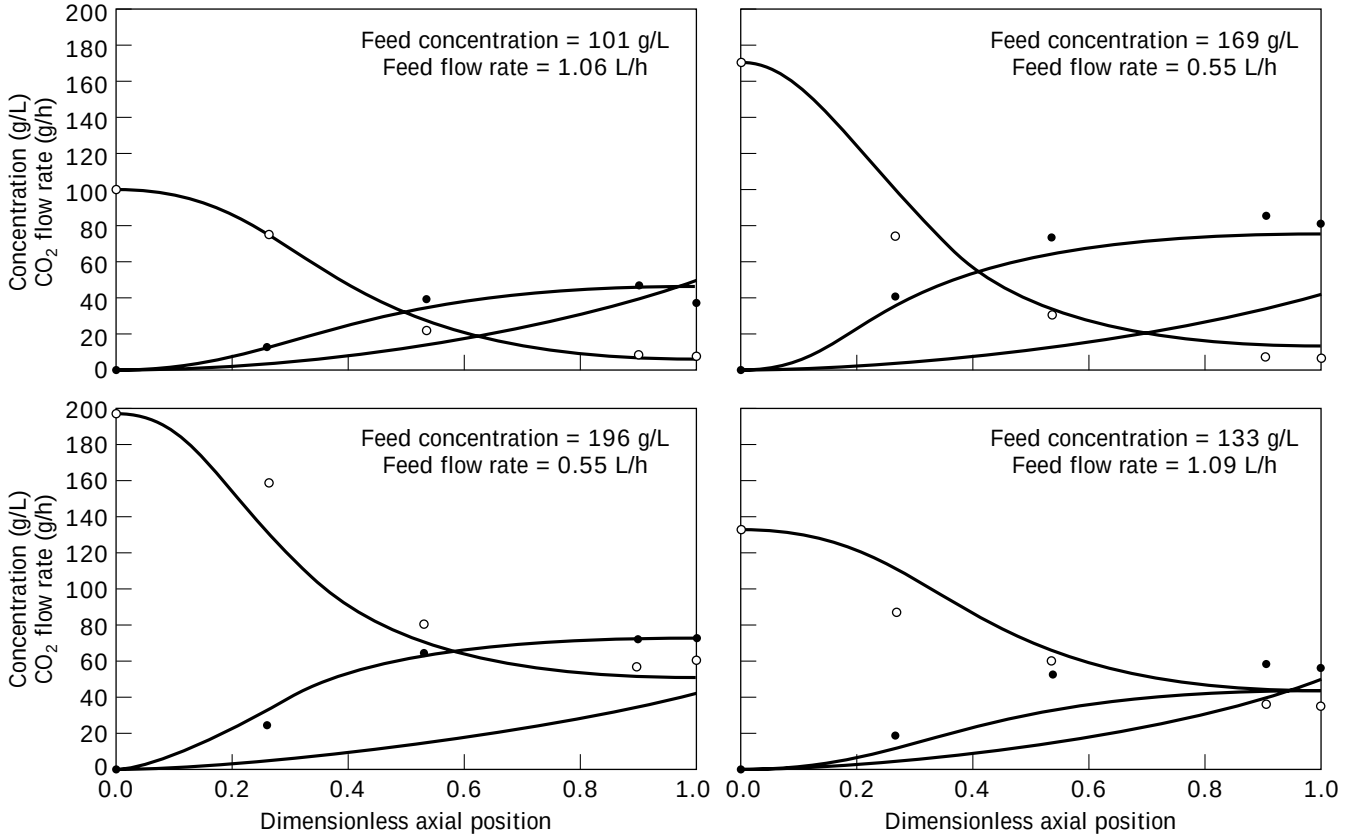

Figure 9. Results of the mathematical model for a tapered fluidized-bed producing ethanol from glucose with *Zymomonas mobilis* cells immobilized in carrageenan beads. Internal concentration profiles with the dimensionless fermenter height: experimental values (points) and values predicted by the model (solid lines). Dotted lines represent the calculated CO_2 flow rate produced by fermentation. *Source*: From Ref. 10.

operation, hydrodynamic behavior and evolution of the immobilized biocatalyst), and the time required in any industrial process to implement any change in technology. Some specific examples from different biotechnological processes illustrate the feasibility of the fluidized bed at a pilot plant and on the industrial scale. The area of wastewater treatment provides examples of high-volume operation and has made use of three-phase fluidized-bed bioreactors, as well as other related designs (such as the up-flow anaerobic sludge blanket reactor), to a significant extent. The wastewater from the baker's yeast industry, particularly from the Gist-brocades company in Delft,

Figure 10. View of an industrial anaerobic wastewater treatment plant based on the operation of fluidized-bed reactors, Gist-brocades, Delft, The Netherlands. *Source*: From Ref. 34.

Netherlands, has been treated with two anaerobic fluidized-bed reactors in series, each one 21 m high and with 390 m^3 total volume, operating with bacterial cells immobilized by attachment onto 0.25- to 0.5-mm-diameter sand particles, a support that is typical for other fluidized-bed reactors applied to anaerobic and aerobic wastewater treatment (34). The volume of the reactor employed for the disengagement of the CH_4 gas obtained was important, and the fluidized-bed volume was 215 m^3. The carbon–oxygen demand (COD) conversion of these reactors is 22 kg/(m^3 day), which is 65% of the COD in the load. A first set of these reactors started operation in 1984, and a second set in 1986. A picture of these industrial units is given in Figure 10. More recently, data from two full-scale an-

aerobic three-phase fluidized-bed plants have also been reported (33). A 700-m^3-total-volume reactor (500-m^3 working volume) has been installed for wastewater treatment at a sugar beet factory of United Northern Sugar Factories Co. in Clauen, Germany, using cells immobilized onto pumice and having COD conversion of 20 kg/(m^3 day). A 734-m^3-total-volume multistage reactor (650- to 700-m^3 working volume) has been installed for wastewater treatment at a yeast factory of Hamburg Co., in Hamburg, Germany, using free cells and a new principle that allows control, in each stage, of the ratio of the recirculated gas amount with respect to the rising gas flow. This enables optimization of the hydrodynamic conditions in each stage, according to the reactor loading. Nitrification of the effluent from a municipal wastewater treatment plant in order to eliminate ammonium salts has also been carried out in large-scale fluidized-bed reactors (35) with a cross-sectional area of 2.2 m^2 and a height of 5 m, using 5 tons of sand particles 0.4–0.6 mm in diameter as support particles for cell biofilm development. The reported results show the feasibility of the system, from both the technical and economic points of view.

Ethanol fermentation has been studied intensively in fluidized-bed reactors and brought up to the pilot-plant level in several cases. A pilot plant with a volume of 1 m^3, using *Saccharomyces cerevisiae* cells immobilized in carrageenan beads has been successfully operated for half a year (36). As an alternative to yeast, the bacteria *Zymomonas mobilis* can also be used. Very promising results have been reported on the operation of a series of two pilot reactors of 55 L each, under nonsterile conditions (37). The support for the immobilization in this case was a macroporous glass particle, Siran, that allowed cell attachment to the internal surface of the pores. After an initial period of sterile colonization of the beads in a conventional stirred tank, the particles, with a high *Z. mobilis* cell concentration, can be transferred to the fluidized bed, which then can be operated at high dilution rates under nonsterile conditions because all the possible contaminants in the feed (a solution of hydrolyzed B-starch) are washed out from the reactor. Complete conversion of 120 g/L sugar concentration with a 4.25-h residence time can be consistently obtained, with ethanol productivities of 18 g/(L h), calculated with the total reactor volume as a basis. A complete technical and economic evaluation of the use of fluidized-bed reactors for the production of ethanol with *Z. mobilis* has shown promising features (38).

Other examples of the use of fluidized-bed bioreactors on the pilot scale in fermentation processes include the production of alcohol-free beer with immobilized yeast in a 50-L pilot-plant fluidized-bed reactor (39) and the production of penicillin using *Penicillium chrysogenum* immobilized in urethane particles in a 160-L pilot-plant reactor (40). *Penicillium chrysogenum* cells have also been used in different studies with fluidized-bed reactors with celite as the support material (41). Also, the area of animal cell culture provides a number of examples of the application of fluidized-bed technology, taking into account that smaller production volumes are usually required in this case. The use of immobilized cells is particularly required for those cells that are anchorage dependent, and a variety of porous carriers and beads have been developed for this purpose. The production of a human anti-HIV-1 antibody using recombinant Chinese hamster ovary cells grown onto a macroporous polyethylene carrier has been carried out in an 84-L-volume pilot-scale fluidized-bed novel reactor equipped with a low shear stress internal impeller for the recirculation of the liquid (42).

BIBLIOGRAPHY

1. D. Kunii and O. Levenspiel, *Fluidization Engineering*, Robert E. Krieger, Huntington, New York, 1977.
2. L.S. Fan, *Gas–Liquid–Solid Fluidization Engineering*, Butterworths, Stoneham, 1989.
3. K. Muroyama and L.S. Fan, *AIChE J.* **31**, 1–34 (1985).
4. G. F. Andrews and J. Przezdziecki, *Biotechnol. Bioeng.* **28**, 802–810 (1986).
5. J.A.M. de Bont, J. Visser, B. Matiasson, and J. Tramper, *Physiology of Immobilized Cells*, Elsevier, Amsterdam, 1990.
6. H.J. Vos, D.J. Groen, J.M. Potters, and K.Ch.A.M. Luyben, *Biotechnol. Bioeng.* **36**, 367–376 (1990).
7. B.H. Davison and C.D. Scott, *Biotechnol. Bioeng.* **39**, 365–368 (1992).
8. L.A.M. Van der Wielen, P.J. Diepen, A.J.J. Straathof, and K.Ch.A.M. Luyben, *Ann. N.Y. Acad. Sci.* **750**, 482–490 (1995).
9. Y. Sun and S. Furusaki, *J. Ferment. Bioeng.* **69**, 102–110 (1990).
10. J.N. Petersen and B.H. Davison, *Appl. Biochem. Biotechnol.* **28/29**, 685–698 (1991).
11. T. Kiesser, G.A. Oertzen, and W. Bauer, *Chem. Eng. Technol.* **13**, 20–26 (1990).
12. N. Qureshi and I.S. Maddox, *J. Chem. Tech. Biotechnol.* **34/35**, 441–448 (1992).
13. G.F. Andrews, *Biotechnol. Gen. Eng. Rev.* **6**, 151–178 (1988).
14. F. Godia and C. Solà, *Biotechnol. Prog.* **11**, 479–497 (1995).
15. W.M. Ohkawa, A. Maezawa, and S. Uchida, *Chem. Eng. Sci.* **52**, 3941–3947 (1997).
16. C. Zheng, B. Rao, and Y. Feng, *Chem. Eng. Sci.* **43**, 2195–2200 (1988).
17. J.-P. Zhang, J.R. Grace, N. Epstein, and K.S. Lim, *Chem. Eng. Sci.* **52**, 3979–3992 (1997).
18. P.F.J. Gommers, L.P. Christoffels, J.G. Kuenen, and K.Ch.A.M. Luyben, *Appl. Microbiol. Biotechnol.* **25**, 1–7 (1986).
19. B.H. Davison, *Appl. Biochem. Biotechnol.* **20/21**, 449–460 (1989).
20. P. Buffière, Ch. Fonade, and R. Moletta, *Chem. Eng. Sci.* **53**, 617–627 (1998).
21. G.F. Andrews and J.P. Fonta, *Appl. Biochem. Biotechnol.* **20/21**, 375–390 (1989).
22. N. Funamizu and T. Takakuwa, *Chem. Eng. Sci.* **51**, 341–351 (1996).
23. L.A.M. Van der Wielen, M.H.H. Van Dam, and K.Ch.A.M. Luyben, *Chem. Eng. Sci.* **51**, 995–1008 (1996).
24. T. Matsumoto, N. Hidaka, Y. Takebayasi, and S. Morooka, *Chem. Eng. Sci.* **52**, 3961–3970 (1997).
25. J. Reese and L.S. Fan, in J. Chaouki, F. Larachi, and M.P. Dudukovuc eds., *Non-invasive Monitoring of Multiphase Flows*, Elsevier, Amsterdam, 1997.
26. J. Villermaux, *Chem. Eng. Sci.* **51**, 1939–1946 (1996).

27. K. Kiared, F. Larachi, Ch. Guy, and J. Chaouki, *Chem. Eng. Sci.* **52**, 3931–3939 (1997).
28. T.C. Bickle and M.G. Thomas, *Ind. Eng. Chem. Process Des. Dev.* **21**, 377–381 (1982).
29. P. Béjar, C. Casas, F. Gòdia, and C. Solà, *Appl. Biochem. Biotechnol.* **34/35**, 467–475 (1992).
30. O. Levenspiel, *The Chemical Reactor Omnibook*, OSU Book Stores, Corvallis, Ore., 1979.
31. D.E. Swaine and A.J. Dauglis, *Biotechnol. Prog.* **4**, 134–148 (1988).
32. J.E. Bailey and D.F. Ollis, *Biochemical Engineering Fundamentals*, McGraw-Hill, New York, 1986, pp. 213.
33. K. Schügerl, *Chem. Eng. Sci.* **52**, 3661–3668 (1997).
34. J.I. Heijnen, A. Mulder, R. Weltevrede, J. Hols, and H.L.I.M. van Leeuwen, *Water Sci. Technol.* **23**, 1427–1436 (1991).
35. P.F. Cooper and S.C. Williams, *Water Sci. Technol.* **22**, 431–442 (1990).
36. M. Nagashima, M. Azuma, S. Noguchi, K. Inuzuka, and H. Samejima, *Biotechnol. Bioeng.* **26**, 992–997 (1984).
37. D. Weuster-Botz, A. Aivasidis, and C. Wandrey, *Appl. Microb. Biotechnol.* **39**, 685–690 (1993).
38. R.M. Busche, C.D. Scott, B.H. Davison, and L.R. Lynd, *Appl. Biochem. Biotechnol.* **34/35**, 395–417 (1992).
39. A. Aivasidis, Ch. Wandrey, H.G. Eils, and M. Katzke, *Proc. 23rd. Congr. Eur. Brew. Conv.*, 569–576 (1991).
40. I. Endo, T. Nagamune, K. Tachi, and T. Kobayashi, in G. Durand, L. Bobichon, and Florent eds., *Int. Biotechnol. Symp.*, Societé Française de Microbiologie, Paris, 1988, pp. 433–441 (1988).
41. T. Keshavarz, R. Eglin, E. Walker, C. Bucke, G. Holt, A.T. Bull, and M.D. Lilly, *Biotechnol. Bioeng.* **36**, 763–770 (1990).
42. M. Reiter, G. Blüml, T. Gaida, N. Zach, F. Unterluggauer, O. Doblhoff-Dier, M. Noe, R. Plail, S. Huss, and H. Katinger, *Bio / Technology* **9**, 1100–1102 (1991).

See also BIOREACTORS, AIR-LIFT REACTORS; BIOREACTORS, CONTINUOUS STIRRED-TANK REACTORS; FERMENTATION MONITORING, DESIGN AND OPTIMIZATION; MASS TRANSFER; SCALE-UP, STIRRED TANK REACTORS.

BIOREACTORS, GAS TREATMENT

GRAHAM ANDREWS
MMBD Consulting
Gresham, Oregon

WILLIAM APEL
Idaho National Engineering and Environmental Laboratory
Idaho Falls, Idaho

KEY WORDS

Biofilters
Biophase
Bioscrubbers
Biotricking filters
Bubble-gasified bioreactors
Cometabolism
Electron acceptors
Electron acceptors
Electron donors
Nutrient addition

OUTLINE

INTRODUCTION

The most common type of bioprocess, at least in the United States, is the aerobic treatment of wastewater, in which contaminants in the aqueous phase are biodegraded with the help of oxygen transferred from the gas phase (air) to generate a metabolic product (carbon dioxide) that, being volatile, is then stripped out of the aqueous phase into the gas. The familiarity of this arrangement should not be allowed to limit our imaginations about the possibilities of bioprocessing. It is perfectly possible to construct a process in which a gas-phase contaminant (hydrogen sulfide) is biodegraded with the help of a nonvolatile oxidant (nitrate), generating a product (sulfuric acid) that remains dissolved in the aqueous phase. The bioreactor for such a process must share many of the features found in aerobic wastewater treatment, such as efficient gas–liquid contacting, cell recycling or immobilization to create a high concentration of biomass, control of temperature and pH, and addition of nutrients in order to create a comfortable environment for microbial metabolism. However, the different objective, the treatment of a gas rather than a liquid, must dictate differences in the details. This point can be illustrated by thinking of a conventional trickling filter not as a device for treating sewage, but as one for removing

oxygen from the air that flows through it. It would work, but terribly inefficiently, with a fractional removal on the order of 1%.

This chapter presents a three-step study of the use of bioprocesses for the removal of undesirable components from gas streams. The existing and potential applications are described first, followed by the types of bioreactors that may be employed. A simple process analysis is then presented to illustrate how the choice and design of the bioreactor is dictated by the particular application, the type of microbial metabolism involved, the concentration and solubility of the contaminant, and so on. It should be noted that there are also a number of potential bioprocesses in which the objective is not the removal of a contaminant from a gas stream, but the bioconversion of gaseous substrates into useful products. They include the partial oxidation of methane to methanol, and the production of ethanol and acetic acid from mixtures of carbon monoxide and hydrogen. Work on these processes is not described in detail, except when doing so illustrates the common problems of bioreactors with gaseous substrates.

MICROORGANISMS AND APPLICATIONS

Due to inherent difficulties in achieving the sterile conditions necessary for prolonged maintenance of pure cultures in field-scale bioreactors, most gas treatment bioreactors contain a mixed culture or consortium of microorganisms. These consortia may be derived from a number of different inocula, from common sources such as sewage-treatment facilities, biofilms from established bioreactors used for similar applications, or soils and waters from areas contaminated with the substrate of interest. In some instances, it is possible to enrich for the desired microbial consortium directly from the bioreactor bed medium, particularly when media components such as soil, compost, peat, or bark chips are used, because these materials naturally contain a mixture of microbes with wide-ranging physiological capacities. Regardless of the inoculum source, the bioreactor must be operated under conditions that select for and maintain, over the life of the bioreactor, microorganisms with the physiological capabilities necessary to catalyze the desired bioconversion. Typical selective factors include the electron donor (i.e., the metabolizable energy source), available terminal electron acceptors, supplemental nutrients, pH, Eh, and temperature.

Regardless of the selection strategy used to achieve a microbial consortium with the desired physiological properties, the use of a consortium versus the attempted use of a pure culture of microbes has a number of practical advantages. As mentioned above, it is difficult to achieve the sterility standards necessary to maintain a pure culture of microbes in a gas treatment bioreactor under field conditions. In addition, a pure culture of microbes is often metabolically incapable of fully degrading a contaminant, so hazardous intermediates may be created and build up within the bioreactor or in effluent streams from the bioreactor. Because mixed consortia inherently tend to be composed of a number of different microbial species with a gamut of physiological capabilities, undesired intermediates that may be created by pure cultures are often fully degraded by consortia. Similarly, in many applications, the concentrations and chemical compositions of gas streams to be treated may be transient. Consortia generally have a higher probability than pure cultures of adapting to this transience. The contaminant gases and vapors that can be successfully biodegraded can be classified by their role in microbial metabolism.

Electron Donors

Microorganisms require a constant supply of metabolic energy, which is normally derived from the oxidation of either organic or inorganic compounds, with these compounds serving as electron donors to the microorganisms. Many environmentally or industrially significant gases and vapors are metabolically oxidizable by microorganisms and can serve as electron donors. Thus, many different types of gas and vapor streams can be and have been, treated microbiologically (1). Microbially oxidizable gases and vapors that have been treated in bioreactors include hydrocarbons, ketones, ammonia, xylene, alcohol, terpene, and carbon disulfide vapors, as well as gases such as methane and hydrogen sulfide (2–10). In the case of carbon-containing substrates (hydrocarbons, carbon monoxide, etc.), the metabolism of these compounds provides heterotrophic microbes not only with an electron source, but also with a source of cellular carbon. Non-carbon-containing substrates such as ammonium, while providing a metabolic electron source, must be metabolized by autotrophic microorganisms capable of obtaining their cellular carbon via the fixation of atmospheric carbon dioxide.

Cometabolism

Some substrates cannot serve as sole energy sources for microorganisms, but are nevertheless potentially bioconvertable. Their biodegradation is achieved in the presence of another compound that serves as the microorganism metabolic electron donor, a process that is termed cometabolism. Trichloroethylene (TCE) provides a well-documented example of a substrate that is oxidized cometabolically by microorganisms. Typical of cometabolic TCE degraders are the methanotrophic bacteria, aerobes that oxidize methane as their sole carbon and energy source (11). This oxidation takes place in a sequential manner, with methane first being converted to methanol, which is in turn oxidized to formaldehyde, formate, and finally, carbon dioxide. Along this oxidative pathway, the methanotrophs generate cellular energy as well as fixing methane-derived carbon into additional biomass. The first step, in which methanol is formed from methane, is catalyzed by the enzyme methane monooxygenase (MMO) (12,13). Although MMO is selective for its natural substrate, it can, under certain conditions, catalyze the oxidation of a variety of other compounds (12–14), including partially chlorinated aliphatic solvents such as TCE. Two distinct forms of MMO have been identified, membrane MMO (mMMO) and soluble (sMMO) (15,16). sMMO, ex-

pressed by methanotrophs growing under copper-limited conditions, supports much higher rates of TCE oxidation than does mMMO, which is expressed under conditions of copper sufficiency (17).

Air streams contaminated with TCE and similar chlorinated solvents are generated by industrial operations and the remediation of contaminated ground and water by air stripping. They can be treated in a bioreactor that is started up with methane as the sole carbon and energy source, while supplying the necessary oxygen and supplemental nutrients under copper-limiting conditions (6). After the methanotrophic consortium is established, the methane load to the reactor can be decreased or fed on an intermittent basis concurrently with TCE vapors. The methanotrophic microbes then will be maintained by the lessened methane feed, while catalyzing the oxidation of the TCE via their sMMO. The reduced or intermittent methane feed not only reduces the amount of methane that must be supplied, but is essential in achieving optimal TCE removal rates since methane itself is an effective competitive inhibitor of TCE oxidation. An alternate, but more expensive, strategy used to avoid this type of competitive inhibition is to supply a catabolic intermediate such as formate in order to provide energy to the methanotrophs, because formate does not compete with TCE for access to the sMMO. It should be noted that a number of other microbial oxygenases have been shown to be capable of catalyzing cometabolic TCE oxidation. These include toluene oxygenases from a number of *Pseudomonas* spp., propane monooxygenases from propanotrophs, and ammonia monooxygenase from *Nitrosomonas europea* (18–21).

Electron Acceptors

Most gas treatment bioreactors remove contaminants from air streams and oxidize them to innocuous end products (CO_2, Cl^-, etc.), using the oxygen in the air as the electron acceptor. However, there are also gas streams containing little or no oxygen where the objective is to remove a compound that can act as an alternative physiological terminal electron acceptor. This approach has been shown to work for compounds like sulfur oxides (SO_x) and nitrogen oxides (NO_x) (8,24,25). NO_x biofilters have been developed using a consortia of denitrifying microbes that have the physiological capacity, as a part of their normal metabolism, to use a variety of NO_x compounds as terminal electron acceptors, reducing them to innocuous nitrogen gas (N_2). This process generally requires low-oxygen conditions because denitrifiers preferentially use oxygen, if present, as their terminal electron acceptor. As a result, selective conditions for denitrifying microbes include a suitable carbon and energy source with a NO_x compound as a terminal electron acceptor, a lack of oxygen, and the presence of supplemental nutrients necessary for microbial growth. The potential application to stack gases raises the question of the maximum temperature at which the microbes will function. Research (25) has shown that naturally occurring thermophilic microbes selected for from compost are capable of reducing nitric oxide (NO) to nitrogen gas (N_2) at temperatures up to 60 °C.

Other processes are far more sensitive than denitrification to trace amounts of oxygen. The sulfite-reducing bacteria responsible for the removal of SO_2 are obligate anaerobes, although they may be active in anoxic microniches, for example, deep in a biofilm. Chlorinated aliphatic solvents will also accept electrons under anaerobic conditions, a degradative mechanism that works best on the completely chlorinated compounds that are not touched by the oxidative enzymes already discussed (22,23). Carbon tetrachloride, for example, will be progressively reduced to chloroform, dichloromethane, and methyl chloride. This mechanism is often categorized as cometabolism, implying that the microbes derive no metabolic benefit from it, but this remains uncertain.

BIOREACTOR TYPES

Figure 1 shows a generic gas treatment bioprocess along with the nomenclature to be used in the subsequent analysis. Gas treatment bioreactors are sometimes described as *gas-phase bioreactors*, but this term is inexact in the sense that the actual reactions happen inside a microbial cell, which is necessarily an aqueous phase. Some reactions carried out in immobilized enzyme reactors do seem to involve direct interaction between the gas and the enzyme (33), although even here the humidity remains a critical variable and the enzyme may be covered with a layer of water a few molecules thick. For our purposes, the bioreactor is divided into a gas phase, a solid phase consisting of any solid packing or biofilm support particles, and a biophase, which contains the water and the microorganisms. The fraction of the bioreactor volume occupied by each phase is called its holdup, and the three values, e_g, e_s, and e_b, must add up to 1.

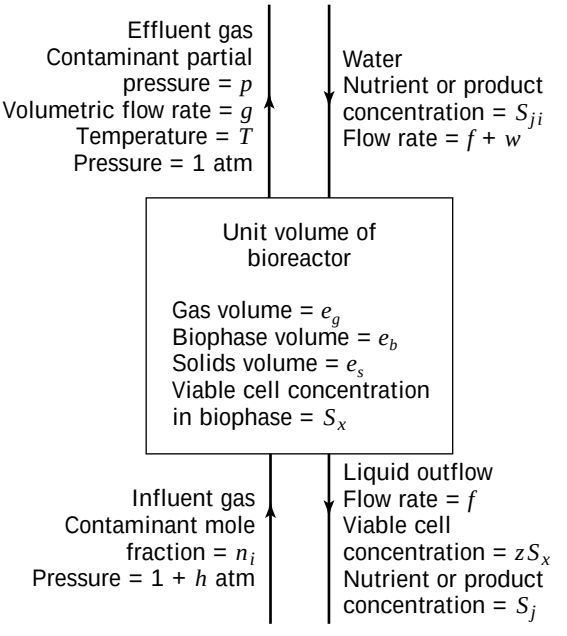

Figure 1. The generic gas-treatment bioreactor.

For convenience, we think in terms of a bioreactor of unit volume and express the gas flow rate as the volume per volume per minute (VVM) flow rate, g, at the effluent gas conditions, taken as temperature T and atmospheric pressure. Others choose to work in terms of the molar outlet gas flow rate (g/RT, where R is the gas constant) or a gas residence time, either the empty bed residence time, $1/g$, or the average time an element of gas actually spends in the reactor, e_g/g. The flow rate of the influent gas is not the same as g because its temperature may not be T, it is at a higher pressure, ($1 + h$ atmospheres, where h is the pressure drop through the reactor), and because various components (contaminant, oxygen, metabolic products, water vapor) are added to, or removed from, the gas stream as it flows through the reactor. When these effects are significant, it is essential to specify exactly what is meant by "gas flow rate."

The objective of some processes is to remove a gaseous contaminant by converting it into a soluble, nonvolatile metabolic product. Some such products, H^+ for example, can be neutralized in the bioreactor, but others, such as the Cl^- from the degradation of chlorinated organics, must be removed in the liquid if they are not to accumulate to concentrations that inhibit the microorganisms. There may therefore be a liquid outflow, f per unit bioreactor volume, and an inflow that must be greater than f to allow for the evaporation rate, w. This outflow tends to wash microorganisms out of the bioreactor, and it is usually beneficial to retain them either by cell recycle or immobilization, making the parameter z in Figure 1 less than 1.

The question is what type of bioreactor should be put in the "black box" in Figure 1. Almost every possible configuration by which a gas can be contacted with a biofilm or a suspension of microorganisms has been employed in some application, and these can be roughly divided into four categories.

Biofilters

The earliest gas-treatment bioreactors were used to control odors in air coming from slaughterhouses and rendering plants and consisted of porous pipes buried in the ground, the noxious compounds being removed by a combination of adsorption and biodegradation as the air flowed up through the soil (26). Applications of the idea have since expanded to include the removal of hazardous, volatile compounds from chemical plants, paint shops, foundries, and a variety of agricultural and food-processing operations. Although often effective, the operation of these simple soil beds depends critically on the local soil and weather conditions. Unless they are covered and/or periodically sprayed with water, they may stop working, either due to becoming waterlogged or to drying out. They have largely been replaced by custom-made biofilters, which are essentially boxes made of plastic, wood, sheet metal, concrete, or even stainless steel, containing a bed of media and a gas distribution system to ensure uniform flow of the gas through the bed.

In terms of the variables defined in Figure 1, biofilters are the small e_b, small f, and small z approach. The biophase consists of individual microorganisms attached to the media, perhaps enough to constitute a thin biofilm. The amount of moisture in this layer is critical, and is controlled by humidification of the inlet gas and/or by spraying water directly over the bed. Little or no water drips out of the bed, making it difficult to provide soluble nutrients and pH control chemicals, or to wash out nonvolatile metabolic products. Biofilters are thus best suited to applications that generate no such products and involve no pH swings, the treatment of air streams containing low levels of volatile organics being the obvious example.

The great advantage of biofilters over the early soil beds is that they allow the choice of the nature and particle size of the bed media. This media must support a high density of attached microorganisms suited to the particular application, perhaps even providing some of the nutrients needed for their growth. The ability to adsorb the contaminant is an advantage because adsorption can provide some contaminant removal during the start-up period, before a large population of well-acclimated microorganisms has developed (sometimes called "the bed-ripening period"), and during any sudden slugs of concentrated contaminant in the influent gas. Also, although the interactions between such adsorption and biodegradation are complex and poorly understood, they are generally favorable to biofilter performance. Finally, the media must be mechanically strong and resistant to disintegration, compacting, and the resulting channeling of gas flow. Soil, compost, peat, and wood-chip mixtures are all inexpensive media that have been used successfully. Materials such as activated carbon and limestone, although more expensive, may be mixed in to provide extra adsorption and pH buffering.

The particle size of the media is critical. Small particles give a huge gas–biophase interfacial area per unit bed volume (a quantity subsequently called "a"), thus eliminating concerns about mass-transfer limitations between the two phases. But beds of small particles have a higher resistance to gas flow, are more prone to waterlogging and plugging by excess biofilm, and if too light, may get blown out of the reactor altogether. A general guideline is to choose the smallest available particles that avoid the latter problems, and then ensure that the shape of the bed is optimized to give the desired contaminant removal with a reasonable pressure drop (see "Scale-Up").

If the life of the bed is found to be finite due to compaction, loss of pH buffering capacity, accumulation of salts from the evaporation of added water and so on, one solution is to employ two beds in series. Bed 1 can provide most of the contaminant removal, while bed 2 polishes the effluent, mainly by adsorption, while developing its own population of well-acclimated microorganisms. When bed 1 is exhausted it can be replaced by bed 2, which is itself replaced by a bed of fresh media. The arrangement of the media on a series of trays in the bioreactor facilitates this mode of operation.

Bubble-Gasified Reactors

Conventional bubble-aerated fermenters make poor gas treatment bioreactors because they are designed for a high rate of transfer of gaseous nutrients and products (O_2 in

and CO_2 out), rather than a high fractional removal of a component from the air stream. This latter objective requires taller bioreactors with longer gas residence times, but tall reactors mean higher pressure drops due to the hydrostatic head. Nevertheless, tall, mechanically agitated bioreactors with multiple impellers have been proposed for removing H_2S from industrial gas streams (29), and bubble columns with no mechanical agitation have been demonstrated for the removal of TCE from air using a toluene-oxidizing organism (30).

These bioreactors are in many ways at the opposite extreme from biofilters. The biophase occupies most of the reactor ($e_b \rightarrow 1$ in Fig. 1), and it is dilute and well-mixed rather than dense and immobilized. The large volume of water makes it easy to add soluble nutrients, control the pH, and remove water containing nonvolatile products. However, care must be taken to not wash out the biomass, because $z = 1$ (Fig. 1) unless there are extra surfaces in the bioreactor for the attachment of a biofilm, or if a cell separation and recycle loop is added. Another major difference is that the gas–biophase interfacial area, a, is not only much smaller than in a biofilter, but is not even a constant, varying with the gas flow rate. Bubble gasified bioreactors are therefore best suited to contaminants like NO_x that are very soluble in water (thus reducing concerns about the gas–liquid mass-transfer rate), whose dissolution in water cause pH swings, and whose metabolism requires large amounts of dissolved nutrients.

Biotrickling Filters

Trickling filters for gas treatment are similar to, but usually taller than, those in use for decades for the secondary treatment of municipal and industrial wastewaters. Like biofilters, they consist of a bed of media through which the gas flows either upward or downward, but unlike biofilters, the microbial culture is recirculated continuously over the bed from a reservoir beneath it. Stone aggregate or wood chips are the traditional media, but even seashells have been used (27). Most modern filters employ ceramic or plastic media, Pall rings, Raschig rings, and so on specifically designed to make a bed with a high surface area to maximize gas transfer, and a high porosity to minimize the pressure drop and the chance of clogging or flooding (28).

These bioreactors can be thought of as intermediate between biofilters and bubble-gasified systems and are best suited to applications between those already described. If the characteristics of the media and the microorganisms are such that most of the biomass stays attached, then a trickling filter is essentially a biofilter with a higher liquid flow and a smaller gas–biophase interfacial area, a, due to the larger media. If on the other hand, most of the biomass stays suspended and the recycle ratio (RR = flow of recycled liquid/f) is high enough to keep the biophase well mixed, then it is functionally similar to a bubble-gasified bioreactor. The main differences are that the pressure drop, h, is usually much smaller, and the interfacial area, a, is a constant that is independent of the gas flow rate.

Bioscrubbers

The systems just described essentially combine two functions, stripping the contaminant from the gas into the aqueous biophase and then subjecting it to biodegradation. But what if the physicochemical conditions in the biophase resulting from the stripping are not suitable for the microbial metabolism? The removal of sulfur dioxide from stack gas is a good example because stack gases contain a small percentage of oxygen that although relatively insoluble, inhibits the bacteria responsible for the reduction of the sulfite formed by the dissolution of SO_2. One solution is the bioscrubber, which consists of an aqueous stripper in which the contaminant is transferred from the gas to water, and a separate bioreactor, in which the liquid effluent from the stripper is essentially treated as wastewater. The bioreactor should be a completely mixed, immobilized-cell type so that a large population can grow up in a well-controlled environment without continuously being recirculated through the potentially toxic environment in the stripper. Several configurations are possible, the simplest being that in which the liquid reservoir at the bottom of a packed-bed stripper is used as the bioreactor. Bioscrubbers are not considered further here because building a separate bioreactor and stripper is necessarily more expensive than combining them in a single unit, and when it is necessary, the two unit operations can be designed by conventional methods.

BIOREACTOR DESIGN

A process variable is any quantity that is under the direct control of the designer or operator of the process. For gas treatment bioreactors, the variables to be fixed by the designer include the bioreactor type, shape, and size, whereas those fixed by the operator include the addition of water, nutrients, and chemicals for pH control. The objective in fixing these variables is to satisfy a set of process requirements that specify the flow rate and composition of the gas stream, the nature and concentration of the contaminant, and the fractional removal required. The difficulty is that many designs, that is, many combinations of the process variables, will meet the process requirements for a particular case. The proper goal of engineering design is not simply to pick one of these designs at random, but to find the single design that meets the requirements at the lowest possible cost. The design of gas treatment bioreactors, like that of any other process, is an economic optimization problem, but one that is so complex that the exact solution cannot be found within the constraints of time and money normally imposed on the design process. The best solution for a particular case will certainly depend on the scale of the problem, the solubility and possible inhibitory effects of the contaminant, the type of microbial metabolism (aerobic or anaerobic, growth associated or cometabolic, etc.) needed to degrade it, and the temperature and pressure of the gas stream. Even coming close to the best solution requires a careful scale-up program in which the insights available from education and experience are used to integrate experiments at different scales with mathematical models that can extrapolate the results from one scale to the design of the equipment at the next scale. The bioreactor analysis presented in this section is intended as a guide to this program, sug-

gesting which bioreactor types be chosen for experimental evaluation in each case, specifying the operating conditions around which the experiments should be designed, and showing how performance may be expected to vary with scale.

Because the design goals are essentially economic, the relationship of the variables shown in Figure 1 to the process costs must be kept in mind. The volume of the commercial-scale bioreactor equals the actual gas flow to be treated (a process requirement) divided by g; a large value for g translates directly into a smaller and, all other things being equal, cheaper bioreactor. The liquid flow, f should be kept as small as possible because providing clean water and disposing of any process wastewater both cost money, as do any nutrients and chemicals that must be added. The pressure drop, h, through the bioreactor may be significant, particularly on a large scale, and it determines the capital cost of the gas compressors and the energy costs for running them. Compressing the feed gas is not only expensive in itself, it heats the feed such that heat exchangers may be needed to cool it to the desired temperature.

Process Analysis

It will be assumed that the biophase is completely mixed and that the gas approximates plug flow through the bioreactor. This provides a realistic description of some bioreactors (bubble columns, some biotrickling filters), and a reasonable starting point for quantitative thinking about the others. More detailed mathematical models are available in the literature for specific types of bioreactors and metabolism (31,32). The equilibrium solubility of the contaminant in the biophase, S^*, will be described by Henry's law, $S^* = p/H$, where p = partial pressure of the contaminant in the gas and H = Henry's law constant. Although this is adequate for relatively insoluble and dilute contaminants, it is a considerable oversimplification for others. For example, the dissolution of oxides of nitrogen (NO_x: a mixture of NO and NO_2) from stack gases into water is an extremely complex process (34,35) that involves the gas-phase chemical oxidation of NO to NO_2 and a dissociation reaction that generates H^+, NO_3^-, and NO_2^- when the gas dissolves. In such cases, Henry's law can only be interpreted in the purely qualitative sense that low H means a soluble gas.

Any complete bioprocess model combines the mass conservation equations that describe the bioreactor with equations that try to approximate the complexities of microbial metabolism. Because the objective here is to compare different bioreactor configurations, it is essential to have consistent descriptions of the metabolism. In most gas treatment applications the contaminant is a major microbial nutrient, either the electron donor or the electron acceptor. Its consumption provides metabolic energy for growth and cell maintenance, so its specific consumption rate, q is given by the yield equation

$$q = \frac{\mu}{Y} + k \qquad (1)$$

where μ is the specific growth rate of cells, Y is the cell-yield coefficient, and k is the cell-maintenance coefficient.

In a well-operated bioreactor, the pH and temperature are carefully controlled and all required nutrients are provided in adequate amounts, making the specific consumption rate a function only of the concentrations of contaminant, S, and any inhibitory product, S_m, dissolved in the biophase. The exact form of this function, written $q(S, S_m)$, will not be specified because it varies among cases, but it must describe the effects on the metabolic rate of substrate limitation, product inhibition, and possibly (when n_i/H is large) substrate inhibition. It is more common to describe the specific cell growth rate, μ, by a Monod-type function of the concentration S, but this is clearly incorrect at the low concentrations found in gas treatment bioreactors, because it predicts that growth stops and substrate uptake continues when no substrate is available ($\mu = 0$ and $q = k$ when $S = 0$). In fact, when a major nutrient is exhausted, its consumption must stop, and the microorganisms go into an endogenous state in which the viable biomass declines, a phenomenon correctly approximated by requiring that $q(S, S_m) = 0$, and thus $\mu = kY$ (equation 1) when $S = 0$. Cell growth now stops at a nonzero "stationary phase" concentration, S_s, corresponding to the point where substrate uptake is just sufficient to satisfy the maintenance requirement, and defined by $q(S_s, 0) = k$.

For cometabolic processes, the contaminant is neither the main electron donor nor the acceptor; two rate equations are needed, and equation 1 contains an extra parameter whose value may be found from knowledge of the degradative pathway. See, for example, the analysis by Andrews of chloroform degradation by methanotrophic bacteria (36). The design of cometabolic bioreactors follows many of the principles described here but is too complex and case specific to be analyzed in detail.

At steady state the conservation of mass requires that the rate of growth of microorganisms in the bioreactor, $\mu e_b S_x$, equals the rate at which they flow out, fzS_x (see Fig. 1 for nomenclature). The loss of microorganisms in mist suspended in the effluent gas may be significant in some bioreactors without demisting devices but is not included explicitly in the analysis. The specific growth rate, μ, a measure of the physiological state of the microorganisms, thus equals zf/e_b, the reciprocal of the mean cell-residence time (the number of cells in the bioreactor divided by the cell outflow rate), which is a quantity under our direct control. This remarkable result, although well known for chemostats, has not been fully appreciated for gas treatment. It follows from equation 1 that the concentrations in the biophase, S and S_m, are constrained by

$$q(S, S_m) = k(1 + D) \qquad (2)$$

where $D = zf/Yke_b$ is the dimensionless dilution rate or reciprocal mean cell-residence time.

The steady-state conservation of mass for the contaminant requires that whatever is removed from the gas phase be transferred to the biophase, where it is either consumed by the microorganisms or flows out in the liquid. For a bioreactor, as opposed to a gas stripper, the latter term

should be negligible, but the flows of dissolved nutrients and nonvolatile metabolic products must be included

$$\frac{g}{RT}(n_i - p) = \frac{k_1 a(n_i - p)}{H \ln\dfrac{(n_i - HS)}{(p - HS)}} = e_b q S_x = \pm\frac{(fS_j - (f + w)S_{ji})}{y_j} \quad (3)$$

where y_j is the amount of component j produced (+ sign) or consumed (− sign) per unit of contaminant consumed (see "Nutrient Addition and Start-Up").

The description of the driving force for mass transfer in terms of the log–mean concentration difference in the second term of this equation follows from the assumption of plug flow of the gas. The expression is not strictly correct when the pressure drop through the bioreactor is large, as in a tall bubble column, because the contaminant partial pressure in the influent is then $(1 + h)n_i$; but this complication is rarely included in practice. The essential points here are that the mass-transfer factor, k_1a, is an empirically determined parameter, that it can be based on different forms of the driving force, and that the best choice depends on the reactor type and must be clearly understood by everyone involved in a project.

Equation 3 can be rearranged to give the fractional removal of the contaminant from the gas, only the product (subscript m) being considered in the last term:

$$x = 1 - \frac{p}{n_i} = (1 - e^{-G})\left(1 - \frac{HS}{n_i}\right) = \frac{S_x}{X}(1 + D) = FD\,\frac{S_m}{S'_m} \quad (4)$$

where $G = k_1aRT/gH$ is the dimensionless mass transfer coefficient; $F = YS'_m/zXy_m$ is the dimensionless product inhibition factor; $X = gn_i/ke_bRT$ is the maximum possible viable cell concentration in the biophase; and S'_m is the product concentration that completely inhibits cell growth.

Rather than solving equations 2 and 4 exactly, which would require the form of the inherent kinetic function $q(S, S_m)$, consider some limiting cases in order of decreasing liquid outflow rate. These cases are used to summarize the bioreactor performance in Figure 2, a graph that can be universal, at least within the limitations of the assumptions, because the parameters describing the contaminant (H, n_i), the reactor (f, k_1a), and the metabolism (k, S'_m) in individual cases have been incorporated into the dimensionless numbers x, D, F, and G.

- *Washout.* $D > (q(n_i/H,0)/k) - 1$: Because the dissolved concentration, S, must obviously be less than that in equilibrium with the feed gas, n_i/H, equation 2 now has no solution, meaning that all of the biomass is washed out of the reactor and there can be no contaminant removal.
- *Substrate limitation.* $D > (1 - e^{-G})/F$: Equation 4 shows that under this condition, $S \to 0$, while $S_m < S'_m$, meaning that microbial kinetics are limited by the availability of substrate rather than product inhibition and the exact value of the inhibition number, F, is irrelevant. If gas-biophase mass transfer is very rapid, the dissolved contaminant is in equilibrium with the outlet gas, giving the best possible bioreactor performance. The shape of this $G = \infty$ line in Figure 2 is simply a reflection of the relationship between $\mu(=zf/e_b)$ and $S(=p/H)$ from the inherent microbial kinetics. Mass-transfer limitation ($G < \infty$) leads to a progressive reduction in the contaminant removal, x.
- *Product inhibition.* $D < (1 - e^{-G})/F$: Now the concentration of metabolic products, S_m reaches inhibitory levels, S'_m, while dissolved contaminant is still available, meaning that metabolism is limited by product inhibition rather than substrate limitation, and the exact value of G is irrelevant. Increasingly stronger inhibition (smaller F) produces a series of curves in Figure 2 whose exact shape depends on the details of the inherent inhibition kinetics. All of these curves pass through the origin because, with no liquid outflow ($D = 0$), any soluble, nonvolatile metabolic products must eventually accumulate to inhibitory levels.

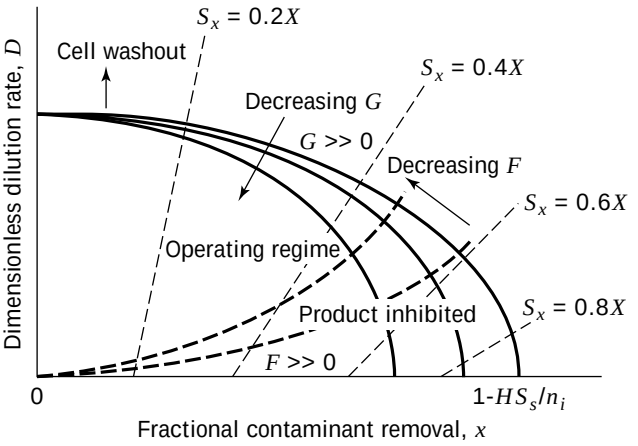

Figure 2. Operating regime for a completely mixed bioreactor.

Consequences for Process Design

Any pair of values of F and G define a regime in Figure 2 within which the bioreactor can operate. The most important result is that for any such pair of values there exists a value of D that maximizes the contaminant removal, x. If the form of the rate equation $q(S, S_m)$ were known, the pointed maximum seen in Figure 2 would be replaced by a smooth curve that defined this optimum design more accurately. In the absence of such detailed modeling the optimum must be found experimentally, the analysis providing a starting point and overall guidance. Because the gas flow rate, g, appears in the denominator of both F and G, the first step is to establish the maximum g for which the desired contaminant removal, x, falls safely within the operating regime. It is clear from equation 4 that a high re-

moval rate (e.g., $x = 0.95$) with reasonable values of $S(\gg Hn_i)$ and $S_m(<0.5\ S'_m)$ requires both $G \sim 3$ and $FD \sim 2$, and such values are reasonable, if approximate, general design goals. Much larger values represent inefficient design because they imply excessive consumption of energy and water.

For processes that produce large amounts of very inhibitory, nonvolatile, soluble metabolic products, the problem is to wash the products out of the bioreactor without washing out the biomass. Mathematically, $y_m/S'_m \to \infty$, making it difficult to keep $FD > 2$ without D exceeding the washout criterion. These are the processes that require cell retention ($z \to 0$), either by cell recycle or by immobilization as a biofilm. For processes with more moderate values of y_m/S'_m, the analysis shows that there exists an optimum set of values of the process variables g, f, and z. Some processes, the aerobic mineralization of hydrocarbons for example, generate only innocuous (H_2O) or gaseous (CO_2) products, so $y_m/S'_m \to 0$, and the analysis suggests operating with no liquid outflow. This not only gives the best effluent-gas quality (Fig. 2 with $F = \infty$) but, because the biomass is in a maintenance condition ($\mu = 0$ when $D = 0$), it also avoids the cost of adding nutrients, such as phosphates, that are needed for microbial growth (see "Nutrient Addition and Start-Up"). In practice there are reasons to avoid this condition. Even if y_m/S'_m is too small to be observed in short-term laboratory experiments, any nonvolatile product must eventually accumulate to inhibitory levels in a continuous bioreactor with no liquid outflow. Salts in the water added to compensate for evaporation or for pH control will also accumulate in the biophase. Also, it must not be forgotten that complete mixing of the biophase is an abstraction never achieved in practice and sometimes, as in the biofilter, not even attempted. The discussion prior to equation 2 shows that any bioreactor with $D = 0$ must have a cell growth rate $\mu = 0$ as an average, but it will contain microniches where cells are dying because conditions are worse than average, and others where conditions are slightly better and cells are growing. Although the growing cells may assimilate some of the material released by the lysis of the dying cells, there must be some long-term accumulation of dead biomass, with consequent reduction in bioreactor performance. Keeping D on the of order of 1, a very low flow rate in most cases can wash out the dead biomass and ensure stable operation for the cost of a few growth nutrients.

The analysis assumed the usual case in which the cell concentration in the bioreactor is kept as high as possible, with sufficient amounts of other nutrients provided to ensure that the contaminant is the limiting nutrient. The quantity X, defined under equation 4, is then the maximum possible viable-cell concentration in the biophase, corresponding to the situation where all of the contaminant flowing into the bioreactor, gn_i/RT, is being used to satisfy the cell maintenance requirement, ke_bX. The actual concentration at any given operating condition, S_x, can be calculated from the fourth term of the equation and is shown in Figure 2 as a function of D and x. There is, however, no guarantee that this concentration corresponds to a dilute, easily mixed cell suspension. If the maintenance requirement, k, is small, and the contaminant loading gn_i is large, it may be a paste of cells too dense to be, for example, pumped around a biotrickling filter. Although it is possible to reduce S_x by restricting the amounts of growth nutrients provided, such artificial reductions in the microbial "catalyst" concentration are generally poor bioprocess design. The alternative is to choose the right type of bioreactor, recognizing that, although the mass of microorganisms in the bioreactor is fixed by the process requirements and the microbial metabolism, the amount of water is a process variable that can be controlled. The concentration, X, is an order of magnitude higher in a trickle-bed type bioreactor where $e_b \approx 0.1$, than in a bubble column where $e_b \approx 1$.

Nutrient Addition and Start-Up

In some processes, the aerobic mineralization of organics in beds of compost for example, the air provides the electron acceptor and the media provides what little growth nutrients are needed. In other processes these substances, and sometimes the electron donor, must be provided in the liquid inflow. The amounts can be estimated from the "stoichiometry" of metabolism, a procedure best illustrated by example. Ongcharit et al. (37) have shown that hydrogen sulfide can be removed from industrial gas streams by the acidophilic, autotrophic, sulfur-oxidizing, denitrifying bacterium *Thiobacillus denitrificans*. Even such esoteric metabolism can be approximated by a pseudo-chemical reaction in which all of the main nutrients and products are written in the ionic form in which they enter or leave the reactor. After performing all of the element and charge balances the result is

$$\begin{aligned} H_2S + (1.6 - 0.2y\gamma)\,NO_3^- + yCO_2 + ypH_2PO_4^- \\ \rightarrow\!\!\rightarrow yCH_hN_nO_oS_sP_p + (0.8 - 0.1y(\gamma + 5n))N_2 \\ + (1 - ys)SO_4^{2-} + (0.4 + y(0.2\gamma - p - 2s))H^+ + wH_2O \end{aligned} \tag{5}$$

The first term on the right-hand side represents the dry weight of the biomass produced. $\gamma = 4 + h - 2o + 6s + 5p$ is a measure of its oxidation/reduction state and is remarkably consistent between species (36) (note that the base oxidation state for nitrogen here is N_2). The actual cell yield is y, the ratio of cells produced to H_2S consumed. For a completely mixed biophase this equals μ/q or, from equations 1 and 2,

$$y = \frac{DY}{(1 + D)} \tag{6}$$

The "stoichiometric coefficients" on the other components in equation 5 then provide the y_j values needed to calculate the concentrations of nutrients and products from the last term in equation 3. These simple calculations can provide a surprising amount of approximate information about process design and development. A feature of the example in equation 5 is the large amount of acid (H^+) produced by the metabolism. Even with the high liquid flow rate allowed by cell immobilization or recycle (29,37) its neutralization requires a high pH in the liquid inflow, so the biophase must be very well mixed if metabolism is

not to be inhibited by pH gradients, suggesting some type of bubble-gasified bioreactor. If all of the NO_3^- and OH^- are provided by their sodium salts, then the salinity in the biophase would be high, suggesting a need for halophilic strains of bacteria. A reasonable alternative would be to explore the use of calcium salts, which would precipitate some of the product sulfate as gypsum, reducing inhibitory effects.

Like all the previous analyses, equation 6 applies only to steady-state operation. Gas treatment bioreactors, like any other bioprocess, are generally started with a relatively small inoculum of acclimated microorganisms, the objective of the start-up period being to increase the population to the steady-state value, S_x. This requires additional growth nutrients, and the initial feed concentration, S_{ji}, can be calculated as above, but with setting the observed cell yield, y, equal to the growth yield coefficient, Y. These concentrations can then be decreased slowly as steady state is approached. Start-up of biofilters is sometimes called ripening of the bed, and it is not always necessary to add growth nutrients, because the microorganisms capable of growth on the contaminant may obtain nutrients from the support material (compost, soil, etc.), or may grow at the expense of cells that die and lyse under conditions in the biofilter. If these sources are not sufficient to produce the biofilm thickness needed for maximum contaminant removal, some nutrient addition after steady-state contaminant removal has been reached will further improve performance. However, excessive nutrient addition must be avoided because modeling (38) suggests that, under contaminant limited conditions, a biofilm will grow much thicker than is needed. The inlet end of the biofilter may plug with useless biofilm.

Just because a steady state exists in theory, it does not follow that it can be reached by any start-up procedure. Of particular concern are those contaminants that are so concentrated (high n_i) and soluble (low H) that they will cause substrate inhibition of the microbial metabolism if their dissolved concentration in the biophase ever reaches equilibrium with the feed (n_i/H). The steady state analyzed above still exists, but $S \ll n_i/H$ only as a consequence of the metabolism of the large numbers of microorganisms present. Starting with a small inoculum, the dissolved concentration in the biophase will be much higher, metabolism will be inhibited, and the biomass may wash out. For similar reasons, batch experiments may produce the erroneous conclusion that the gas cannot be treated biologically. A proper start-up procedure may involve dilution of the feed gas and careful control of the dilution rate and nutrient addition, until a dense, well-acclimated microbial culture has developed.

Gas-Biophase Mass Transfer

Figure 2 shows that high levels of contaminant removal require high values of the dimensionless mass-transfer factor, G, which is actually the product of two dimensionless numbers: H/RT, an inverse measure of the contaminant solubility, and k_1a/g, a measure of the efficiency with which the gas flow generates mass transfer. This is not usually a difficulty for biofilters with their thin biophase and very large a but how can it be achieved for other bioreactor types? Measurements of gas–liquid mass transfer factors (28) are often given as correlations of the form

$$k_1a = AU_g^c \tag{7}$$

The superficial gas velocity U_g is related to the flow rate g by $U_g = gL$, where L is the bioreactor height. Consider first an idealized bubble column, a hypothetical device in which all the bubbles are the same size, and doubling U_g simply doubles their number. The exponent c must then be 1, making $k_1a/g = AL$, a constant dependent upon scale but independent of gas-flow rate. In real bubble columns, with their imperfect bubble dispersion, c is closer to 0.7, but this still implies that G varies only slightly with g. The copious data available for oxygen transfer from air (28) shows that, at normal gas flows (g on the order of 1 VVM), k_1a/g is on the order of 1 at the laboratory scale, rising toward 10 in commercial-scale equipment. Assuming for the purposes of illustration that k_1 for a gas is proportional to its diffusivity in water raised to the 2/3 power (strictly valid only for relatively insoluble gases, for which most of the mass-transfer resistance is on the liquid side of the gas–biophase interface), this can be used to estimate G and the maximum possible fractional removal, $1 - e^{-G}$, (equation 4 with $S \to 0$) for contaminant gases of low, medium, and high solubility. The results shown in Table 1 suggest that bubble columns would be useless for insoluble contaminants like carbon monoxide, but worth consideration for moderately soluble contaminants like hydrogen sulfide. Most hydrocarbon vapors fall into the former category, but many alcohols and chlorinated aliphatic solvents are in the latter (30). For very soluble contaminants, such as sulfur dioxide, G tends to be unnecessarily large in bubble columns, and while acceptable removal with a moderate pressure drop could be achieved in very short, wide columns, this configuration has not been explored in practice.

The addition of a mechanical agitator can increase k_1a by roughly one order of magnitude, mainly by breaking up the gas flow into many small bubbles with a large interfacial area. Equation 7 still applies, but the A parameter becomes a function of the mechanical power input per unit reactor volume. Unfortunately, agitation also undermines the assumption that the gas moves though the reactor in plug flow. In a mechanically agitated tank, the gas bubbles are assumed to recirculate several times so that the gas phase is completely mixed; a sample of gas containing many bubbles taken from anywhere in the tank would have the same composition as the outlet gas. The effect on the driving force for mass transfer can be seen by comparing the concentration profiles shown in Figure 3a and b. Mathematically, the long-mean concentration difference used in equation 3 must be replaced by the more familiar effluent partial pressure driving force ($p/H - S$), which makes the maximum possible removal not ($1 - e^{-G}$), but $G/(1 + G)$. These two functions are virtually identical at small G, which explains why the exact definition of the driving force is not an issue for aeration (oxygen is an insoluble gas, $H/RT = 30$ at 20 °C, and its small fractional removal from the air stream in conventional fermenters is

Table 1. Performance of Bioreactors for which k_1a/g = 1–10 for O_2

Contaminant gas	H/RT at 20 °C	G	Maximum possible removal	
			Mixed gas phase $G/(1 + G)$	Plug flow gas $1 - \exp(-G)$
CO	37	0.023–0.23	0.022–0.19	0.023–0.20
H_2S	0.41	1.8–18	0.65–0.95	0.84–1
SO_2	0.0088	88–880	0.99–0.999	1

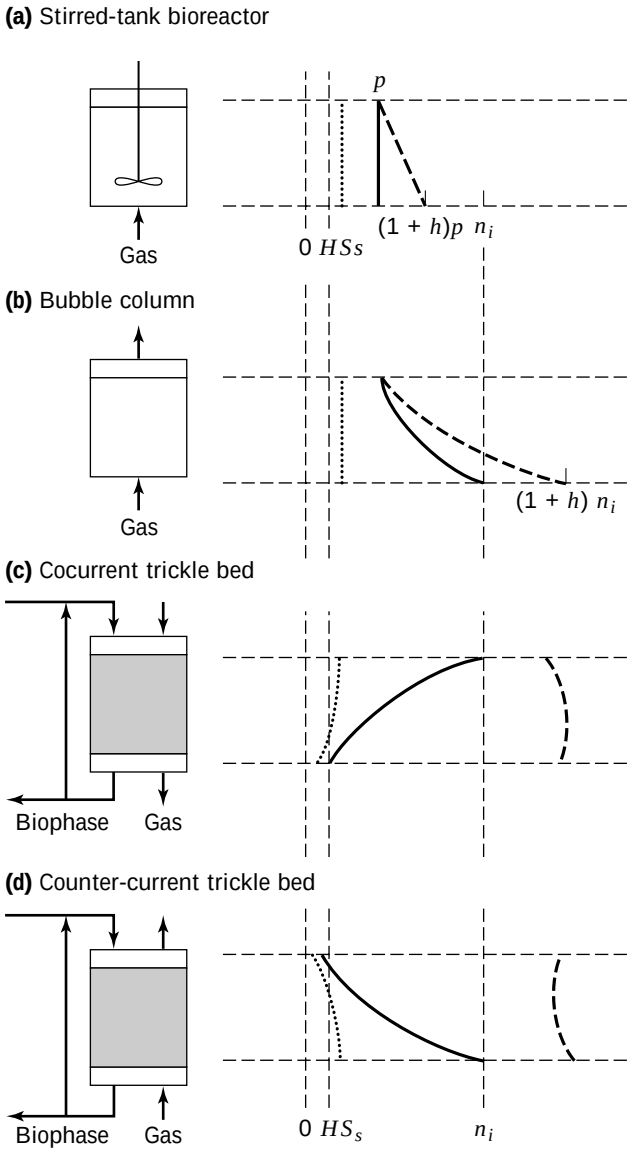

Figure 3. Concentration Profiles in Different Bioreactors. (**a**), (**b**) Partial pressure in gas phase, dot-dash line (**c**), (**d**) Viable biomass concentration, dot-dash line. Dotted line, partial pressure in biophase = HS; solid line, mole fraction in gas phase.

unimportant). However, a goal of 95% contaminant removal now requires not $G > 3$, but $G > 19$, which gives some idea of the lower effectiveness of a completely mixed gas phase. The numbers in Table 1 show that this lower effectiveness cancels out the increased k_1a leading to conclusions similar to those for bubble columns. The extra expense of mechanical agitation is rarely justified in gas treatment bioreactors, although reactors designed for a high k_1a/g with large aspect (height:diameter) ratios and multiple impellers to prevent bubble coalescence (29) have been proposed for removing hydrogen sulfide. Stirred tanks have been used successfully (39) for the microbial production of ethanol and acetic acid from carbon monoxide and hydrogen (another insoluble gas; H/RT = 51 at 20 °C), but the objective there was high volumetric productivity, rather than complete gas consumption. Several tanks were used in series, and they were pressurized to several atmospheres to improve gas transfer.

In contrast to bubble-gasified reactors, the gas–biophase interfacial area in biotrickling filters is almost constant, fixed by the choice of packing media and only slightly influenced by U_g and the superficial velocity at which the liquid is pumped over the bed U_1. This makes it possible to achieve the necessary value of G for contaminants of almost any solubility by appropriate choice of the packing media and the gas flow per unit volume, g. Many types of packing are available and the best choice in a particular situation is a complex trade-off between the following considerations:

- Less soluble contaminants will need the large a provided by smaller media and the small g implied by the lower permeability of such media to gas flow. For these contaminants, most of the gas–biophase mass-transfer resistance is on the biophase side of the interface, so in correlations of the form of equation 7, $c \to 0$, but A is a fairly strong function of U_1.
- More soluble contaminants can achieve the same G with the smaller a and larger g given by larger media. In this case most of the mass-transfer resistance is on the gas side of the interface, so $c > 0$ and A is less dependent on U_1.
- The conservation of mass shows that the change in concentration of a nonvolatile metabolic product in the biophase as it moves down the bed is $U_g x n_i y_m / U_1 RT$. If this number is small then the biophase approximates complete mixing. If it is large, then the concentration gradients, including that of pH, may be large enough to inhibit metabolism.

- Although a high liquid flow improves mixing and mass transfer, there is a definite upper limit of U_1 at which the bed floods. This limit is predictable (28) and is much smaller for small media.
- It is difficult to generalize about the attachment of the microorganisms to the media because this depends on both the nature of the media and the type of biomass involved. However, it is clear that a bed of small media with attached biomass may quickly become plugged if the contaminant is sufficiently concentrated and the biofilm is allowed to grow. It is reasonable to suppose that the larger the media and the higher the liquid velocity, the more cells will be suspended in the liquid rather than being attached. The z parameter in Figure 1 will be correspondingly larger.
- A biophase containing suspended and attached biomass may, if too thick or too dense, have its own mass-transfer resistance (38). While such resistance is usually to be avoided, it may be beneficial. For example, in trying to separate one electron acceptor, NO_x, from stack gases that contain another, O_2, which is preferred by the microorganisms, it should be possible to take advantage of the much higher solubility of the NO_x to create locally anaerobic environments in the biophase.

Somewhere among all of these considerations is a best choice of media for any situation. For dilute, less-soluble contaminants whose metabolism does not produce any nonvolatile metabolic products, the biotrickling filter will look more like a biofilter, with small media, little liquid flow, and attached biomass. For more soluble contaminants which do generate such products, it will tend toward the other extreme of high liquid flows and a completely mixed biophase. If there seems to be no sensible solution, the answer may be to adopt a bioscrubber. Although more expensive, it greatly simplifies the design problem by separating gas–liquid mass transfer from the microbiological considerations. It is certainly preferable to think in terms of this continuum of possibilities and to choose the one best suited to a particular application, rather than considering the different types of gas treatment bioreactors as completely separate technologies, each of which can be forced to fit any job.

Biophase Mixing and the Minimum Effluent Concentration

The single bioreactors with a completely mixed biophase analyzed here have an obvious drawback: all of the microorganisms are exposed to the same physicochemical environment, it is the worst possible environment for metabolism, with the lowest nutrient concentrations and the highest concentrations of metabolic products. One consequence appears in Figure 2. Even with no mass transfer resistance ($G = \infty$), no product inhibition ($F = \infty$), and no wastage of biomass ($D = 0$), the analysis suggests that complete contaminant removal is still impossible. With no biomass outflow there is no net cell growth, and all of the contaminant is used for maintenance metabolism (equation 2 with $\mu = D = 0$ gives $q = k$). Under these conditions, the dissolved contaminant concentration is not zero, but the stationary phase concentration, S_s, so the partial pressure in the effluent gas cannot be less than HS_s, and the fractional removal, x, can never exceed $(1 - HS_s/n_i)$, even with perfect mass transfer (equation 4 with $G = \infty$). This maximum removal also exists for completely mixed biological wastewater treatment systems, but in that case it does not matter because S_s is much less than common effluent standards. It may matter for some insoluble gas-phase contaminants because the corresponding minimum-achievable partial pressure, HS_s, may be significant, even when S_s is small. Bioreactors with a completely mixed biophase are a poor choice for such contaminants.

The simplest improvement would be two bioreactors through which the gas flows in series and between which the microbial culture is continuously recirculated. Reactor 1 would have a relatively high effluent partial pressure and dissolved contaminant concentration, providing a good environment for metabolism and cell growth. If the process variables are fixed correctly (a complete analysis is beyond the scope of this chapter) reactor 2 could run with a dissolved concentration $S < S_s$. The biomass in reactor 2 would then be in an endogenous state, but this would no longer matter because fresh, viable cells would be continuously supplied from reactor 1, and the dying cells would either flow back there to recover or be lost in the liquid effluent. The liquid inflow would go to reactor 1, where the growth nutrients are needed, and where it would dilute the concentrations of any metabolic products.

The more bioreactors in series, the better the average physicochemical environment for metabolism. Columns containing many sieve trays or bubble-cap trays have long been used for gas–liquid contacting in the chemical process industry and should be considered for the biological treatment of gases in cases where the biomass grows best in suspension and the contaminant is relatively dilute, insoluble, and a poor microbial substrate (i.e., HS_s/n_i is large). These columns are inherently countercurrent contacting devices with the gas flowing upward while the microbial culture falls down from tray to tray. An individual microorganism experiences a series of environments with ever-increasing dissolved contaminant concentration, S, until it is suddenly pumped back to the top tray where conditions are endogenous ($S < S_s$), but where it can continue metabolizing contaminant and survive long enough to start through the cycle again. Nutrient addition and pH control can be done on each tray as needed, and the liquid effluent can be taken from near the top of the column where cell viability is lowest.

A similar effect, with the gas closer to the theoretical optimum of plug flow, can be achieved in an upflow biotrickling filter with a small liquid recycle ratio. The only drawbacks are that pH control and nutrient addition can now only be done at the top of the bed, and the liquid can only be removed from the bottom, which is not necessarily the best arrangement. If all the microbial cells are suspended, the concentration profiles of viable biomass and contaminant will be as shown in Figure 3d. In real trickle beds some of the biomass remains attached, which is a great advantage over tray columns when a nonvolatile metabolic product is generated, because it allows a large

liquid outflow to remove the product without the danger of washing out the biomass. (Mathematically, D is small because z is small, even though f is large.) Biotrickling filters can also be operated in the gas-downflow, cocurrent mode, which gives concentration profiles (again assuming suspended biomass) more like those shown in Figure 3c. Now, the microorganisms moving down the bed experience an ever-worsening environment for metabolism, with lower S and higher product concentration S_m. They leave the bottom of the bed in an endogenous, low-viability state, which is very suitable for the liquid outflow stream, but which may cause a significant lag phase when cells are recycled to the better environment at the top of the bed. The question of whether the cocurrent mode works better can only be answered definitively by experiments on a particular gas stream.

In biofilters the biophase is far from being completely mixed. It consists of an immobilized mass of up to xXe_b viable cells per unit bioreactor volume (less if cell growth has been limited by some nutrient other than the contaminant), and one of the goals of media selection is to provide sufficient surface area so that these cells can be distributed as a biofilm thin enough to avoid mass transfer limitation due to diffusion through the film. However, simple models (38) suggest that biofilters should share the minimum effluent partial pressure, HS_s, predicted earlier for bioreactors with a completely mixed biophase, because biofilms exposed to any lower partial pressures near the biofilter effluent would be in an endogenous state and eventually die. Experience suggests otherwise, probably because the adsorption of the contaminants on the media increases their effective concentration in the microorganisms' immediate environment. It follows that highly adsorptive support particles, such as compost or activated carbon, will work best, and that biofilters can treat very insoluble, hydrophobic contaminants if they adsorb well.

Scale-Up

First-stage scale-up experiments can be done in a reactor of any size that is convenient or available, as long as it is large enough so that the flows of gas and liquid are not significantly altered by entrance effects, channeling, or wall effects. Ideally, several different bioreactor types or packing materials are studied, but this is not always possible. The objective is to vary the gas flow, g, the liquid flow, f, nutrient addition, Sji, and so on, to determine how the specified contaminant removal can be achieved most economically. The scale-up problem is then to extrapolate the results in order to calculate the necessary volume (volume = gas flow to be treated/g) and shape (specifically the height, L) of the commercial-scale bioreactor, which must satisfy the process requirements without further experimentation immediately after start up. The best combination of process variables found in the experiments must be close to the optimum identified by the point at the right end of the operating region in Figure 2. To preserve this solution at the commercial scale, the dimensionless numbers D, F, and G that define this point must be kept the same between scales. Scaling up a gas treatment bioreactor is thus an example of Reynold's similarity principle, which states that two physical situations are similar only if the all of the relevant dimensionless numbers are identical.

Consider first the case where there is no inhibitory metabolic product and the process needs little or no liquid outflow. $F(\rightarrow\infty)$ and $D(\rightarrow 0)$ both drop from the list of relevant dimensionless numbers, and the scale-up problem reduces to finding combinations of gas flow, g, and bioreactor height, L, that keep G constant between scales. Given a mass-transfer correlation of the form of equation 7, G can be written $ARTL^c/Hg^{(1-c)}$. The problem is illustrated graphically in Figure 4, where lines of constant G are drawn on a log–log plot of g versus L. If the small-scale experiments have found different combinations of g and L that produce the specified contaminant removal, x, then this data should fall on such a line, labeled *empirical* in Figure 4, because the theory suggests that "constant x" implies "constant G." Also shown in Figure 4 is an upper limit on the gas superficial velocity, $U_g = gL$, caused by physical phenomena such as slugging of bubble columns, fluidization of the media in upflow biofilters, or flooding of the impeller in stirred tanks. This limit may be slightly different at different scales. Two extreme cases of the scale-up problem can be identified.

For a biofilter or a biotrickling filter treating sparingly soluble contaminants, the mass-transfer factor is little affected by the gas velocity, implying that $c = 0$ and making the empirical line horizontal. Several important phenomena are lumped into the parameter A, but there is no reason to expect them to vary with scale because microorganisms cannot "know" if they are in a small or large bioreactor. Consequently, performance on the large scale is defined by the same horizontal line, meaning that scale-up is done at constant g, or equivalently at constant gas-residence time ($=1/g$). Because $g = U_g/L$, constant g can be achieved either with a deep bed and a high gas velocity, the right end of the $c = 0$ line in Figure 4, or with a shallow bed and a low velocity, the left end of the line. Although the former are easier and cheaper to build, they have a much higher pressure drop though the bed, meaning higher costs for gas compression and possibly subsequent

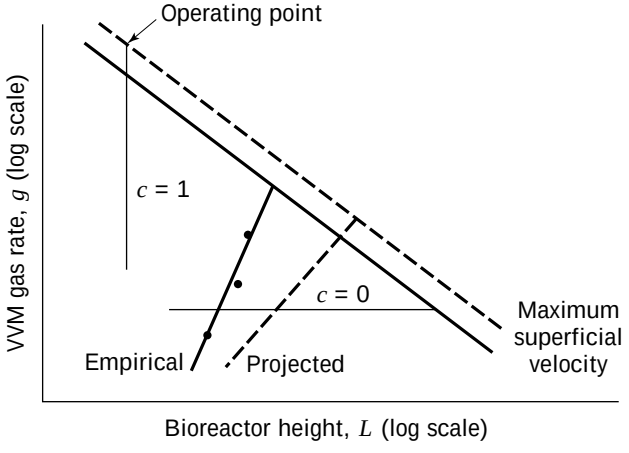

Figure 4. Dotted line, large scale; solid line, small scale.

cooling to return the gas to a temperature tolerable to the microorganisms. The latter are much cheaper to operate and work well as long as the beds are deep enough (at least several hundred times the particle size) to avoid problems of channeling and short-circuiting of the gas flow. Many biofilters consist of shallow beds of media on trays arranged in various configurations in a reactor designed to ensure an even flow of gas into the beds.

At the other extreme is the ideal bubble column described in the section "Gas Biophase Mass Transfer" for which $c = 1$. The value of G, and thus the contaminant removal, is now independent of gas flow but proportional to bioreactor height. Scale-up must therefore be done by keeping L constant but increasing the reactor width, the large-scale bioreactor operating at maximum g in order to minimize its volume (the *operating point* in Figure 4). Although this ideal bubble column is an abstraction, it illustrates a paradox that can arise in scaling up practical bubble columns (for which $c \cong 0.7$); if the desired removal can be achieved in a small-scale column, then a bubble column is probably not the best solution at the commercial scale. For very soluble contaminants, the L needed to obtain the desired fractional removal may be in the range of laboratory reactors, around 1 m. Scale-up would produce a very unusually shaped large-scale bioreactor, a similar height but several meters wide. There would be no point in making it any deeper, except to provide a safety factor in the design, and it could not be made any narrower and still meet the process requirements. For insoluble contaminants the necessary L may be several meters. The conclusion from laboratory experiments would then be that a bubble column is not a feasible bioreactor, even though the desired contaminant removal may be achievable (albeit with a high pressure drop) with the reactor heights used at the commercial scale.

All practical situations fall between these two extremes, so neither simple scale-up rule, constant g or constant L, is necessarily appropriate. The empirical line will have a positive slope, and a similar line for the same G at the larger scale can be projected from it if any variations of the parameters A and c with scale can be estimated from the published literature, experience, consultations with equipment manufacturers, and so on. The design of the large-scale bioreactor can be anywhere along this projected line in Figure 4, the exact design point again being constrained by the maximum U_g line, but essentially an economic trade-off between the large bioreactors demanded by a small g and the large pressure drops associated with a large L. The essential point is that the shape, and the size of the large-scale bioreactor are fixed by this procedure and should not be chosen based simply on guesswork or convenience.

Some bioreactor types allow design flexibility because they have variables that can be adjusted when drawing the projected line. Both A and c tend to decrease with scale in any bubble-gasified reactor due to poorer gas dispersion, but in mechanically agitated tanks, A is a function of the power input per unit volume, which can be varied to some extent. For trickle beds and biofilters, both A and the bed permeability are predictably related to packing size, allowing the packing to be chosen to give the large-scale reactor both a convenient shape and a reasonable pressure drop. Note that, whether or not such changes are made between scales, the estimates on which the projected line in Figure 4 is based should always be conservative in order to provide a factor of safety in the large-scale design.

When product inhibition is significant, the liquid outflow, f, becomes a critical variable, and all three dimensionless numbers D, F, and G must be kept constant if the physicochemical environment of the biomass (S, S_m) and the optimum bioreactor performance established in the small-scale experiments are to be extrapolated to the large scale. An exact solution is possible only when the retention of the biomass by cell immobilization or recycle (the z parameter) can be controlled, although when retention is almost complete ($z \to 0$) only the product DF (from which z cancels) is important, implying that the liquid flow, f, must be kept proportional to the gas flow, g. Biotrickling filters have an extra dimensionless number, the liquid recycle ratio, RR, which introduces the extra difficulty that increasing the bed height, while keeping f and RR constant increases the liquid superficial velocity [$U_l = Lf(1 + RR)$], thus changing the mass-transfer situation and possibly flooding the bed. The procedure just described will not work in these more complex situations (constant x no longer implies constant G), but the general considerations still apply, including the physical limits on the gas superficial velocity, the desirability of tall small-scale bioreactors to reduce uncertainties, the need for compromise between capital and energy costs, and the possibility of predicting a very inconvenient aspect ratio for the large-scale bioreactor. Judgment and calculation are needed in each case because the trivial solution to the scale-up problem—"build a bigger bioreactor with the same shape, f, and g as the small one"—is unlikely to be the best. Gas treatment bioreactors are one of the few devices whose performance tends to improve with scale, but taking advantage of this tendency in practice is not straightforward.

NOMENCLATURE

a	Gas–biophase interfacial area per unit bioreactor volume
A,c	Constants in mass-transfer correlation
D	$zf/e_b Yk$ = dimensionless liquid flow rate
e	Hold-up
f	Liquid outflow rate per unit bioreactor volume
F	$YS'_m/zy_m X$ = dimensionless product-inhibition number
g	Volumetric gas outflow rate per unit bioreactor volume (the VVM gas rate)
G	$k_1 aRT/Hg$ = dimensionless mass-transfer-effectiveness number
h	Gauge pressure (atm) at gas inlet
H	Henry's law constant
k	Cell maintenance coefficient
k_1	Gas-to-biophase mass-transfer coefficient
L	Bioreactor height
n_i	Mole fraction of contaminant in feed gas

p Partial pressure (atm) of contaminant in effluent
q Specific consumption rate of contaminant
R Gas constant
S Dissolved concentration in biophase
S_s Stationary phase contaminant concentration (concentration at which $\mu = 0$)
S'_m Product concentration that totally inhibits metabolism
T Outlet gas temperature
U_g Superficial gas velocity at bioreactor outlet
U_1 Superficial liquid velocity in a trickle bed
X gn_i/ke_bRT = maximum possible cell concentration in biophase
x $1 - p/n_i$ = fractional removal of contaminant
w Evaporation rate per unit bioreactor volume
y Mole of nutrient consumed or product formed per unit of contaminant metabolized
Y Cell-yield coefficient
z Cell concentration in liquid effluent/cell concentration in biophase
γ Available electrons per carbon equivalent of biomass
μ Specific growth rate of biomass

Subscripts

i Inlet conditions
j Any nutrient or product
m Metabolic product
x Biomass

BIBLIOGRAPHY

1. G. Leson and A.M. Winer, *J. Air & Waste Management Assoc.* **41**, 1045–1053 (1991).
2. D.S. Hodge, V.F. Medina, R.L. Islander, and J.S. Devinny, *Environ Technol.* **12**, 655–662 (1991).
3. W.A. Apel, W.D. Kant, F.S. Colwell, B. Singleton, B.D. Lee, G.F. Andrews, A.M. Espinosa, and E.G. Johnson, *Emerging Technologies in Hazardous Waste Management IV*, American Chemical Society, Washington, D.C., 1994, pp. 142–159.
4. S. Dharmavaram, J. Casey, and C. van Lith, *Proc. Air Waste Management Association*, 93-WP-52C.01, Denver, Colo., June 13–18, 1993.
5. I. Togashi, M. Suzuki, M. Hirai, M. Shoda, and H. Kubota, *J. Ferment. Technol.*, **64**, 425–432 (1986).
6. W.A. Apel, P.R. Dugan, M.R. Wiebe, E.G. Johnson, J.H. Wolfram, and R.D. Rogers, *Emerging Technologies in Hazardous Waste Management*, vol. 3, American Chemical Society, Washington, D.C., 1993, pp. 411–428.
7. W.A. Apel, B.D. Lee, M.R. Walton, L.L. Cook, and K.B. Dinerstein, *Proceedings of the Air & Waste Management Association*, 95-TP9C.07, San Antonio, Tex., June 18–23, 1995.
8. P. Plumb, K.H. Lee, and K.L. Sublette, *Appl. Biochem. Biotechnol.* **24/25**, 785–797 (1990).
9. J. Croonenberghs, F. Varani, and P. Le Fevre, *Proceedings of the Air & Waste Management Association*, 94-RP115B.06., Cincinnati, Ohio, June 19–24, 1994.
10. Y. Yang, A.P. Tongas, and J.R. Blunk, *Proceedings of the Air & Waste Management Association*, 94-RA115A.04., 1994.
11. R. Whittenbury, K.C. Phillips, and J.E. Wilkinson, *J. Gen. Microbiol.* **61**, 205–218 (1970).
12. C.L. Haber, L.N. Allen, S. Zhao, and R.S. Hanson, *Science.* **221**, 1147–1153 (1983).
13. J. Pilkington, and H. Dalton, *Methods in Enzymology*, vol. 88, Academic, New York, 1990, pp. 181–190.
14. J. Colby, D.I. Stirling, and H. Dalton, *Biochem. J.* **165**, 395–402 (1977).
15. D. Scott, J. Brannan, and I. Higgins, *J. Gen. Microbiol.* **125**, 63–72 (1981).
16. Stanley, S. Prior, D.J. Leak, and H. Dalton, *Biotechnol. Lett.* **5**, 487–492 (1983).
17. R. Oldenhuis, R.L.J.M. Vink, D.B. Janssen, and B. Witholt, *Appl. Environ. Microbiol.* **55**, 2819–2826 (1989).
18. V. Hecht, D. Brebbermann, P. Bremer, and W.D. Deckwer, *Biotechnol. Bioeng.* **47**, 461–469 (1995).
19. B.R. Folsom, P.J. Chapman, and P.H. Pritchard, *Appl. Environ. Microbiol.* **56**, 1279–1285 (1990).
20. D. Arciero, T. Vannelli, M. Logan, and A.B. Hooper, *Biochem. Biophys. Res. Commun.* **159**, 640–643 (1989).
21. L.P. Wackett, G.A. Brusseau, S.R. Householder, and R.S. Hansen, *Appl. Environ. Microbiol.* **55**, 2960–2964 (1989).
22. M. Kastner, *Appl. Environ. Microbiol.* **57**, 2039–2046 (1991).
23. J.N. Petersen, R.S. Skeen, K.M. Amos, and B.S. Hooker, *Biotechnol. Bioeng.* **43**, 521–528 (1994).
24. J.M. Barnes, W.A. Apel, and K.B. Barrett, *J. Hazard. Mat.* **41**, 315–326 (1995).
25. W.A. Apel, J.M. Barnes, and K.B. Barrett. *Proceedings of the Air & Waste Management Association*, San Antonio, Tex., June 18–23, 1995.
26. Bohn H.L., *J. Air Pollut. Control Assoc.* **25**, 953–95 (1975).
27. M. Shields, M. Reagin, R. Gerger, C. Somerville, R. Schaubhaut, R. Campbell, and J. Hu-Primmer, in R.E. Hinchee, A. Leeson, L. Senprini, and S.K. Ong eds., Bioremediation of Chlorinated and Polycyclic Aromatic Compounds, Lewis, Ann Arbor Mich. 1994, pp. 50–65.
28. R.H. Perry and C.H. Chilton, *Chemical Engineers Handbook*, 6th ed., McGraw Hill, New York, 1988.
29. H.M. Lizama and E.N. Kaufmann, in D.S. Holmes and R.W. Smith eds., Minerals Bioprocessing II, TMS, Warrendale, Penn, 1995, pp. 241–253.
30. B.D. Ensley, Dept. of Energy Report DOE/CH-9207, 1992.
31. Z. Shareefden and B.C. Baltzis, *Chem. Eng. Sci.* **49**, 4347–4360 (1994).
32. R.M. Diks and S.P. Ottengraf, *Bioprocess Eng.* **6**, 93–99 (1991).
33. S. Lamare and M. Legoy, *Trends in Biotechnology* **11**, 413–419 (1993).
34. R.M. Counce and J.J. Perona, in N. Cheremisenoff ed., *Handbook of Heat and Mass Transfer*, vol. 2, Gulf, Houston, Tex., 1986, pp. 953–966.
35. Y.N. Lee and S.E. Schwartz, *J. Phys. Chem.* **85**, 840–848 (1981).
36. G.F. Andrews, Appl. Biochem. Biotechnol. **51/52**, 329–338 (1994).
37. C. Oncharit, Y.T. Shah, and K.L. Sublette. Chem. Eng. Sci. **45**, 2383–2389 (1990).
38. G.F. Andrews and K.S. Noah, *Biotechnol. Prog.* **11**, 498–509 (1995).
39. K.T. Klasson, M.D. Ackerson, E.C. Classen, and J.L. Gaddy, *Fuel* **72**, 1673–1678 (1993).